Methanol Steam Reforming for Fuel Cell Applications

Sandra Teixeira Sá

Dissertation presented for the degree of

Doctor in Chemical and Biological Engineering

by the

University of Porto

Supervisors

Adélio Miguel Magalhães Mendes, Associated Professor

José Manuel Ribeiro de Sousa, Assistant Professor

LEPAE - Laboratory of Engineering Processes, Environment and Engineering

Chemical Engineering Department

Faculty of Engineering – University of Porto

Porto, 2011

Acknowledgments

I would like to acknowledge the financial support of the Portuguese Foundation for Science and Technology (FCT) for my PhD grant (SFRH/BD/30385/2006) and for the projects PTDC/EQU-EQU/71617/2006 and PTDC/CTM/108454/2008. I would also like to thank LEPAE, DEQ and FEUP, for giving me the conditions to carry out my work.

I am particularly thankful to my supervisors Professor Adélio Mendes and Professor José Sousa, for their guidance and for the long hours of helpful discussions. To Prof. Adélio for always finding time for me in his busy schedule, for believing in me and never letting me give up. To Prof. Sousa for all his patience during the models' development and the hard work in the units' assembly.

I would like to thank my father- and mother-in-law for translating the abstract to French. I would not be able to do it myself!

My thankful words also go to all my labmates: thank you for your friendship and support. Many thanks to all the members of our "Steam Reforming and Fuel Cells Group" for all the helpful weekly discussions. I am also thankful to Dr. Lúcia Brandão for always being available to help me, and to Dr. Alfredo Tanaka for his useful insights regarding carbon membranes. Thank you Alfredo for finding the one sealant that actually worked in my membranes!

To all my friends, thank you for your support and advice, but mostly for the joy and optimism that you always give me. A special word to Luísa, thank you for your true friendship, and for being there for me with kind words and support. Your strength and determination has helped me so many times!

To my father, for your guidance and the values you have taught me. To my brother Filipe, for the affection and for always being there for me. Thank you both for

your unconditional love and your never-ending support. To all my family, thank you for never letting me feel alone.

My deepest gratitude goes to you Nuno for giving me the strength and will to carry on. Thank you for your patience and for showing me that there is always a solution for each problem. Thank you for all your love and for making me truly happy.

To my mom…

Contents

Part II: Modelling

Part III: Experimental

Abstract

In a time where environment problems are one of the world biggest concerns, it is imperative to search and develop new and clean sources of energy. A promising environmentally friendly technology is the production of electrical power with fuel cells. More specifically, polymer electrolyte membrane fuel cells (PEMFC) are a suitable power generation device for small scale and transport applications. Although they are very attractive by their low or zero gas emissions, fuel cells require hydrogen as a fuel, which is extremely difficult to store and to transport. Steam reforming of methanol allows a hydrogen production *in situ*, avoiding the hydrogen storage and transportation problems.

The present thesis is focused on the production of hydrogen by methanol steam reforming. This work comprises simulation studies concerning the configuration of membrane reactors; kinetic modelling of a commercial $CuO/ZnO/Al_2O_3$ catalyst; and operation of a carbon membrane reactor.

This work starts with a theoretical approach, where membrane reactor (MR) configurations for the production of PEMFC grade hydrogen were investigated in two simulation studies. The purpose of these studies was to determine in which operating and design conditions a membrane reactor could produce a PEMFC grade hydrogen stream. In a comparative study between carbon molecular sieve (CMS) and palladium membrane reactors, CMS-MR presented higher hydrogen recoveries, while the Pd-MR had the advantage of producing a pure hydrogen stream. A combined CMS+Pd membrane reactor was also investigated, revealing some advantages towards each membrane reactor. In a different study, the enhancement of the CMS-MR performance by the presence of a preferential oxidation (PROX) catalyst in the permeate side was addressed. It was found that the presence of the PROX catalysts in the permeate side was able to convert almost all of the carbon monoxide into carbon dioxide. It was concluded that this system is appropriate to produce a PEMFC grade hydrogen stream.

With the purpose of studying the steam reforming reaction and validate the previously developed mathematical model, the reaction kinetics and the membranes' permeabilities were experimentally determined. A commercial $CuO/ZnO/Al_2O_3$ catalyst (G66 MR, Süd-Chemie) was used for the kinetic study, where several kinetic expressions were used to fit the experimental data. The kinetic rate expressions with best fit were used to simulate the packed bed reactor with a one-dimensional model, which was able to predict very accurately the experimental conversion of methanol and the CO concentration.

The permeability of carbon membranes for single gas and gas mixtures was also investigated. A membrane module of CMS hollow fibres from Carbon Membranes Ltd. was assembled, in order to perform permeance measurements at 150 and 200 °C. The results at 150 °C were particularly interesting in terms of ideal selectivity for CMS application in low temperature MSR membrane reactors.

The reaction of methanol steam reforming was studied in a carbon membrane reactor, comprising the previously studied CMS membranes and $CuO/ZnO/Al_2O_3$ catalyst. The catalytic activity experiments were performed at 200 °C, atmospheric pressure in the retentate side and vacuum in the permeate side. A sweep gas configuration was simulated with a one-dimensional model, which revealed that using steam as sweep gas brings several advantages to the reactor's performance. The results confirmed the potential of using MSR in a carbon membrane reactor to produce humidified hydrogen directly usable for PEMFC applications.

Sumário

Numa época em que os problemas ambientais são uma preocupação mundial, é crucial procurar e desenvolver novas fontes de energia limpas. Uma tecnologia promissora e amiga do ambiente é a produção de energia eléctrica com células de combustível. Mais concretamente, as células de combustível de electrólito de membrana polimérica (PEMFC) são um dispositivo de geração de energia adequado para aplicações de pequena escala e transporte. Embora sejam ambientalmente atractivas devido às baixas emissões gasosas, as células de combustível necessitam de hidrogénio como combustível, um gás que é extremamente difícil de armazenar e transportar. A reformação do metanol permite a produção de hidrogénio *in situ*, evitando assim os problemas de armazenamento e transporte deste gás.

A presente tese visa o estudo da produção de hidrogénio por reformação de metanol com vapor de água. Este trabalho abrange estudos de simulação relativos à configuração de reactores de membrana; cinética de um catalisador comercial $CuO/ZnO/Al_2O_3$; e a operação de um reactor de membrana de carbono.

Este trabalho começa com uma abordagem teórica, na qual foram realizados dois estudos de simulação onde a configuração de reactores de membrana (MR) para a produção de hidrogénio destinado a alimentação a PEMFC é abordada. Estes estudos foram realizados com o objectivo de determinar quais as condições operatórias em que um reactor de membrana pode produzir uma corrente de hidrogénio adequada a uma PEMFC. Num estudo comparativo entre um reactor de membrana de peneiro molecular de carbono (CMS) e um reactor de membrana de paládio, o CMS-MR originou uma maior recuperação de hidrogénio, enquanto o Pd-MR apresentou a vantagem de produzir uma corrente pura de hidrogénio. Foi também estudado um MR com a combinação das membranas CMS+Pd que revelou algumas vantagens em relação a cada um dos MR. Foi ainda estudada a melhoria do desempenho de um CMS-MR quando na presença de um catalisador de oxidação preferencial (PROX) no permeado. Verificou-se uma conversão quase completa de monóxido de carbono a

dióxido de carbono pelo catalisador de PROX. Foi concluído que o sistema em causa é adequado para a produção de hidrogénio para a alimentação a PEMFC.

Tendo como objectivo o estudo da reacção de reformação de metanol e a validação do modelo matemático desenvolvido anteriormente, a cinética da reacção bem como as permeabilidades das membranas foram determinadas experimentalmente. O estudo cinético foi efectuado com um catalisador comercial $CuO/ZnO/Al_2O_3$ (G66 MR, Süd-Chemie), onde várias expressões cinéticas foram usadas para ajustar os pontos experimentais. As expressões cinéticas de velocidade com melhor ajuste foram usadas para simular um reactor de leito fixo com um modelo matemático, o qual foi capaz de prever com grande precisão a conversão de metanol e a concentração de CO.

A permeabilidade das membranas de carbono a gases puros e misturas foi também investigada. Para tal, foi construído um módulo de membranas de CMS, fornecidas pela empresa Carbon Membranes Ltd., para a medição da permeância a 150 e 200 °C. Os resultados a 150 °C foram particularmente interessantes em termos de selectividade para aplicação de CMS em reactores de membrana em regime de baixa temperatura.

A reacção da reformação de metanol foi ainda estudada num reactor de membrana com as membranas de CMS e o catalisador $CuO/ZnO/Al_2O_3$. As experiências de actividade catalítica foram realizadas a 200 °C, pressão atmosférica no retido e vácuo no permeado. Por fim, foi simulada uma configuração com vapor de água como gás de arrasto, que revelou diversas vantagens no que diz respeito ao desempenho do reactor. Os resultados confirmaram o potencial da reformação de metanol num reactor de membrana de carbono para alimentar directamente uma PEMFC.

Sommaire

À une époque où les problèmes d'environnement sont l'une des plus grandes préoccupations du monde, il est impératif de rechercher et de développer de nouvelles sources d'énergies propres. Une technologie prometteuse et respectueuse de l'environnement est la production d'énergie électrique avec des piles à combustible. Plus précisément, la pile à combustible d'électrolyte à membrane polymère (PEMFC) est un dispositif de puissance appropriée pour la production à petite échelle et les applications de transport. Bien qu'elles soient très attractives par leurs faibles ou nulles émissions de gaz, les piles à combustible nécessitent de l'hydrogène comme combustible, qui est extrêmement difficile à stocker et à transporter. Le reformage du méthanol permet la production de l'hydrogène in situ, en évitant les problèmes de stockage et de transport.

Cette thèse se concentre sur la production d'hydrogène par reformage du méthanol. Ce travail comprend des études de simulation sur la configuration des réacteurs à membrane; modélisation cinétique d'un catalyseur commercial $CuO/ZnO/A_{l2}O_3$ et l'exploitation d'un réacteur à membrane de carbone.

Ce travail commence par une approche théorique, où les configurations du réacteur à membrane (MR) pour la production d'hydrogène ont été étudiées dans deux simulations. Le but de ces études était de déterminer dans quelles conditions d'exploitation et la conception d'un réacteur à membrane pourrait produire un flux d'hydrogène pour la PEMFC. Dans une étude comparative entre les réacteurs à membrane en tamis moléculaire de carbone (CMS) et les réacteurs à membrane de palladium, CMS-MR a présenté les récupérations d'hydrogène plus élevées, tandis que le Pd-MR a eu l'avantage de produire un flux d'hydrogène pur. Un réacteur à membrane combinée CMS + Pd a également été étudié, révélant des avantages sur les autres réacteurs à membrane. Dans une autre étude, l'amélioration de la performance du CMS-MR par la présence d'un catalyseur d'oxydation préférentielle (PROX) dans le côté du perméat a été adressée. Il a été constaté que la présence des

catalyseurs PROX dans le côté du perméat était capable de convertir la quasi-totalité du monoxyde de carbone en dioxyde de carbone. On peut conclure que ce système est approprié pour produire un flux d'hydrogène pour la PEMFC.

Dans le but d'étudier la réaction de reformage du méthanol et de valider le modèle mathématique développé précédemment, la cinétique de la réaction et la perméabilité des membranes ont été déterminées expérimentalement. Un catalyseur commercial $CuO/ZnO/Al_2O_3$ (G66 MR, Süd Chemie) a été utilisé pour l'étude cinétique, où plusieurs expressions cinétiques ont été utilisées pour ajuster les données expérimentales. Les expressions cinétiques avec le meilleur ajustement ont été utilisées pour simuler le réacteur à lit fixe avec un modèle unidimensionnel, qui a été en mesure de prédire très précisément la conversion expérimentale de méthanol et la concentration de CO.

La perméabilité des membranes de carbone pour un seul gaz et mélanges de gaz a également été étudiée. Un module à membrane de fibres CMS de Carbon Membranes Ltd. a été assemblé, afin d'effectuer des mesures de perméabilité à 150 et 200 °C. Les résultats à 150 °C ont été particulièrement intéressants en termes de sélectivité idéale pour les applications CMS en réacteurs à membrane de basse température.

La réaction de reformage du méthanol a été étudiée dans un réacteur à membrane de carbone, comprenant les membranes précédemment étudiées CMS et de catalyseur $CuO/ZnO/Al_2O_3$. Les expériences d'activité catalytique ont été réalisées à 200 °C, la pression atmosphérique dans le côté rétentat et le vide dans le côté du perméat. Une configuration de gaz de balayage a été simulée avec un modèle unidimensionnel, qui a révélé que l'utilisation de la vapeur comme gaz de balayage présente plusieurs avantages pour les performances du réacteur. Les résultats ont confirmé le potentiel de l'utilisation de la MSR dans un réacteur à membrane de carbone pour produire de l'hydrogène humidifié directement utilisable pour des applications de type PEMFC.

Figure Captions

Table Captions

Part I

Introduction

Chapter 1. Introduction

In the last decades, the world population has experienced a significant growth along with increasing energy demands. The dependency on fossil fuels and the foreseen depletion of the world reserves in a near future are among of the world's biggest concerns. According to the United States Energy Information Administration, the world's production of primary energy has increased at an average annual rate of 2.3 % between 1996 and 2006. As it is clear from Figure 1.1, fossil fuels represent most of the primary energy produced.

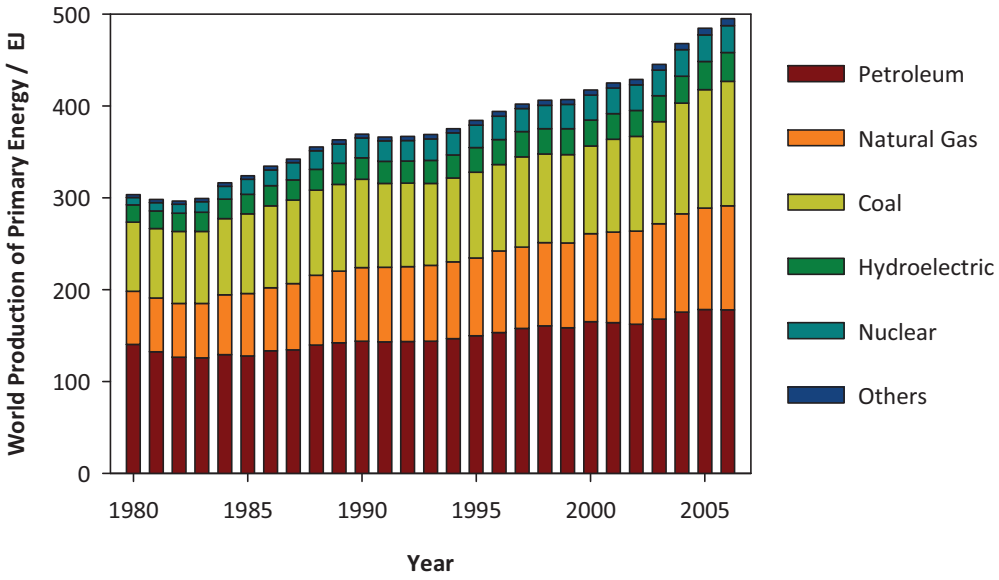

Figure 1.1 – World production of primary energy from 1996 to 2006 according to the United States Energy Information Administration

Dependency on fossil fuels, increasing greenhouse emissions, global warming and other environmental concerns, are triggering the search for new and clean energy sources. One of the most promising technologies involved in this quest is the environmentally friendly fuel cell [1-4].

1.1. Fuel cells

The operation of a fuel cell is very similar to a battery, where electricity is generated from an electrochemical reaction. However, fuel cells present the advantage of not losing their charge like batteries. Fuel cells transform chemical energy from a fuel continuously supplied in electrical energy, while batteries store their own chemical energy source [5]. Although there are many types of fuel cells, their operation is very similar. The fuel (most commonly hydrogen) is supplied to the anodic side while the oxidant enters the fuel cell through the cathodic side. An electrochemical reaction generates and pushes electrons from the anode through an external circuit to the cathode, creating an electrical current. Fuel type, operating temperature and charge carrier ion that crosses the electrolyte, can differ depending on the type of electrolyte used in the fuel cell. A brief description of the most common fuel cells is presented in the following sections.

1.1.1. Solid oxide fuel cell

Solid oxide fuel cells (SOFC) operate at high temperatures (700-1000 °C) which allow fast kinetics without expensive materials. Hydrogen is used as fuel and oxygen as oxidant. The operating efficiency of a SOFC is around 60 % and its main applications are stationary power generation and auxiliary power systems [6, 7]. The SOFC electrolyte is a solid, nonporous metal oxide that can be shaped into various forms such as tubular, planar, or monolithic. The main advantage of high operating temperature is the possibility of internal fuel reforming, thus eliminating the need of a fuel processor [7]. Additionally, SOFC is not poisoned by carbon monoxide. However, high operating temperatures can also cause deterioration of the fuel cell components.

1.1.2. Polymer electrolyte membrane fuel cell

Polymer electrolyte membrane fuel cells (PEMFC) use hydrogen as fuel and oxygen, usually from air, as oxidant. The electrolyte of a PEMFC is a polymer protonic

conductive membrane that allows protons to cross from the anode to the cathode side [8]. Having a solid phase polymer electrolyte membrane and operating at low temperatures (< 90 °C), makes PEMFC much easier to seal and assemble than other fuel cells [8]. Low operating temperatures also allows faster start-up than high temperature fuel cells. PEMFC presents ca. 35-60 % efficiency and requires high purity hydrogen as fuel, especially in what concerns the concentration of carbon monoxide [1, 6]. The PEMFC anodic catalysts are usually made of supported platinum on which carbon monoxide strongly adsorbs, and even small amounts of CO can cause a significant decrease in the catalytic activity and in the output power of the fuel cell. This detrimental effect is commonly known as CO poisoning. Some studies advise a CO concentration limit of 10 ppm [9, 10] for low temperature operation (< 90 °C) in order to avoid CO poisoning. The hydrogen purity requirements of the International Organization for Standardization (ISO 14687) are even lower for PEMFC for road vehicles applications, where a limit of 0.2 ppm is imposed [11].

In high temperature polymer electrolyte membrane fuel cells (HT-PEMFC) the low CO limits described above are not applied [12]. With the recent developments of temperature resistant polymer membranes, such as acid-doped polybenzimidazole (PBI) membranes, the CO tolerance is significantly higher [13]. In fact, the CO effect has been reported as almost negligible at high temperatures such as 140 °C [14]. In 2008, the company Global Energy Innovations presented a HT-PEMFC for the temperature range of 160-180 °C. The membrane electrode assembly (assembled stack of electrodes, catalyst and polymer electrolyte membrane) Celtec®-P MEA supplied by BASF Fuel Cell Inc., tolerates large concentrations of carbon monoxide (3 % at 160 °C) [15].

With only water and heat as emissions, PEMFC are appropriate for vehicles and mobile applications. Recently, electric cars powered by PEMFC were introduced in the market, as the ones presented in Figure 1.2.

Figure 1.2 – Honda FCX Clarity Fuel Cell Electric Vehicle (at the left) [16]; Mercedes-Benz F-CELL prototype [17] (at the right).

An alternative type of PEMFC is the direct methanol fuel cell (DMFC), where hydrogen is replaced by methanol as fuel. At the anodic side of the DMFC, methanol is oxidized in the presence of water, producing CO_2. When high concentrations of methanol are used, methanol diffuses through the membrane, which is called methanol cross-over. In order to reduce methanol cross-over, lower methanol concentrations are employed, with the drawback of reducing the cell voltage. Although DMFC present lower power density than hydrogen fuelled PEMFC, they are suitable to power portable electronic devices. In fact, Toshiba has already presented some prototype cell phones and laptop computers powered by DMFC - Figure 1.3. According to Toshiba, the DMFC delivers long continuous operation with an energy density up to five times that of a typical lithium-ion battery.

Figure 1.3 – Toshiba DMFC laptop prototype [18] (at the left); Toshiba DMFC cell phone prototype presented at CEATEC Japan 2008 conference [19] (at the right).

PEMFC are seen as the leading candidate for automotive power applications. As explained above, purified hydrogen is required to feed a PEMFC in order to maintain a good performance. In the next section, the production and transportation of hydrogen for PEMFC application is discussed.

1.2. Hydrogen as energy carrier

1.2.1. Hydrogen sources

Hydrogen is not a primary energy source, but an intermediate for storing and carrying energy. It can be produced from several sources, such as natural gas, biomass, gasoline, coal, methanol and water. Fossil fuels are the major source for hydrogen production, Figure 1.4, and also the less expensive ones. Water electrolysis, on the other hand, is a very expensive process and only represents 3.9 % of worldwide hydrogen production.

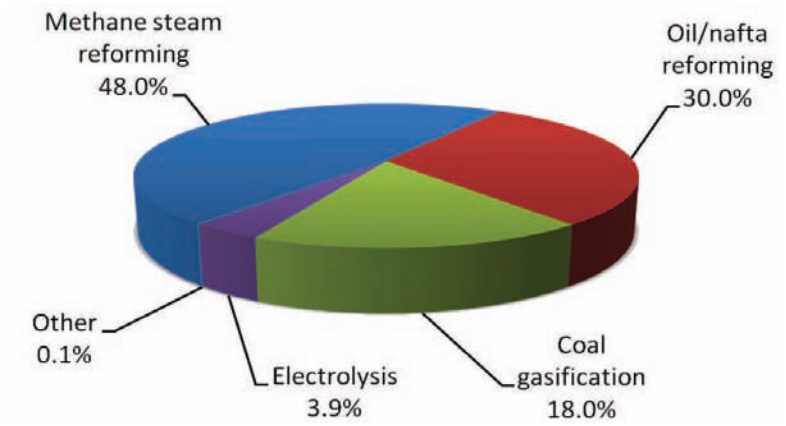

Figure 1.4 – Primary energy sources for hydrogen production [20].

Methane steam reforming is currently the least expensive method for hydrogen production [21, 22]. Methane is wide available, has a pipeline delivery infrastructure and has a high hydrogen to carbon ratio [23]. In the reforming reaction, methane reacts with steam in the presence of a metal catalyst. Hydrogen and carbon monoxide

are formed at high temperatures (> 500 °C), followed by a water gas shift reactor to convert CO to CO_2 [24]. According to the United States Energy Information Administration, the natural gas reserves are enough for ca. 110 more years. Nevertheless, this is still a limited source and increasing demands can result in a cost increase. Other hydrocarbon and alcohol fuels can also be used to produce hydrogen by steam reforming, partial oxidation or autothermal reforming. Well known fuels as propane, gasoline or diesel are an option, although they must be desulfurized first.

Coal is the fossil fuel with the highest reserves and is responsible for approximately half of the electric power supply in the United States [25]. However, coal combustion has major environmental drawbacks, such as the emission of nitrogen oxides (NOx) and sulfur dioxide. A different approach is to produce hydrogen from coal by gasification [26, 27]. In this process, coal is exposed to steam and controlled amounts of oxygen/air at high pressure and temperature. The reaction produces carbon monoxide, hydrogen and carbon dioxide. A water gas shift reactor can then be used to convert CO to CO_2. The high carbon content of coal results in high carbon dioxide emissions, which is a major disadvantage of this fuel. Carbon capture and storage can be used to overcome this problem.

Representing 3.9 % of the primary energy sources for hydrogen production, electrolysis is an expensive but clean process [20]. Electricity is provided to the electrolyser, composed by two electrodes. Water molecule is split into oxygen at the anode and hydrogen at the cathode. The production of hydrogen via electrolysis can result in an environmentally friendly technology, depending on the source of the electricity used [28]. Hydrogen can be produced from current nuclear reactors by electrolysis of water, without emitting CO_2 or other pollutant gases [23]. Another environmentally friendly option is the use of renewable energy sources, such as wind power. Generating electricity with wind turbines is a promising technology, although the electrolyser costs can still be reduced and the integration of the wind turbine with the electrolyser can be improved [29].

Finally, hydrogen can be produced by solar thermo-chemical water splitting, a process that requires high temperatures [28]. The water molecule is decomposed producing a gaseous mixture of hydrogen and oxygen. Water molecules dissociation is enhanced at high temperatures, which can be obtained with concentrated solar energy [30]. However, a water dissociation of only 25 % has been reported at high temperatures near 2225 °C [31]. Significant lower reaction temperatures (800-1300 °C) can be achieved with the use of redox pair cycles, based on redox materials that can act as effective water splitters at lower temperatures [31, 32].

1.2.2. Hydrogen storage and transportation

After hydrogen production, it is necessary to transport it to the final consumer or application. Unlike liquid fuels that can be easily stored, hydrogen has very low density and requires special storage conditions. Hydrogen can be stored in the gaseous form, liquefied or in solid materials [33, 34].

In the gaseous form, hydrogen must be compressed at several hundred atmospheres. The energy required for the storage of compressed hydrogen at 700 bar in lightweight compound bottles or tanks is ca. 22 % of its internal energy [31, 35]. In the liquid state, hydrogen is more compact than in the gas phase, and it can be stored in smaller vessels. Hydrogen is cooled down to cryogenic temperatures which require a high amount of energy. Around 30 % of the hydrogen energy content is spent in the liquefaction process [36]. Another important aspect is the loss of hydrogen by boil off. Boil off is the small amount of gas that evaporates due to heat leakage, that must be permitted for safety reasons. Considering the liquefied hydrogen for transportation applications, this hydrogen leak could be used while the vehicle was in operation, minimizing the losses. However, once stopped, the vehicle would have to be vented to avoid safety hazards.

The use of liquid organic hydrides (LOH) for hydrogen storage is also possible. The hydrogen storage is based in the dehydrogenation of LOH (such as methylcyclohexane, cyclohexane and decahydronaphthalene) and hydrogenation of

corresponding aromatics [37, 38]. LOH can store ca. 6-8 wt.% of hydrogen and are suitable for hydrogen transportation from centralized generation facilities to fuelling stations [38]. Most of the dehydrogenation catalysts reported in the literature are Pt-based, with reaction temperatures in the range of 210-350 °C [38-41]. This process still requires some improvements towards the development of more efficient and less expensive catalysts for LOH dehydrogenation [38].

Another approach to store hydrogen is the use of chemical hydrides in the form of slurry. Water-reactive chemical hydrides present higher gravimetric densities than metal hydrides. For instance, compounds like $LiBH_4$, $NaBH_4$ and $Al(BH_4)_3$ can carry ca. 18 wt.%, 11 wt.% and 17 wt.% of hydrogen, respectively [36, 37]. The chemical hydride slurry or solution has the advantage of being in the semi-liquid state, thus can be stored in most conventional tanks. However, the hydrogen release mechanism is slow and requires thermal management and regeneration of the chemical hydride. Hydrogen is released when exposed to water in a highly exothermic reaction which needs to be handled carefully. On the other hand, the regeneration process is highly endothermic, relatively inefficient and expensive [37].

Solid materials such as metal hydrides can also be used for hydrogen storage [34, 38, 42]. In metal hydride storage, hydrogen is supplied to the container forming a hydride in an exothermic reaction. The extraction of hydrogen is endothermic, which requires heat supply for hydrogen release [36]. The main disadvantage of this process is the weight of metal hydride required. Although they are very compact when compared to compressed hydrogen vessels, they are extremely heavy, which increases the transportation costs. More specifically, the absorbed hydrogen represents an average of only 1-3 % of the total weight of the tank, which makes it unpractical for transport applications [23, 31, 36].

1.2.3. Fuel hydrogen carriers

As described in the previous sections, there are disadvantages in each method of hydrogen storage and transportation. Energy losses, high costs or even safety hazards

are issues that need to be improved. Concerning small-scale applications such as PEMFC, *in situ* hydrogen production is a suitable alternative to its transportation. Common fuel processors for hydrogen production are based on the reforming of hydrocarbons and alcohols. Several hydrogen carriers can be considered for this application, such as methane, ethanol, methanol and dimethyl ether [43-47]. Liquid fuels as methanol and ethanol are easy to handle and do not require special storage or transportation conditions. Another important factor is the reforming temperature. Methane is reformed above 500 °C [24], while ethanol reacts around 400 °C [48] and dimethyl ether in the temperature range of 250-350 °C [49, 50]. The lowest reforming temperature range is presented by methanol, 200-300 °C [51-53]. However, this fuel is highly toxic and must be handled with caution. The emerging technology of dimethyl ether steam reforming will most likely play an important role in hydrogen production for PEMFC applications in a near future [47, 49, 50, 54]. Dimethyl ether is non-toxic and easily liquefied at low pressure, which facilitates its storage and transportation. However, this recent process is still not fully studied and more efficient catalysts must be developed. Methanol steam reforming, on the other hand, has been vastly studied and promising results with low temperature catalysts have been reported [51-53, 55, 56]. In the next section, the production of hydrogen through methanol steam reforming is addressed. Methanol production and safety issues are also discussed.

1.3. Methanol as hydrogen carrier

1.3.1. Methanol production

Methanol is a colourless liquid traditionally used for the production of chemicals such as formaldehyde and acetic acid. Initially called “wood alcohol”, methanol was produced by the distillation of wood from the early 1800s until the mid-1920s [23]. A more efficient process, based on H_2, CO and CO_2 mixtures, replaced wood distillation

and has been used since then. Methanol production from synthesis gas occurs according to eqs. (1.1)-(1.3) [57, 58]:

$$CO + 2H_2 \rightleftharpoons CH_3OH \qquad \Delta H_{298} = -90.9\,kJ \cdot mol^{-1} \qquad (1.1)$$

$$CO_2 + 3H_2 \rightleftharpoons CH_3OH + H_2O \qquad \Delta H_{298} = -41.0\,kJ \cdot mol^{-1} \qquad (1.2)$$

$$CO_2 + H_2 \rightleftharpoons CO + H_2O \qquad \Delta H_{298} = -49.8\,kJ \cdot mol^{-1} \qquad (1.3)$$

Synthesis gas can be obtained by several sources, namely coal, natural gas, petroleum or heavy oils. However, the most suitable feedstock for methanol production is natural gas. It has a high hydrogen content, low energy consumption and low operation costs.

1.3.2. Methanol safety

Methanol is known by its toxicity and rapid absorption by ingestion or inhalation. Nonetheless, a technical report from the United States Department of Energy from 1991 stated that gasoline is considered more hazardous to health than methanol [59]. Methanol fuel stations could operate very similarly to gasoline ones, with modifications to avoid skin exposure to methanol. In the refuelling process, inhalation of small amounts of methanol (2-3 mg) is easily metabolized by the human body, thus is not considered dangerous [23, 60]. Another safety issue is the possibility of fire and explosion. In comparison to gasoline, methanol is less volatile and less likely to ignite. Under the same conditions, methanol would emit 2-4 times less vapours than gasoline. In a study from the United States Environmental Protection Agency about methanol safety, it was considered that methanol is safer, and less likely to cause deadly or damaging fires than gasoline [61]. In this way, as long as safety precautions are followed, methanol should not be considered a more hazardous fuel than gasoline.

Concerning the containers' materials for methanol storage and transportation, certain metals must be avoided due to corrosion, such as magnesium and aluminium. Methanol also attacks common elastomeric materials, as rubber and polyurethane.

Corrosion resistant materials such as stainless steel and carbon steel are recommended [62].

1.3.3. Production of hydrogen from methanol

Methanol is a suitable fuel for hydrogen production due to its high hydrogen to carbon ratio, low boiling point and the absence of C-C bonds. In this section, possible routes for hydrogen production from methanol are addressed, namely decomposition, partial oxidation, steam reforming and combined steam reforming.

Methanol decomposition (MD) - MD is the reverse of methanol synthesis reaction, producing carbon monoxide and hydrogen (eq. (1.4)) [63, 64].

$$CH_3OH \rightleftharpoons CO + 2H_2 \qquad \Delta H_{298} = 92.0\,kJ\cdot mol^{-1} \tag{1.4}$$

The high production of carbon monoxide makes methanol decomposition reaction not appropriate for hydrogen production for PEMFC applications.

Partial oxidation of methanol - methanol reacts with oxygen in an exothermic reaction producing carbon dioxide and hydrogen as follows [65, 66]:

$$CH_3OH + 1/2O_2 \rightarrow CO_2 + 2H_2 \qquad \Delta H_{298} = -192.2\,kJmol^{-1} \tag{1.5}$$

Some hydrogen can be lost in this process, decreasing the hydrogen selectivity.

Methanol steam reforming (MSR) - Methanol and steam react in an endothermic reaction, producing hydrogen and carbon dioxide according to eq. (1.6):

$$CH_3OH + H_2O \rightleftharpoons CO_2 + 3H_2 \qquad \Delta H_{298} = 49.7\,kJ\cdot mol^{-1} \tag{1.6}$$

The presence of carbon monoxide in the reaction products is attributed to the side reactions methanol decomposition (eq. (1.4)) and water gas shift (WGS):

$$CO + H_2O \rightleftharpoons CO_2 + H_2 \qquad \Delta H_{298} = -41.2\,kJ\cdot mol^{-1} \tag{1.7}$$

The production of hydrogen by MSR has been vastly studied in the literature [46, 52, 67-69]. If some oxygen is added to the reactor, partial oxidation of methanol will occur, via a process called combined methanol steam reforming [70, 71]. The combination of the partial oxidation and steam reforming reactions brings some

advantages when compared to MSR alone, such as higher reaction rates and thermo-balanced conditions.

1.3.4. Methanol steam reforming catalysts

A large number of studies can be found in the literature regarding the development of new catalysts for MSR [67, 72-74]. Two major catalysts groups can be considered, copper-based and group 8-10 metals.

The most common catalysts for the MSR reaction are the copper-based ones. They present high activity and selectivity, but also have pyrophoric characteristics and deactivate by thermal sintering [75, 76]. On the other hand, group 8-10 catalysts are highly stable and present similar selectivities (production of CO in comparison to CO_2), with the drawback of lower activities [67, 77]. Comparing the activity of both groups, copper-based catalysts emerge as the most active ones. For instance, Patel *et al.* [78] has reported a Cu/Zn/Zr/Al catalyst with 261 $\mu mol_{H2} \cdot g_{cat}^{-1} \cdot s^{-1}$ at 260 °C, and a Cu/Zn/Ce/Al with 244 $\mu mol_{H2} \cdot g_{cat}^{-1} \cdot s^{-1}$ at 260 °C. On the other hand, Xia *et al.* [56] produced a very promising $Pd/ZnO/Al_2O_3$ catalyst with 113.9 $\mu mol_{H2} \cdot g_{cat}^{-1} \cdot s^{-1}$ at 265 °C, confirming that group 8-10 catalyst can also present high activities.

Most catalysts are active in the temperature range of 200-300 °C, but promising results have been reported in the literature for temperatures below 200 °C [51, 52, 55, 79, 80]. The increasing research on MSR catalysts is resulting in the production of new and more efficient catalysts. However, deactivation and stability problems of copper catalysts still need to be solved. Although Pd alloy catalysts are a good alternative, their activity can still be improved.

1.3.5. Integrated methanol steam reforming/PEMFC applications

Several applications for methanol reformers coupled with PEMFC have already been tested. In 1994, the first vehicle with this technology was presented by DaimlerChrysler, the Necar 1, with the dimensions of a van due to the size of the fuel cell. Three years later, the Necar 3 was presented powered by a 50-kW PEMFC fuelled

by an on-board methanol reformer. On November 2000, an improved and more compact system was presented for the Necar 5. With a 75-kW PEMFC, Necar 5 was able to achieve 150 $km \cdot h^{-1}$.

Figure 1.5 – DaimlerChrysler's methanol fuelled vehicles Necar 3 [81] and Necar 5 [82].

In 2002, Casio announced the development of a small-scale reformer/PEMFC system for portable devices, with around half the weight of a laptop lithium ion rechargeable battery. A micro reactor formed on a silicon wafer was used to produce hydrogen by MSR.

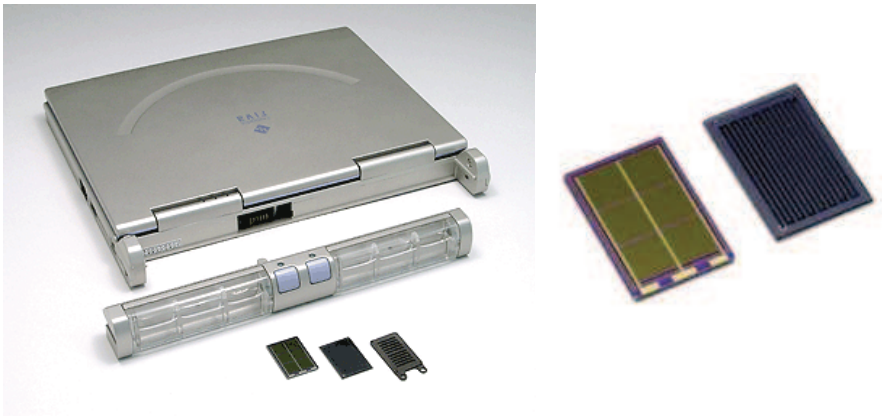

Figure 1.6 – Casio laptop computer powered by a methanol reformer with PEMFC system; detailed view of the methanol micro reformer at the right side of the figure [83].

More recently, UltraCell Corporation presented a new fuel cell power source device in 2005. The UltraCell device has twice the energy density of common lithium batteries

and is suitable for portable applications. The device is composed by a methanol micro reformer that generates hydrogen for a PEMFC, which can provide continuous power for long periods of time. An upgraded version, XX55, was presented in 2008 with a higher peak power and efficiency.

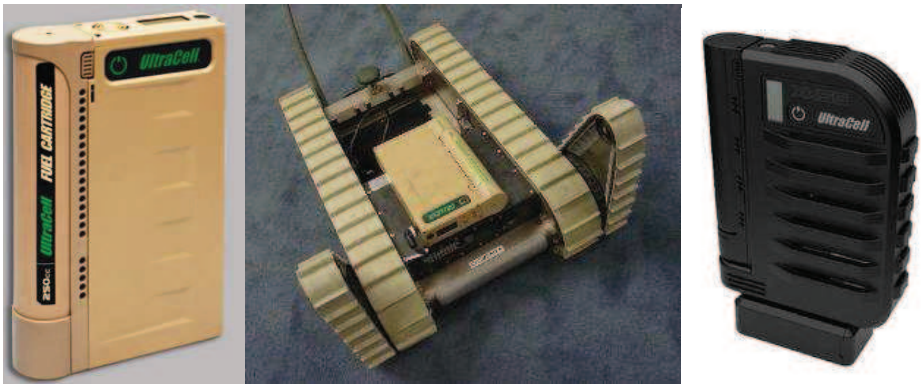

Figure 1.7 – UltraCell XX25 system (at the left side); UltraCell system powering a military robot (at the center); UltraCell XX55 system (at the right side) [84].

Element One, E1, a company from Oregon founded in 2010, designs, develops, and manufactures hydrogen reformers and purifiers for companies providing PEMFC systems. Pegasus Me-50 Hydrogen Generator was launched in November 2010, and is designed to support the requirements of a 5 kW PEMFC.

Figure 1.8 – Pegasus Me-50 Hydrogen Generator from Element One, Oregon [85].

Finally, a recent start-up company, PowerCell Sweden, is currently developing a fuel reformer combined with a PEMFC, the PowerPac system. This system is being designed to be very flexible in what concerns the type of fuel required. In addition to diesel, PowerPac can be fuelled with dimethyl ether, ethanol or methanol.

Figure 1.9 – PowerPac system from PowerCell-Sweden, under development [86].

In our research group, new catalysts are currently being developed for low temperature steam reforming and low CO production (150-180 °C). These innovative catalysts are particularly important for systems with methanol reformers coupled with HT-PEMFC as the ones presented above. Since the steam reforming reaction is endothermic and the fuel cell operation is exothermic, their combination allows higher overall energy efficiencies. Moreover, the water produced by the fuel cell can be recycled and supplied to the reformer.

Despite the promising applications, the methanol steam reforming process can still be improved. Significant amounts of carbon monoxide are produced which is a poison for PEMFC [87]. The removal of CO and other impurities requires a purification step that will be discussed in the next section.

1.4. Hydrogen purification

1.4.1. Gas separation

Gas separation can be performed by different processes, such as cryogenic distillation, pressure swing adsorption or permeation [88-90]. Cryogenic distillation can achieve high recoveries and good separations, but also demands high energy consumption and is very expensive. Pressure swing adsorption, on the other hand, is able to deliver high purity compounds, but with the drawback of low recoveries [88]. A simpler and versatile alternative technology is based on gas separation through membrane permeation [91, 92]. Membranes are compact and light weighted, which allows small units with reduced assembling costs. In addition, this technology can be coupled with a reaction unit, combining reaction and separation in the same device.

1.4.2. Membranes

1.4.2.1. Organic membranes

Polymer membranes can be divided in porous (high permeabilities and low selectivities) and dense membranes (low permeabilities and high selectivities). One of the main drawbacks of these membranes is the polymer's sensitivity to high temperatures and aggressive chemical environments [93]. Additionally, polymers can be swollen or plasticized when exposed to low concentrations of hydrocarbons or carbon dioxide.

1.4.2.2. Inorganic membranes

Gas separation with inorganic membranes such as carbon, glass or silica membranes, is based on a molecular sieving effect through small pores [94]. Concerning the hydrogen separation from a gas mixture, amorphous silica membranes can present high hydrogen permeability and selectivity, but are not easy to produce without defects [94]. Glass membranes present low hydrogen fluxes and

are extremely fragile. On the other hand, they show good thermal stability and chemical resistance [94]. Zeolite membranes do not present high hydrogen selectivity due to pinholes and voids between zeolite crystals [94].

Carbon molecular sieve membranes are promising candidates for gas separations, due to their separation properties and high temperature resistance [95]. CMS membranes are suitable for a large temperature range, as reported in a study by Sznejer *et al.* [96], where they were tested in the temperature range of 25-400 °C. These membranes are, however, stable above 200 °C only for reducing atmospheres. CMS can be prepared in different configurations as flat sheet, membrane supported on tube, capillary, and hollow fibre. Compared to polymer membranes, CMS present higher permeabilities and selectivities, as well as higher stability in the presence of organic vapours [95, 97]. However, CMS membranes are very brittle and require special handling.

Palladium-based membranes are very popular for hydrogen separation due to their high selectivity towards hydrogen. The transport mechanism is based on the sorption of hydrogen on the palladium surface, diffusion of the atomic hydrogen through the metal, and recombination at the other side of the membrane. The main disadvantages of Pd-based membranes are the high Pd price and poisoning by sulphur and chlorine containing species, carbon monoxide, water vapour and strongly adsorbing hydrocarbons [97]. These membranes are usually used in the temperature range of 200-500 °C, but ultrathin Pd membranes can operate at lower temperatures such as 150 °C [98]. However, these membranes suffer from mechanical instabilities, such as easy peeling from the support material and defect formation due to hydrogen embrittlement [98].

1.4.3. Membrane reactors

Methanol steam reforming membrane reactors have been vastly studied in the literature [99-105]. Besides the clear advantage of reducing the number of process

units, the presence of a membrane enhances the reactor performance as well. In MSR, the desired purified gas is hydrogen, the PEMFC fuel, thus a hydrogen selective membrane is used. While hydrogen is removed from the reaction side, the MSR reaction equilibrium shifts towards the products, increasing the conversion of methanol.

The most common membranes used for this application are the palladium-based ones [106-108]. As described above, Pd membranes are highly selective and allow the production of a pure hydrogen stream. However, these membranes present low permeabilities and are favoured by high temperatures. Carbon molecular sieve membranes are a suitable alternative to Pd-based membranes for temperatures below ca. 200 °C [105, 109]. They are less expensive, present higher permeabilities and their selectivity is favoured by low temperatures. Therefore, a good compromise between permeability and selectivity can be obtained at low reaction temperatures (below 200 °C).

1.5. Scope of the thesis

The application of PEMFC in mobile or portable devices has been increasing the past few years. A combination of methanol reformers with PEMFC has already shown promising results but require further research. Accordingly, this thesis aims to study and optimize the production of PEMFC grade hydrogen by methanol steam reforming.

The present work is divided in four parts. In **Part I** the importance of fuel cells is presented, along with an overview of the possible methods for hydrogen production. The use of methanol as hydrogen carrier is addressed as well as the current applications of this technology for fuelling PEMFC. **Part II** (**Chapter 2** and **Chapter 3**) comprises two modelling studies concerning the configuration of membrane reactors. The purpose of these studies is to determine in which conditions a membrane reactor can produce a PEMFC grade hydrogen stream. In **Chapter 2**, a comparative study between carbon molecular sieve and palladium membrane reactors is presented. In

Chapter 3, the enhancement of the CMS-MR performance by the presence of a preferential oxidation catalyst in the permeate side is addressed. **Part III (Chapter 4** and **Chapter 5**) consists of two experimental studies over a $CuO/ZnO/Al_2O_3$ catalyst. The experimental units used in these works are described in **Appendix A**. **Chapter 4** presents a kinetic study where several kinetic expressions are used to fit the experimental data. The same catalyst is used in the carbon membrane reactor described in **Chapter 5**. The permeabilities of carbon membranes for single gas and gas mixtures are also investigated in this chapter. Permeance measurements are performed at 150 and 200 °C, with a membrane module of CMS hollow fibres (Carbon Membranes Ltd.). The reaction of methanol steam reforming is studied in a carbon membrane reactor, comprising the previously studied CMS membranes and $CuO/ZnO/Al_2O_3$ catalyst. Finally, the general conclusions are presented in **Part IV** along with future work suggestions.

List of Abbreviations and symbols

Abbreviations	Definition
DMFC	direct methanol fuel cell
HT-PEMFC	high temperature polymer electrolyte membrane fuel cells
LOH	liquid organic hydrides
MSR	methanol steam reforming
NOx	nitrogen oxides
PBI	acid-doped polybenzimidazole
PEMFC	polymer electrolyte membrane fuel cells
SOFC	solid oxide fuel cells
WGS	water gas shift

References

[1] Y. Wang, K.S. Chen, J. Mishler, S.C. Cho, X.C. Adroher, A review of polymer electrolyte membrane fuel cells: Technology, applications, and needs on fundamental research, Appl. Energy, 88 (2011) 981-1007.

[2] X. Zhang, S.H. Chan, G. Li, H.K. Ho, J. Li, Z. Feng, A review of integration strategies for solid oxide fuel cells, J. Power Sources, 195 (2009) 685-702.

[3] B. Smitha, S. Sridhar, A.A. Khan, Solid polymer electrolyte membranes for fuel cell applications--a review, J. Membr. Sci., 259 (2005) 10-26.

[4] S.J. Peighambardoust, S. Rowshanzamir, M. Amjadi, Review of the proton exchange membranes for fuel cell applications, Int. J. Hydrogen Energy, 35 (2010) 9349-9384.

[5] R.P. O'Hayre, S.W. Cha, W. Colella, F.B. Prinz, Fuel Cell Fundamentals, Jonh Wiley & Sons, Inc., New York, 2006.

[6] Comparison of Fuel Cell Technologies, Energy Efficiency and Renewable Energy - Fuel Cell Technologies Program, U.S. Department of Energy.

[7] J.M. Andújar, F. Segura, Fuel cells: History and updating. A walk along two centuries, Renewable Sustainable Energy Rev., 13 (2009) 2309-2322.

[8] F. Barbir, PEM Fuel Cells: Theory and Practice, Elsevier Academic Press, 2005.

[9] J. Larmaine, A. Dicks, Fuel cell systems explained, 2nd ed., West Sussex, 2003.

[10] A. Rodrigues, J.C. Amphlett, R.F. Mann, B.A. Peppley, P.R. Roberge, Carbon monoxide poisoning of proton-exchange membrane fuel cells, Energy Conversion Engineering Conference, 1997. IECEC-97., Proceedings of the 32nd Intersociety, 1997, pp. 768-773 vol.762.

[11] International Organization for Standardization, ISO/TS 14687-2, Hydrogen fuel - product specification - Part 2: proton exchange membrane (PEM) fuel cell applications for road vehicles, 2008.

[12] J. Zhang, Z. Xie, J. Zhang, Y. Tang, C. Song, T. Navessin, Z. Shi, D. Song, H. Wang, D.P. Wilkinson, Z.-S. Liu, S. Holdcroft, High temperature PEM fuel cells, J. Power Sources, 160 (2006) 872-891.

[13] S.K. Das, A. Reis, K.J. Berry, Experimental evaluation of CO poisoning on the performance of a high temperature proton exchange membrane fuel cell, J. Power Sources, 193 (2009) 691-698.

[14] S. Bose, T. Kuila, T.X.H. Nguyen, N.H. Kim, K.-t. Lau, J.H. Lee, Polymer membranes for high temperature proton exchange membrane fuel cell: Recent advances and challenges, Prog. Polym. Sci., In Press, Corrected Proof.

[15] V.P. McConnell, High-temperature PEM fuel cells: Hotter, simpler, cheaper, Fuel Cells Bull., 2009 (2009) 12-16.

[16] http://automobiles.honda.com/fcx-clarity/.

[17] www.emercedesbenz.com.

[18] http://www.fuelcelltoday.com/reference/image-bank/Portable/Toshiba-DMFC-laptop.

[19] http://www.cellphonebeat.com/entry/toshiba-bringing-fuel-cell-powered-cell-phone-next-year/.

[20] B.C.R. Ewan, R.W.K. Allen, A figure of merit assessment of the routes to hydrogen, Int. J. Hydrogen Energy, 30 (2005) 809-819.

[21] M.F. Hordeski, Hydrogen & Fuel Cells: Advances in Transportation and Power, Fairmont Press, 2008.

[22] M.F. Hordeski, Alternative Fuels - The Future of Hydrogen, 2nd ed., Fairmont Press Inc. , 2008.

[23] G.A. Olah, A. Goeppert, G.K.S. Prakash, Beyond Oil and Gas: The Methanol Economy, 2nd ed., WILEY-VCH Verlag GmbH & Co. KGaA, Weinheim, 2006.

[24] Y. Chen, Y. Wang, H. Xu, G. Xiong, Hydrogen production capacity of membrane reformer for methane steam reforming near practical working conditions, J. Membr. Sci., 322 (2008) 453-459.

[25] J.G. Speight, Handbook of Coal Analysis, John Wiley & Sons, 2005.

[26] M.F. Irfan, M.R. Usman, K. Kusakabe, Coal gasification in CO2 atmosphere and its kinetics since 1948: A brief review, Energy, 36 (2010) 12-40.

[27] G. De Micco, G.G. Fouga, A.E. Bohé, Coal gasification studies applied to H2 production, Int. J. Hydrogen Energy, 35 (2010) 6012-6018.

[28] J.D. Holladay, J. Hu, D.L. King, Y. Wang, An overview of hydrogen production technologies, Catal. Today, 139 (2009) 244-260.

[29] The Hydrogen Economy. Opportunities, Costs, Barriers, and R&D Needs, National Academies Press, Washington, 2004.

[30] A. Steinfeld, Solar thermochemical production of hydrogen--a review, Solar Energy, 78 (2005) 603-615.

[31] B. Coelho, A.C. Oliveira, A. Mendes, Concentrated solar power for renewable electricity and hydrogen production from water-a review, Energy Environ. Sci., 3 (2010) 1398-1405.

[32] A.G. Konstandopoulos, C. Agrofiotis, Hydrosol : Advanced monolithic reactors for hydrogen generation from solar water splitting, Revue des Energies Renouvelables, 9 (2006) 121 – 126.

[33] S. Satyapal, J. Petrovic, C. Read, G. Thomas, G. Ordaz, The U.S. Department of Energy's National Hydrogen Storage Project: Progress towards meeting hydrogen-powered vehicle requirements, Catal. Today, 120 (2007) 246-256.

[34] D.K. Ross, Hydrogen storage: The major technological barrier to the development of hydrogen fuel cell cars, Vacuum, 80 (2006) 1084-1089.

[35] U. Bossel, B. Eliasson, G. Taylor, The Future of the Hydrogen Economy: Bright or Bleak?, European Fuel Cell Forum, 2005.

[36] I. Cumalioglu, A. Ertas, Y. Ma, T. Maxwell, State of the Art: Hydrogen storage, J. Fuel Cell Sci. Technol., 5 (2008).

[37] T. Riis, E.F. Hagen, P.J.S. Vie, Ø. Ulleberg, Hydrogen production and storage R&D: priorities and gaps, Int. Energy Agency, Hydrogen Implementing Agreement, (2006).

[38] R.B. Biniwale, S. Rayalu, S. Devotta, M. Ichikawa, Chemical hydrides: A solution to high capacity hydrogen storage and supply, Int. J. Hydrogen Energy, 33 (2008) 360-365.

[39] N. Kariya, A. Fukuoka, T. Utagawa, M. Sakuramoto, Y. Goto, M. Ichikawa, Efficient hydrogen production using cyclohexane and decalin by pulse-spray mode reactor with Pt catalysts, Appl. Catal. A, 247 (2003) 247-259.

[40] I. Kobayashi, K. Yamamoto, H. Kameyama, A proposal of a spray pulse operation for liquid film dehydrogenation: 2-Propanol dehydrogenation on a plate catalyst, Chemical Engineering Science, 54 (1999) 1319-1323.

[41] S. Hodoshima, H. Nagata, Y. Saito, Efficient hydrogen supply from tetralin with superheated liquid-film-type catalysis for operating fuel cells, Appl. Catal. A, 292 (2005) 90-96.

[42] B. Sakintuna, F. Lamari-Darkrim, M. Hirscher, Metal hydride materials for solid hydrogen storage: A review, Int. J. Hydrogen Energy, 32 (2007) 1121-1140.

[43] A. Qi, B. Peppley, K. Karan, Integrated fuel processors for fuel cell application: A review, Fuel Process. Technol., 88 (2007) 3-22.

[44] M. Ni, D.Y.C. Leung, M.K.H. Leung, A review on reforming bio-ethanol for hydrogen production, Int. J. Hydrogen Energy, 32 (2007) 3238-3247.

[45] H.F. Abbas, W.M.A. Wan Daud, Hydrogen production by methane decomposition: A review, Int. J. Hydrogen Energy, 35 (2010) 1160-1190.

[46] D.R. Palo, R.A. Dagle, J.D. Holladay, Methanol Steam Reforming for Hydrogen Production, Chem. Rev., 107 (2007) 3992-4021.

[47] C. Ledesma, U.S. Ozkan, J. Llorca, Hydrogen production by steam reforming of dimethyl ether over Pd-based catalytic monoliths, Appl. Catal. B, 101 (2011) 690-697.

[48] S. Tosti, A. Basile, F. Borgognoni, V. Capaldo, S. Cordiner, S.D. Cave, F. Gallucci, C. Rizzello, A. Santucci, E. Traversa, Low temperature ethanol steam reforming in a Pd-Ag membrane reactor Part 1: Ru-based catalyst, J. Membr. Sci., 308 (2008) 250–257.

[49] S. Kudo, T. Maki, K. Miura, K. Mae, High porous carbon with Cu/ZnO nanoparticles made by the pyrolysis of carbon material as a catalyst for steam reforming of methanol and dimethyl ether, Carbon, 48 (2010) 1186-1195.

[50] X. Wang, X. Pan, R. Lin, S. Kou, W. Zou, J.-X. Ma, Steam reforming of dimethyl ether over Cu-Ni/[gamma]-Al2O3 bi-functional catalyst prepared by deposition-precipitation method, Int. J. Hydrogen Energy, 35 (2010) 4060-4068.

[51] J. Agrell, H. Birgersson, M. Boutonnet, I. Melián-Cabrera, R.M. Navarro, J.L.G. Fierro, Production of hydrogen from methanol over Cu/ZnO catalysts promoted by ZrO2 and Al2O3, J. Catal., 219 (2003) 389-403.

[52] G. Águila, J. Jiménez, S. Guerrero, F. Gracia, B. Chornik, S. Quinteros, P. Araya, A novel method for preparing high surface area copper zirconia catalysts: Influence of the preparation variables, Appl. Catal. A, 360 (2009) 98-105.

[53] J.W. Ha, A. Kundu, J.H. Jang, Poly-dimethylsiloxane (PDMS) based micro-reactors for steam reforming of methanol, Fuel Process. Technol., 91 (2010) 1725-1730.

[54] T. Fukunaga, N. Ryumon, N. Ichikuni, S. Shimazu, Characterization of CuMn-spinel catalyst for methanol steam reforming, Catal. Commun., 10 (2009) 1800-1803.

[55] L. Gao, G. Sun, S. Kawi, A study on methanol steam reforming to CO2 and H2 over the La2CuO4 nanofiber catalyst, J. Solid State Chem., 181 (2008) 7–13.

[56] G. Xia, J.D. Holladay, R.A. Dagle, E.O. Jones, Y. Wang, Development of highly active Pd-ZnO/Al2O3 catalysts for microscale fuel processor applications, Chem. Eng. Technol., 28 (2005) 515-519.

[57] J.-P. Lange, Methanol synthesis: a short review of technology improvements, Catal. Today, 64 (2001) 3-8.

[58] G. Wang, Y. Zuo, M. Han, J. Wang, Cu-Zr-Zn catalysts for methanol synthesis in a fluidized bed reactor, Appl. Catal. A, 394 (2011) 281-286.

[59] Assessment of Costs and Benefits of Flexible and Alternative Fuel Use in the US Transportation Sector, Technical Report No. 7: Environmental, Health, and Safety Concerns, United States Department of Energy, Washington, DC, 1991.

[60] Methanol in fuel cell vehicles Human toxicity and risk evaluation (Revised), Statoil, Norway,, 2001.

[61] Methanol Fuels and Fire Safety, Fact Sheet OMS-8, EPA 400-F-92-010, U.S. Environmental Protection Agency, Office of Mobile Sources, Washington, DC, 1994.

[62] Methanol Health And Safety Guide No. 105, IPCS - International Programme on Chemical Safety, 1997.

[63] G. Marbán, A. López, I. López, T. Valdés-Solís, A highly active, selective and stable copper/cobalt-structured nanocatalyst for methanol decomposition, Appl. Catal. B, 99 (2010) 257-264.

[64] S. Goodarznia, K.J. Smith, Properties of alkali-promoted Cu-MgO catalysts and their activity for methanol decomposition and C2-oxygenate formation, J. Mol. Catal. A: Chem., 320 (2010) 1-13.

[65] W.-S. Chen, F.-W. Chang, L.S. Roselin, T.-C. Ou, S.-C. Lai, Partial oxidation of methanol over copper catalysts supported on rice husk ash, J. Mol. Catal. A: Chem., 318 (2009) 36-43.

[66] L. Mo, A.H. Wan, X. Zheng, C.-T. Yeh, Selective production of hydrogen from partial oxidation of methanol over supported silver catalysts prepared by method of redox coprecipitation, Catal. Today, 148 (2009) 124-129.

[67] Q. Zhang, R.J. Farrauto, A PdZn catalyst supported on stabilized ceria for stoichiometric methanol steam reforming and hydrogen production, Appl. Catal. A, 395 (2011) 64-70.

[68] A. Basile, A. Parmaliana, S. Tosti, A. Iulianelli, F. Gallucci, C. Espro, J. Spooren, Hydrogen production by methanol steam reforming carried out in membrane reactor on Cu/Zn/Mg-based catalyst, Catal. Today, 137 (2008) 17–22.

[69] S.H. Israni, M.P. Harold, Methanol steam reforming in single-fiber packed bed Pd-Ag membrane reactor: Experiments and modeling, J. Membr. Sci., 369 (2011) 375-387.

[70] B. Lindström, J. Agrell, L.J. Pettersson, Combined methanol reforming for hydrogen generation over monolithic catalysts, Chem. Eng. J., 93 (2003) 91-101.

[71] C.-C. Chang, C.-T. Chang, S.-J. Chiang, B.-J. Liaw, Y.-Z. Chen, Oxidative steam reforming of methanol over CuO/ZnO/CeO2/ZrO2/Al2O3 catalysts, Int. J. Hydrogen Energy, 35 (2010) 7675-7683.

[72] S. Sá, H. Silva, L. Brandão, J.M. Sousa, A. Mendes, Catalysts for methanol steam reforming--A review, Appl. Catal. B, 99 (2010) 43-57.

[73] T. Tanabe, S. Kameoka, A.P. Tsai, Microstructure of leached Al-Cu-Fe quasicrystal with high catalytic performance for steam reforming of methanol, Appl. Catal. A, 384 (2010) 241-251.

[74] Y. Men, G. Kolb, R. Zapf, M. O'Connell, A. Ziogas, Methanol steam reforming over bimetallic Pd-In/Al2O3 catalysts in a microstructured reactor, Appl. Catal. A, 380 (2010) 15-20.

[75] J. Papavasiliou, G. Avgouropoulos, T. Ioannides, Steady-state isotopic transient kinetic analysis of steam reforming of methanol over Cu-based catalysts, Appl. Catal. B, 88 (2009) 490–496.

[76] G. Huang, B.-J. Liaw, C.-J. Jhang, Y.-Z. Chen, Steam reforming of methanol over CuO/ZnO/CeO2/ZrO2/Al2O3 catalysts, Appl. Catal. A, 358 (2009) 7–12.

[77] T. Conant, A.M. Karim, V. Lebarbier, Y. Wang, F. Girgsdies, R. Schlögl, A. Datye, Stability of bimetallic Pd-Zn catalysts for the steam reforming of methanol, J. Catal., 257 (2008) 64-70.

[78] S. Patel, K.K. Pant, Influence of preparation method on performance of Cu(Zn)(Zr)-alumina catalysts for the hydrogen production via steam reforming of methanol, J. Porous Mater., 13 (2006) 373-378.

[79] B. Lindström, L.J. Pettersson, P. Govind Menon, Activity and characterization of Cu/Zn, Cu/Cr and Cu/Zr on -alumina for methanol reforming for fuel cell vehicles, Appl. Catal. A, 234 (2002) 111-125.

[80] C.-Z. Yao, L.-C. Wang, Y.-M. Liu, G.-S. Wu, Y. Cao, W.-L. Dai, H.-Y. He, K.-N. Fan, Effect of preparation method on the hydrogen production from methanol steam reforming over binary Cu/ZrO2 catalysts, Appl. Catal. A, 297 (2006) 151-158.

[81] http://www.n24.de/news/newsitem_4303361.html.

[82] http://tpe09.free.fr/images2/v41.jpg.

[83] http://world.casio.com/info/2002/fuelcell.html.

[84] http://www.ultracellpower.com/.

[85] http://www.e1na.com/.

[86] http://www.powercell.se/.

[87] H.P. Dhar, L.G. Christner, A.K. Kush, Nature of CO Adsorption during H2 Oxidation in Relation to Modeling for CO Poisoning of a Fuel Cell Anode, J. Electrochem. Soc., 134 (1987) 3021-3026.

[88] M. Takht Ravanchi, T. Kaghazchi, A. Kargari, Application of membrane separation processes in petrochemical industry: a review, Desalination, 235 (2009) 199-244.

[89] N.N. Li, A.G. Fane, W.S.W. Ho, T. Matsuura, Advanced Membrane Technology and Applications, John Wiley & Sons, 2008.

[90] A.L. Kohl, R.B. Nielsen, Gas Purification, 5th ed., Elsevier, 1997.

[91] C.A. Scholes, K.H. Smith, S.E. Kentish, G.W. Stevens, CO2 capture from pre-combustion processes--Strategies for membrane gas separation, Int. J. Greenhouse Gas Control, 4 (2010) 739-755.

[92] K. Briceño, R. Garcia-Valls, D. Montané, State of the art of carbon molecular sieves supported on tubular ceramics for gas separation applications, Asia-Pac. J. Chem. Eng., 5 (2010) 169-178.

[93] P. Bernardo, E. Drioli, G. Golemme, Membrane Gas Separation: A Review/State of the Art, Ind. Eng. Chem. Res., 48 (2009) 4638-4663.

[94] R. Bredesen, K. Jordal, O. Bolland, High-temperature membranes in power generation with CO2 capture, Chemical Engineering and Processing, 43 (2004) 1129-1158.

[95] M.-B. Hägg, J.A. Lie, A. LindbrÅThen, Carbon Molecular Sieve Membranes, Annals of the New York Academy of Sciences, 984 (2003) 329-345.

[96] G.A. Sznejer, I. Efremenko, M. Sheintuch, Carbon Membranes for High Temperature Gas Separations: Experiment and Theory, AIChE J., 50 (2004).

[97] J.E. Koresh, A. Soffer, The Carbon Molecular Sieve Membranes. General Properties and the Permeability of CH₄/H₂ Mixture, Taylor & Francis, 1987, pp. 973 - 982.

[98] D.A. Pacheco Tanaka, M.A. Llosa Tanco, T. Nagase, J. Okazaki, Y. Wakui, F. Mizukami, T.M. Suzuki, Fabrication of Hydrogen-Permeable Composite Membranes Packed with Palladium Nanoparticles, Advanced Materials, 18 (2006) 630-632.

[99] A. Basile, F. Gallucci, L. Paturzo, A dense Pd/Ag membrane reactor for methanol steam reforming: Experimental study, Catal. Today, 104 (2005) 244-250.

[100] A. Basile, F. Gallucci, L. Paturzo, Hydrogen production from methanol by oxidative steam reforming carried out in a membrane reactor, Catal. Today, 104 (2005) 251–259.

[101] A. Basile, G.F. Tereschenko, N.V. Orekhova, M.M. Ermilova, F. Gallucci, A. Iulianelli, An experimental investigation on methanol steam reforming with oxygen addition in a flat Pd–Ag membrane reactor, Int. J. Hydrogen Energy, 31 (2006) 1615 – 1622.

[102] A.S. Damle, Hydrogen production by reforming of liquid hydrocarbons in a membrane reactor for portable power generation—Model simulations, J. Power Sources, 180 (2008) 516-529.

[103] M.D. Falco, Pd-based membrane steam reformers: A simulation study of reactor performance, Int. J. Hydrogen Energy, 33 (2008) 3036 – 3040.

[104] F. Gallucci, A. Basile, Co-current and counter-current modes for methanol steam reforming membrane reactor, Int. J. Hydrogen Energy, 31 (2006) 2243 - 2249.

[105] X. Zhang, H. Hu, Y. Zhu, S. Zhu, Methanol Steam Reforming to Hydrogen in a Carbon Membrane Reactor System, Ind. Eng. Chem. Res., 45 (2006) 7997-8001.

[106] M.-H. Rei, G.-T. Yeh, Y.-H. Tsai, Y.-L. Kao, L.-D. Shiau, Catalysis-spillover-membrane. III: The effect of hydrogen spillover on the palladium membrane reactor in the steam reforming reactions, J. Membr. Sci., 369 (2010) 299-307.

[107] A. Basile, P. Pinacci, A. Iulianelli, M. Broglia, F. Drago, S. Liguori, T. Longo, V. Calabrò, Ethanol steam reforming reaction in a porous stainless steel supported palladium membrane reactor, Int. J. Hydrogen Energy, 36 (2010) 2029-2037.

[108] A. Iulianelli, T. Longo, A. Basile, Methanol steam reforming in a dense Pd–Ag membrane reactor: The pressure and WHSV effects on CO-free H2 production, J. Membr. Sci., 323 (2008) 235–240.

[109] S. Sá, H. Silva, J.M. Sousa, A. Mendes, Hydrogen production by methanol steam reforming in a membrane reactor: Palladium vs carbon molecular sieve membranes, J. Membr. Sci., 339 (2009) 160-170.

Part II

Modelling

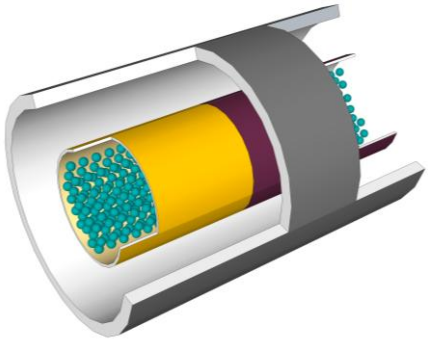

Chapter 2. Hydrogen production by methanol steam reforming in a membrane reactor: Pd vs. CMS membranes[1]

Abstract

In this study, the production of hydrogen by methanol steam reforming in a membrane reactor (MR) was simulated using a one-dimensional mathematical model. The model assumes axially dispersed plug-flow with pressure drop for the retentate side, and plug flow behaviour with no axial dispersion and no pressure drop for the permeate side. Two types of membranes were simulated, namely a carbon molecular sieve (CMS) membrane and a palladium (Pd) membrane. The simulation results showed that the CMS membrane reactor presents higher hydrogen recoveries, while the Pd membrane reactor has the advantage of producing a pure hydrogen stream. It was also studied a membrane reactor with two membrane sections, one made of CMS and the other made of palladium. This new configuration revealed some advantages compared to the reactor equipped with either membrane type alone. For instance, the highest hydrogen recovery was obtained with the CMS/Pd-MR.

[1] S. Sá, H. Silva, J.M. Sousa, A. Mendes, Hydrogen production by methanol steam reforming in a membrane reactor: Palladium vs carbon molecular sieve membranes, J. Membr. Sci., 339 (2009) 160-170.

2.1. Introduction

Nowadays, worldwide environmental concerns are triggering the search for clean energy sources. Lowering the emissions of gases that contributes to the greenhouse effect and global warming is imperative, and fuel cells are providing an attractive solution to this problem. Presenting only heat and water as emissions, hydrogen fuel cells are an important source of clean electrical power [1-4]. To generate power, polymer electrolyte membrane fuel cells (PEMFC) require hydrogen as fuel. However, direct use of hydrogen in the PEMFC presents distribution and storage problems caused by its low energy density per normal volume. Hydrogen production *in situ* from hydrocarbon fuels comes as a possible solution to this problem [5-7]. Methanol presents several advantages compared to other fuels, namely: is liquid at atmospheric conditions, has high hydrogen to carbon ratio, and its reforming temperature is relatively low (200-300 °C) [8-10]. In what concerns methanol supply, it can be produced from a variety of sources, including natural gas, coal and biomass. Alternatively to steam reforming, methanol can be fed directly to a fuel cell (DMFC – direct methanol fuel cell) in order to generate power. However, compared to the PEMFC, these devices present lower efficiency, lower power density and higher catalyst usage, which results in higher costs [11]. Taken all into concern, methanol steam reforming is seen as a reliable source of hydrogen for fuel cell applications.

According to the literature [12, 13], three chemical reactions can be considered in the methanol steam reforming process: the methanol steam reforming itself (MSR, eq. (2.1)), and the side reactions methanol decomposition (MD, eq. (1.4)) and water gas shift (WGS, eq. (1.7)):

$$CH_3OH + H_2O \rightleftharpoons CO_2 + 3H_2 \qquad \Delta H_{298} = 49.7\,kJ\cdot mol^{-1} \qquad (2.1)$$

$$CH_3OH \rightleftharpoons CO + 2H_2 \qquad \Delta H_{298} = 92.0\,kJ\cdot mol^{-1} \qquad (2.2)$$

$$CO + H_2O \rightleftharpoons CO_2 + H_2 \qquad \Delta H_{298} = -41.2\,kJ\cdot mol^{-1} \qquad (2.3)$$

Besides the non-reacted methanol and water, the reaction products are hydrogen (desired product), carbon dioxide and carbon monoxide. To feed a fuel cell, the hydrogen stream needs purification, mainly because carbon monoxide poisons the anodic catalyst of the fuel cell and its concentration must be lower than 10 ppm [14]**.** This could be done in several ways, namely using a permselective membrane. Combining in the same device both operations, reaction and separation, membrane reactors present several advantages towards conventional reactors. Besides reducing the number of process units, a MR could also achieve conversions higher than the ones obtained in a conventional reactor at the same operating conditions. Gallucci *et al.* [15], for example, showed how methanol conversion, hydrogen production and hydrogen selectivity can be enhanced by using a membrane reactor over the values obtained in a traditional reactor. Matzakos *et al.* [16] also used a membrane reactor for hydrogen production, and presented an integrated process with a steam reformer and a fuel cell. In their work, the authors describe an overall process-flow diagram, showing that an integrated system is viable.

The choice of the membrane kind to use in a membrane reactor must consider both cost and performance. Several studies have been published concerning the use of palladium based membrane reactors [9, 17-20]. Palladium membranes are highly selective to hydrogen and allow the production of a pure H_2 stream, at least theoretically. However, these membranes suffer from hydrogen-embrittlement cracking during thermal cycling and readily evidence surface contamination by sulphur-containing species [21]. Moreover, they are expensive, so a cheaper solution is strongly needed. Although these membranes are only permeable to hydrogen, they have limited applications due to their low permeability compared to porous inorganic membranes [22, 23]. As a possible alternative, CMS membranes are less expensive and present higher permeabilities than Pd membranes. As a drawback, they are brittle and present lower selectivities to hydrogen.

The use of carbon molecular sieve membranes in methanol steam reforming reactors has not been extensively studied. Zhang *et al.* [10], for example, presented

an experimental study comparing a traditional reactor with a CMS membrane reactor for this reaction. They concluded that higher methanol conversion and lower carbon monoxide yield were achieved, enhancing the potential of these membranes. Harale *et al.* [24] studied a CMS membrane reactor for another application: the water gas shift reaction. The membranes presented very high hydrogen permeation fluxes, reinforcing the idea that higher flow rates and lower membrane areas can be used with such membrane reactors.

These promising results justify the need of a detailed study of the potential advantages of CMS membranes over the palladium membranes. In this thought line, the present work aims to analyze and compare the advantages and disadvantages of both Pd and CMS membrane reactors to conduct the methanol steam reforming. Its main objective is to analyze in which conditions each of the membranes perform better than the other and how can both membranes be integrated simultaneously in the same reactor in order to get a synergy. To perform such study, it was developed a one-dimensional comprehensive mathematical model of a packed-bed membrane reactor. A set of simulation results are then provided which illustrate some key points about the use of this membrane reactor, namely the methanol conversion, carbon monoxide concentration in the hydrogen rich stream and hydrogen recovery. The goal is to maximize the methanol conversion and the hydrogen recovery, keeping the CO concentration at the permeate side below 10 ppm.

2.2. Development of the Membrane Reactor Model

Figure 2.1 shows the scheme of the simulated membrane reactor. It consists of a tubular membrane with surface area A^M, housing a packed-bed of catalyst in the inner side and a permeate chamber on the outer side. A gas phase stream of methanol and water is fed to the reaction side, producing hydrogen, carbon dioxide and carbon monoxide. At the permeate side, water vapour is used as sweep gas. Two types of

membranes are considered in this work: a palladium membrane and a carbon molecular sieve membrane.

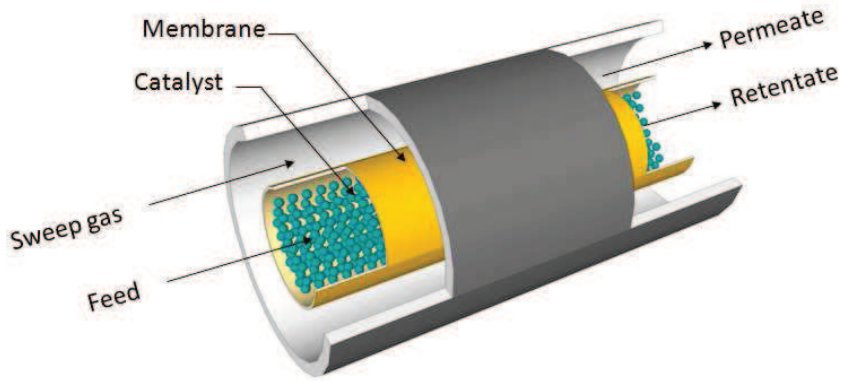

Figure 2.1 – Scheme of the simulated membrane reactor.

The mathematical model proposed comprises the steady-state mass balance equations for the reaction and permeate sides, as well as the respective boundary conditions. This model considers isothermal conditions and ideal gas behaviour. The retentate is assumed to follow an axially dispersed plug flow pattern, with pressure drop described by the *Ergun* equation [25] and filled with a methanol steam reforming catalyst with an uniform cross-sectional void fraction. The permeate is assumed to be plug flow with no axial dispersion, with no pressure drop and flowing in co-current.

2.2.1. Retentate (Reaction) Side

Partial Mass Balance

$$-\frac{d}{dz}\left(u^R p_i^R\right)+D_{ax}\frac{d}{dz}\left(P^R\frac{d}{dz}\left(\frac{p_i^R}{P^R}\right)\right)-\frac{2}{A^R}r^M\Re TN_i+\frac{m_{cat}}{V^R}\Re TR_i=0 \tag{2.4}$$

Total Mass Balance

$$-\frac{d}{dz}\left(u^R P^R\right)-\frac{2}{A^R}r^M\Re T\sum_i N_i+\frac{m_{cat}}{V^R}\Re T\ {}_{cat}R_i=0 \tag{2.5}$$

Pressure drop

$$-\frac{dP^R}{dz} = 150\frac{u^R}{d_p^2}(1- \ )^2 + \frac{7}{4}\frac{_{gas}\left(u^R\right)^2}{d_p}\frac{1-}{} \tag{2.6}$$

Boundary Conditions

The partial mass balance is a second order differential equation, thus, two boundary conditions are needed [26]. When the pressure drop cannot be considered negligible, it must be imposed one boundary condition in z = 0 and other in z = 1, as follows:

$$z=0: \quad D_{ax}\frac{d}{dz}\left(\frac{p_i^R}{P^R}\right) = u^R\frac{p_i^R - p_i^{R,in}}{P^R} \text{ and } u^R = u^{R,in} \tag{2.7}$$

$$z=1: \quad \frac{d}{dz}\left(\frac{p_i^R}{P^R}\right) = 0 \text{ and } P^R = P^{R,out} \tag{2.8}$$

where the superscript *R* stands for retentate side, *i* refers to the i^{th} component, *z* is axial coordinate, *u* is the interstitial velocity, *p* is the partial pressure, *P* is the total pressure, D_{ax} is the effective axial dispersion coefficient, r^M is the internal radius of the membrane, A^R is the cross sectional area of the retentate chamber, V^R is the volume of the retentate chamber, is the void fraction of the catalyst bed, $\Re$ is the gas constant, *T* is the absolute temperature, *N* is the flux through the membrane, and m_{cat} is the mass of catalyst, d_P is the catalyst particle diameter, is the gas viscosity and $_{gas}$ is the gas density. *R* is the rate of consumption or formation of the individual species, which is given by:

$$R_i = \sum_j \ _{ij} r_j \tag{2.9}$$

where r_j is the reaction rate of reaction *j* (described below) and $_{ij}$ is the stoichiometric coefficient for species *i* in the reaction *j*, taken negative for reactants, positive for reaction products, and null for the components that do not take part in the reaction.

Kinetic Model

The reaction rate expressions used in this model are the ones developed by Peppley *et al.* [13]. It is assumed that the reaction occurs only at the catalyst surface, and that there is no mass transfer resistance between the bulk gas and the catalyst surface.

$$r_{MSR}=\frac{k_{MSR}K_{CH_3O^{(1)}}\left(\frac{p_{CH_3OH}}{p_{H_2}^{1/2}}\right)\left(1-\frac{p_{H_2}^3 p_{CO_2}}{K_{MSR}^e p_{CH_3OH}p_{H_2O}}\right)C_{S1}^T C_{S1a}^T S_A}{\left(1+K_{CH_3O^{(1)}}\frac{p_{CH_3OH}}{p_{H_2}^{1/2}}+K_{HCOO^{(1)}}p_{CO_2}p_{H_2}^{1/2}+K_{OH^{(1)}}\frac{p_{H_2O}}{p_{H_2}^{1/2}}\right)\left(1+K_{H^{(1a)}}^{1/2}p_{H_2}^{1/2}\right)} \tag{2.10}$$

$$r_{WGS}=\frac{k_{WGS}K_{OH^{(1)}}\left(\frac{p_{CO}p_{H_2O}}{p_{H_2}^{1/2}}\right)\left(1-\frac{p_{H_2}p_{CO_2}}{K_{WGS}^e p_{CO}p_{H_2O}}\right)C_{S1}^{T\ 2}S_A}{\left(1+K_{CH_3O^{(1)}}\frac{p_{CH_3OH}}{p_{H_2}^{1/2}}+K_{HCOO^{(1)}}p_{CO_2}p_{H_2}^{1/2}+K_{OH^{(1)}}\frac{p_{H_2O}}{p_{H_2}^{1/2}}\right)^2} \tag{2.11}$$

$$r_{MD}=\frac{k_{MD}K_{CH_3O^{(2)}}\left(\frac{p_{CH_3OH}}{p_{H_2}^{1/2}}\right)\left(1-\frac{p_{H_2}^2 p_{CO}}{K_{MD}^e p_{CH_3OH}}\right)C_{S2}^T C_{S2a}^T S_A}{\left(1+K_{CH_3O^{(2)}}\frac{p_{CH_3OH}}{p_{H_2}^{1/2}}+K_{OH^{(2)}}\frac{p_{H_2O}}{p_{H_2}^{1/2}}\right)\left(1+K_{H^{(2a)}}^{1/2}p_{H_2}^{1/2}\right)} \tag{2.12}$$

where k_j and K_j^e are the reaction rate and equilibrium constants for reaction *j*, respectively; K_i is the adsorption coefficient for surface species *i*, C_{S1}^T and C_{S2}^T are the total catalyst surface concentration of sites 1 and 2, respectively, C_{S1a}^T and C_{S2a}^T are the total catalyst surface concentration of sites 1*a* and 2*a*, respectively, and S_A is the surface area of the catalyst.

2.2.2. Permeate Side

Partial Mass Balance

$$\frac{d}{dz}\left(u^P p_i^P\right)-\frac{2}{A^P}r^M\Re TN_i=0 \tag{2.13}$$

Total Mass Balance

$$P^P \frac{du^P}{dz} - \frac{2}{A^P} r^M \Re T \sum_i N_i = 0 \tag{2.14}$$

Boundary Conditions

$$z = 0: \quad p_i^P = p_i^{P,in} \text{ and } u^P = u^{P,in} \tag{2.15}$$

where superscript P stands for permeate side and A^P is the cross sectional area of the permeate chamber

2.2.3. Membrane Permeation Equation

The mass transfer of each component through the membrane is assumed to be described by its local driving force and a global mass transfer coefficient, according to the following equation:

$$N_i(z) = L_i \left\{ \left(p_i^R(z) \right)^n - \left(p_i^P(z) \right)^n \right\} \tag{2.16}$$

where L is a permeance coefficient and n is 1/2 for the palladium membrane (Sieverts' law) and 1 for the CMS membrane. The film transport resistance at the interface gas/membrane is considered negligible and the permeability coefficients are assumed constant.

2.2.4. Dimensionless Equations

The model variables were made dimensionless with respect to the retentate feed ($u^{R,in}$), to hydrogen (L_{H2} and M_{H2}) and to the reactor length, $\boldsymbol{l_{reactor}}$. Changing for dimensionless variables and introducing suitable dimensionless parameters, equations (2.4)-(2.8) and (2.13)-(2.16) become as follows:

$$-\frac{d}{dx}\left(u^{R^*} p_i^{R^*}\right) + \frac{1}{Pe}\frac{d}{dx}\left(P^{R^*} \frac{d}{dx}\left(\frac{p_i^{R^*}}{P^{R^*}} \right) \right) - \Gamma T^* N_i^* + DaT^* R_i^* = 0 \tag{2.17}$$

$$-\frac{d}{dx}\left(u^{R^*} P^{R^*}\right) - \Gamma T^* \sum_i N_i^* + DaT^* \sum_i R_i^* = 0 \tag{2.18}$$

$$-\frac{dP^{R*}}{dx} = \quad u^{R*} + \quad \frac{\rho^{*}_{gas}}{T^{*}}\left|u^{R*}\right|u^{R*} \tag{2.19}$$

$$x=0: \quad \frac{1}{Pe}\frac{d}{dx}\left(\frac{p_i^{R*}}{P^{R*}}\right) = u^{R,in*}\frac{p_i^{R*}-p_i^{R,in*}}{P^{R*}} \text{ and } u^{R*} = u^{R,in*} \tag{2.20}$$

$$x=1: \quad \frac{d}{dx}\left(\frac{p_i^{R*}}{P^{R*}}\right)=0 \text{ and } P^{R*} = P^{R,out*} \tag{2.21}$$

$$\frac{d}{dx}\left(u^{P*}p_i^{P*}\right) - \Gamma \quad T^{*}N_i^{*} = 0 \tag{2.22}$$

$$P^{P*}\frac{du^{P*}}{dx} - \Gamma \quad T^{*}\sum_i N_i^{*} = 0 \tag{2.23}$$

$$x=0: \quad p_i^{P*} = p^{P,in*} \text{ and } u^{P*} = u^{P,in*} \tag{2.24}$$

$$N_i^{*}(x) = L_i^{*}\left[\left(p_i^{R*}(x)\right)^{n} - \left(p_i^{P*}(x)\right)^{n}\right] \tag{2.25}$$

where $= \frac{150(1-\quad)^2 u_{ref} l_{reactor}}{^2 d_p^2 P_{ref}}$, $= \frac{1.75(1-\quad)M_{ref}u_{ref}^2 l_{reactor}}{d_p \Re T_{ref}}$, $p_i^{*} = \frac{p_i}{P_{ref}}$, $P^{*} = \frac{P}{P_{ref}}$,

$u^{*} = \frac{u}{u_{ref}}$, $R_i^{*} = \frac{R_i}{k_{SR,ref}C_{S1}^{T}C_{S1a}^{T}S_A}$, $L_i^{*} = \frac{L_i}{L_{ref}}$, $x = \frac{z}{l_{reactor}}$, $Da = \frac{m_{cat}\Re T_{ref}k_{SR,ref}C_{S1}^{T}C_{S1a}^{T}S_A}{u_{ref}A^{R}P_{ref}}$,

$= \frac{A^R}{A^P}$, $\Gamma = \frac{A^M \Re T_{ref} P_{ref}^{n-1} L_{ref}}{u_{ref}A^R}$, $Pe = \frac{l_{reactor}u_{ref}}{D_{ax}}$, M_{ref} is the reference molar mass, L_{ref} is the reference permeance coefficient of the membrane, x is the dimensionless axial coordinate of the reactor, Pe is the Peclet number for mass transfer, Da is the Damköhler number, Γ is the dimensionless permeation contact time (ratio between permeate flow of reference component when fed pure for null permeate pressure and the total molar feed flow), $k_{MSR,ref}$ is the rate constant for the steam reforming reaction at the reference temperature, P_{ref} is the reference pressure (set to 100 kPa), T_{ref} is the reference temperature (set to 298 K), u_{ref} is the reference velocity, A^M is the permeation area of the membrane and $l_{reactor}$ is the reactor's length.

2.2.5. Numerical solution strategy

To simulate the steam reforming membrane reactor, it is necessary to solve equations (2.17)-(2.19) and (2.22)-(2.23) with the respective boundary conditions. In order to overcome numerical instability problems, it was used the same strategy adopted already [27] for solving the equations: a time derivative term was added to their right-hand side, transforming this problem into a pseudo-transient one. The resultant partial differential equations were spatially discretized using the finite volumes method [28]. The time advancement was accomplished by LSODA [29], a numerical package developed at the Lawrence Livermore National Laboratory. The solution was considered to be in steady state when the time derivative of each dependent variable and for each of the spatial coordinate was smaller than a pre-defined value.

2.3. Discussion

In order to compare the performance of the membrane reactors equipped with Pd and CMS membranes, a systematic study on the effect of the most important operating variables and parameters was made. Such comparison focused on the analysis of the methanol conversion, H_2/CO reaction selectivity, CO concentration at the permeate side and hydrogen recovery. Ideally, methanol conversion and hydrogen recovery should be as high as possible, while the CO concentration should be below 10 ppm. The developed mathematical model was validated using the experimental data by Basile *et al.* [30] and by Zhang *et al.* [10]. As it can be realized from Figure 2.2, the model agrees well with the experimental data.

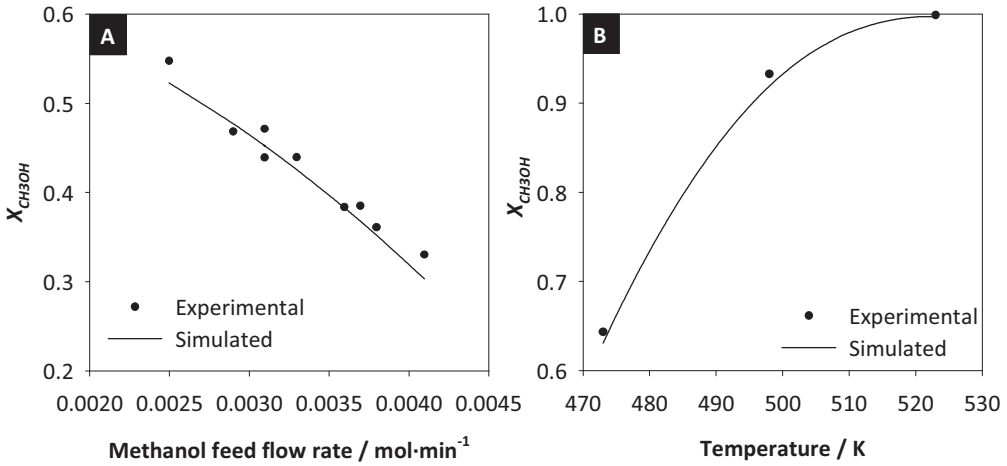

Figure 2.2 – Experimental and simulated data for the: **(A) -** CMS membrane reactor [10]; **(B) -** Pd membrane reactor [30].

The sweep gas used was water vapour and the sweep ratio (ratio between the inlet permeate velocity and the inlet retentate velocity) was set to 1 [31]. Compared to nitrogen, the advantage of using steam as sweep gas is mainly related to the simplicity of its separation from the hydrogen stream by condensation. Moreover, recent studies from Dong *et al.* [32] reported higher hydrogen production and recovery when compared to the use of nitrogen as a sweep gas. The operating parameters for the simulation are presented in Table 2.1. The steam to carbon ratio was varied from 1 to 4 according to what is commonly used in the literature [33]. The temperature was in the range of 473-573 K [31] and the reaction pressure varied from 1 to 3 bar [18]. In order to obtain high driving forces, the permeate pressure was varied from 0.01 to 0.8 bar. The hydrogen permeance was taken from the work of Harale *et al.* [24] for the CMS membrane, and from the work of Basile *et al.* [34] for the Pd membrane. The permeance data were used to estimate the permeation contact time values, using feed flow rates and membrane areas commonly used in the literature [10, 33]. The *Da* number interval was estimated using the kinetic data from the work of Peppley *et al.* [13] and the commonly used catalyst mass and feed flow rates [10, 33].

Table 2.1 – Parameters for the simulation

$Da \in [0.01, 100]$	$\Gamma \in [1, 4]$
$P^{R,out} \in [100, 300]$ kPa	$P^{P} \in [1, 80]$ kPa
$T \in [473, 573]$ K	$S/C\,(H_2O/CH_3OH) \in [1, 4]$
L_{ref}(Pd) =1.57x10^{-7} kmol·m^{-2}·s^{-1}·kPa$^{-0.5}$	L_{ref}(CMS) = 3.53x10^{-7} kmol·m^{-2}·s^{-1}·kPa^{-1}
$L_{H_2}^{Pd*}$ = 1	$L_{H_2}^{CMS*}$ = 1
$L_{H_2O}^{CMS*}$ = 0.313	$L_{CH_3OH}^{CMS*}$ = 0.001
$L_{CO_2}^{CMS*}$ = 0.080	L_{CO}^{CMS*} = 0.015

2.3.1. Methanol conversion

Palladium and palladium-silver membranes are used in membrane reactors to separate hydrogen from a gas mixture. Due to their unique characteristics of being permeable only to this gas, they allow the formation of a pure hydrogen stream that can be used to feed fuel cells. However, due to their relatively low permeability, the reactor must operate with high membrane areas, to recover most of the hydrogen produced. In order to obtain the desirable recoveries of hydrogen at a lower membrane area, CMS membranes can be used instead. These membranes present relatively high permeabilities, but they have the drawback to be permeable to other species, resulting in a not pure hydrogen permeate stream.

The permeation behaviour of the two membranes can have a significant effect in the membrane reactor performance. To evaluate such influence, it was simulated the methanol conversion (X_{CH_3OH} , eq.(2.26)) as a function of the Damköhler number and temperature, for both CMS and Pd membrane reactors – Figure 2.3.

$$X_{CH_3OH} = \frac{F_{CH_3OH}^{R,in*} - F_{CH_3OH}^{R,out*} - F_{CH_3OH}^{P,out*}}{F_{CH_3OH}^{R,in*}} \tag{2.26}$$

where F_i is the dimensionless flow rate: $F_i^* = \frac{p_i^* u^*}{T^*}$.

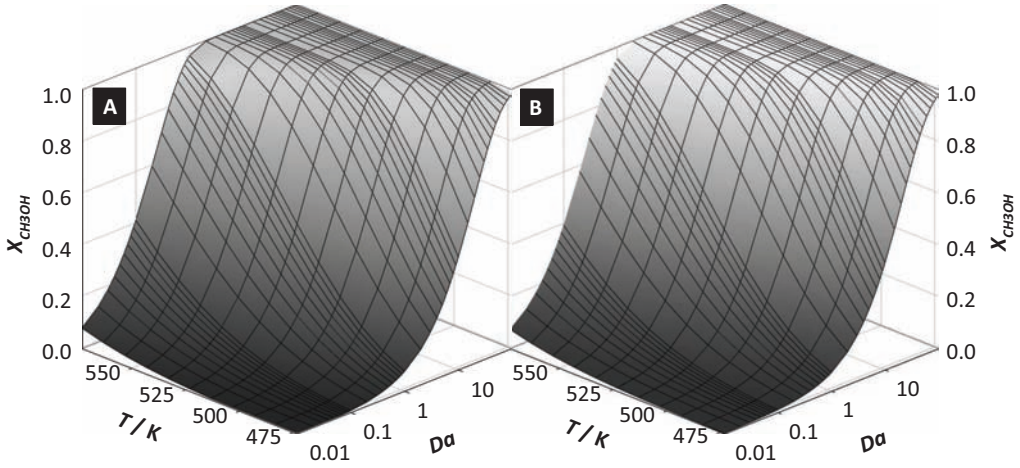

Figure 2.3 – Methanol conversion as a function of the temperature and Damköhler number for: **(A) -** CMS membrane reactor; **(B) -** Pd membrane reactor; *S/C* = 1.5, Γ = 2, $P^{R,out*} = 1$ and $P^{P*} = 0.1$.

The methanol conversion pattern achieved in both membrane reactors is very similar, which could indicate that the permeation behaviour of the two membranes has no effect in the reactor's performance in what concerns the consumption of methanol. In Figure 2.4 it can be seen the methanol conversion of both reactors as a function of the Damköhler number for a given temperature; it is now clear that both reactors perform very closely.

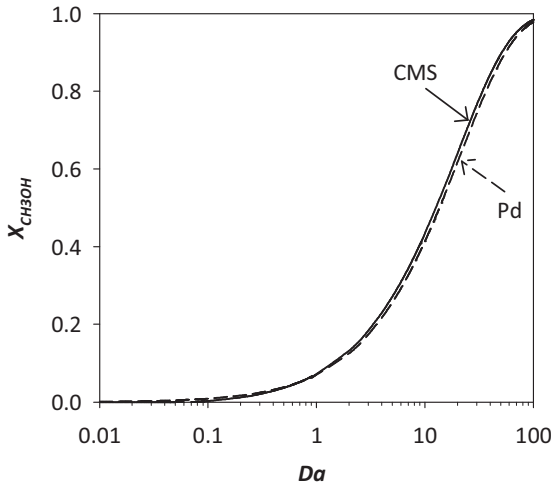

Figure 2.4 – Methanol conversion as a function of the Damköhler number for a palladium membrane reactor and a CMS membrane reactor *S/C* = 1.5, *T* = 473 K, $\Gamma = 2$, $P^{R,out*} = 1$ and $P^{P*} = 0.1$.

Although the differences between the conversions achieved by both MR are almost unnoticeable, it is important to know what are their causes and in which conditions are they more or less important. The methanol steam reforming and secondary reactions (MD and WGS), are equilibrium limited reactions. For these reactions, the conversion is determined by the reaction rate and by the concentration of reactants (which should be as high as possible) and the concentration of products (which should be maintained as low as possible). In opposite to what occurs in the Pd-MR, water permeates through the CMS membrane, diminishing its concentration at the reaction side. At low to medium Damköhler numbers, this has a negligible impact, because the needs of water for the reaction are relatively low. Conversely, at medium to high Damköhler numbers, the reaction is faster, consuming more water. The permeation of this species through the membrane should deplete it from the reaction side faster than for the non permeable membrane (consumption only by reaction), thus decreasing the conversion. However, the simulated results show a different pattern. This apparent contradiction is related to the change in the residence time of the reaction mixture in the reaction zone. More specifically, the permeation of all

species in the CMS-MR lowers the total retentate flow rate, increasing the residence time of the reaction mixture, thus enhancing methanol conversion. Corroborating what has been said, Figure 2.5 shows the difference between the gas velocities at the retentate side for both membrane reactors.

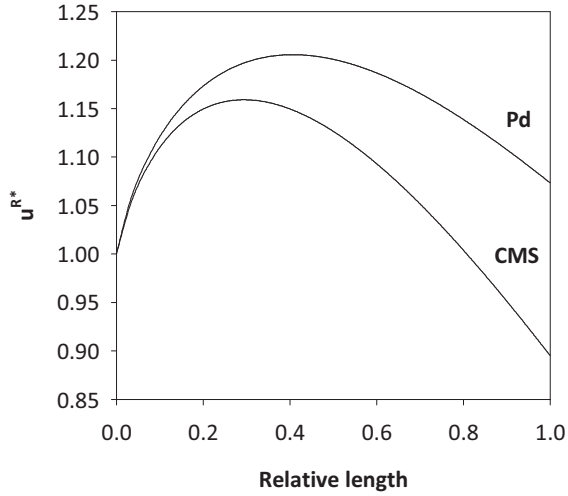

Figure 2.5 – Relative gas velocity at the retentate side along the reactor's length pressure for a palladium membrane reactor and a CMS membrane reactor. *S/C* = 1.5, *T* = 473 K, $\Gamma = 2$, *Da* = 40, $P^{R,out*} = 1$ and $P^{P*} = 0.1$.

To improve methanol conversion, the permeate pressure can be reduced in order to increase the driving force for hydrogen permeation. The removal of hydrogen from the reaction side shifts the MSR and the MD reactions toward the products, resulting in higher methanol conversion. However, it should be taken into account that in a CMS-MR the water flux through the membrane can occur from the retentate to the permeate side or vice-versa, according to the driving force. To determine if the reaction conversion is positively or negatively affected by water permeation from the permeate to the retentate side, the influence of the total permeate pressure was studied - Figure 2.6 (A).

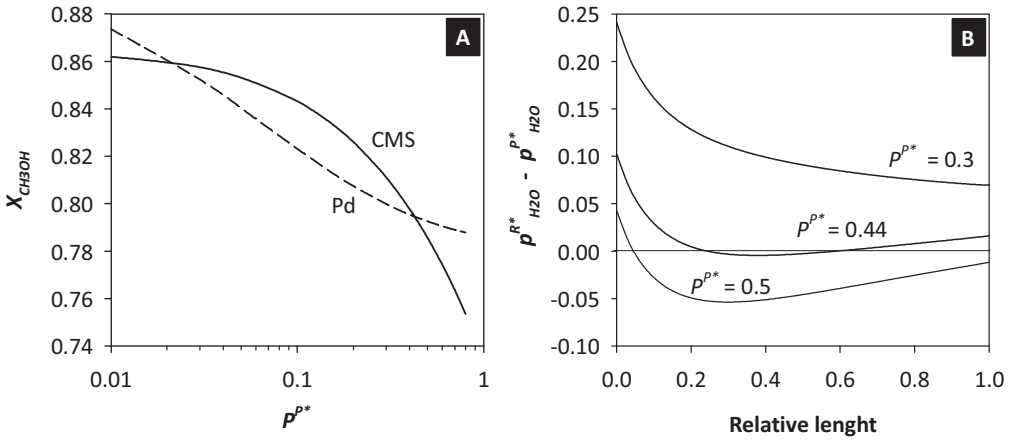

Figure 2.6 – (A) - Methanol conversion as a function of the total relative permeate pressure for a palladium membrane reactor and a CMS membrane reactor. **(B) -** Difference between the water partial pressure at the reaction side ($p^{R*}_{H_2O}$) and the permeate side ($p^{P*}_{H_2O}$) along the reactor's length; *S/C* = 1.5, *T* = 473 K, $\Gamma = 2$, *Da* = 40, $P^{R,out*} = 1$

It is clear from Figure 2.6 that for an intermediate relative permeate pressure region, the CMS-MR presents better performance than the Pd-MR, concerning methanol conversion. In fact, the permeate pressure in the CMS-MR does not need to be as low as the one in the Pd-MR to achieve the same conversion. For the same reason, the sweep gas flow rate does not have to be as high as the one in the Pd-MR. Outside this region, Pd-MR presents higher conversions. When a CMS membrane is used, the effect of water depletion by permeation must be considered, in opposite to what happens in a Pd membrane. At very low relative permeate pressures, below P^{P*}≈0.02 in the present case, water is depleted in the reaction side due to its high permeation rate (high driving force), lowering subsequently the methanol conversion relatively to the one achieved by the Pd-MR. Above P^{P*}≈0.02, the conversion of the CMS-MR becomes higher than the one achieved by the Pd-MR. As P^{P*} increases, the loss of water by permeation decreases also, being no longer depleted from the reaction side. Additionally, the permeation of water from the retentate side increases the residence time of the reaction mixture, as discussed before, enhancing the

methanol conversion. Finally, above $P^{P*}\approx 0.44$, the water partial pressure at the retentate side is lower than the one at the permeate side, which causes a permeation flux from the permeate to the retentate side. This is shown in Figure 2.6 (B) where the water partial pressure difference between retentate and permeate is given along the reactor's length. The water inlet from the permeate side increases its concentration at the reaction side, subsequently augmenting the total retentate flow rate. Although the increase of the H_2O/CH_3OH ratio promotes the reaction to move towards the products, thus increasing the conversion, the increase of the total flow rate in the reaction zone decreases the amount of methanol consumed due to a decrease in the residence time. Therefore, the CMS membrane reactor is penalized relatively to the Pd membrane reactor for this region of permeate pressures.

It is also important to analyse how the hydrogen driving force is affected by the pressure. The driving force for CMS and the Pd membranes is not the same: when Pd is used, the Sieverts law is applied (n = 0.5 in eq. (2.25)); on the other hand, when CMS is used n = 1. Figure 2.7 shows the difference between the CMS-MR and the Pd-MR dimensionless hydrogen driving force, (Δ_{DF}, eq. (2.27)) as a function of the hydrogen partial pressure at the permeate side, for various hydrogen retentate pressures.

$$\Delta_{DF} = \frac{\left(p_{H_2}^R - p_{H_2}^P\right)}{p_{H_2}^R} - \frac{\left(\left(p_{H_2}^R\right)^{0.5} - \left(p_{H_2}^P\right)^{0.5}\right)}{\left(p_{H_2}^R\right)^{0.5}} \tag{2.27}$$

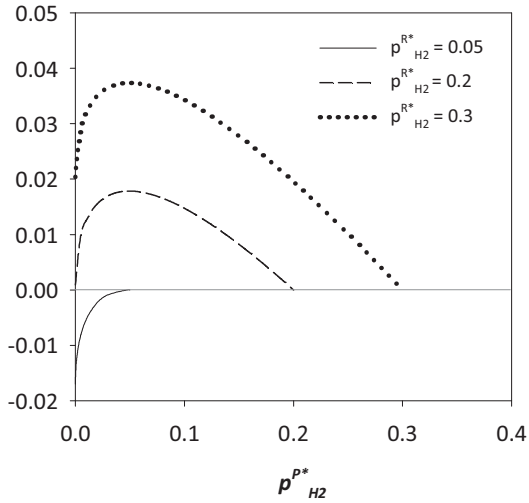

Figure 2.7 – Difference between the CMS-MR and the Pd-MR hydrogen driving force, as a function of the hydrogen partial pressure at the permeate side, for various hydrogen retentate pressures.

According to Figure 2.7, the CMS-MR presents a higher driving force when the amount of hydrogen at the retentate side is higher, which indicates that CMS membranes are more adequate to recover higher hydrogen concentrations and Pd membranes are more suitable for lower hydrogen concentrations.

2.3.2. H_2/CO Selectivity

Besides the conversion of methanol, it is important to analyse the reaction selectivity towards the desired product - hydrogen. For this reason, the MSR reaction should be favoured relatively to the MD reaction, in order to reduce the formation of CO. The amount of hydrogen produced relatively to the amount of CO can be characterized by the H_2/CO selectivity [35], given by equation (2.28):

$$S_{H_2/CO} = \frac{F_{H_2}^{R,out*} + F_{H_2}^{P,out*}}{F_{CO}^{R,out*} + F_{CO}^{P,out*}} \tag{2.28}$$

The influence of the Damköhler number and the permeation contact time in the H_2/CO selectivity is presented in Figure 2.8. It is important to clarify that the

permeation contact time represents the ratio between a reference permeation flow and the feed flow. Knowing that the permeance of the reference component (hydrogen) for CMS and Pd membranes is very different, the permeation flux is also different. As so, for a given feed flow rate, both membranes can present the same permeation contact time value as long as the product $L_{ref} \cdot A^{M}$ is the same for both of them.

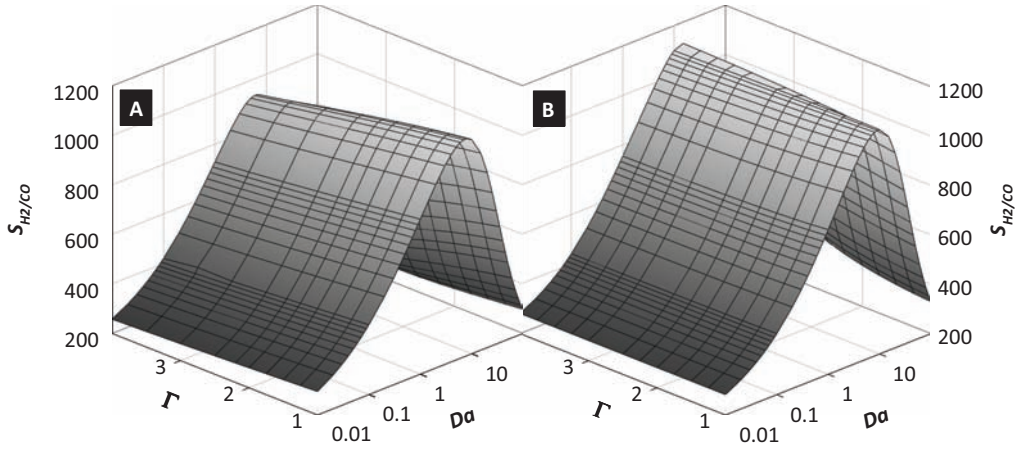

Figure 2.8 – H_2/CO selectivity as a function of the dimensionless permeation contact time and the Damköhler number for: **(A) -** CMS membrane reactor; **(B) -** Pd membrane reactor. *S/C* = 1.5, *T* = 473 K, $P^{R,out*} = 1$ and $P^{P*} = 0.1$.

As it can be seen in Figure 2.8, the H_2/CO selectivity increases with the *Da* number until a maximum value is reached. Afterwards, for high *Da* numbers, H_2/CO selectivity decreases. When the reaction rates are relatively low, $Da = [0.01, 1]$, the consumption of the reactants is also low, thus the water partial pressure at the retentate side is high. As the *Da* number increases, this excess of steam shifts the MSR and the WGS reactions towards the products, producing hydrogen and consuming carbon monoxide, thus increasing the selectivity. At high *Da* numbers, the reaction rates are also high and the gas mixture composition at the reaction side is altered due to the high methanol conversion. In particular, the concentration of water diminishes and the concentration of carbon dioxide increases. This combination shifts

the reverse water gas shift (rWGS) reaction towards the products, consuming hydrogen, producing carbon monoxide and decreasing the reaction selectivity.

The influence of the permeation contact time on the membrane reactor performance, on the other hand, is dependent of the membrane type. The higher the value of Γ, the higher is the fraction of the feed flow that permeates, that is, the stage cut. Concerning the Pd-MR, an increase in the permeation contact time value results in higher hydrogen permeation flux compared to the total feed flow rate. The removal of hydrogen from the retentate side shifts the MSR and the WGS reactions towards the products, producing more hydrogen and consuming carbon monoxide. Conversely, in the CMS-MR, an increase of the permeation contact time value results in higher relative permeation fluxes for all species. The permeation of hydrogen and carbon dioxide has a positive influence in the H_2/CO selectivity, promoting the MSR and the WGS reaction to move towards the products. However, the permeation of water has the opposite effect: it promotes the rWGS reaction, more carbon monoxide is produced, and the H_2/CO selectivity decreases. In addition, less water is available for the MSR reaction and less hydrogen is produced. This effect overrides the others and the H_2/CO selectivity decreases.

Comparing the performance of both membranes in what concerns the H_2/CO selectivity, the CMS-MR presents slightly higher values at low to medium *Da* numbers, while the Pd-MR shows higher values at medium to high *Da* numbers - Figure 2.9. Due to the lower retentate flow rate of the CMS-MR, mostly due to the water permeation, the extent of all reactions is higher at first. However, the low concentration of water at high *Da* numbers will promote the rWGS reaction over the others. In the Pd membrane reactor, water does not permeate, so the rWGS is not so highly enhanced. Therefore, its concentration at the reaction side is then kept higher than in the CMS-MR, resulting in higher H_2/CO selectivity.

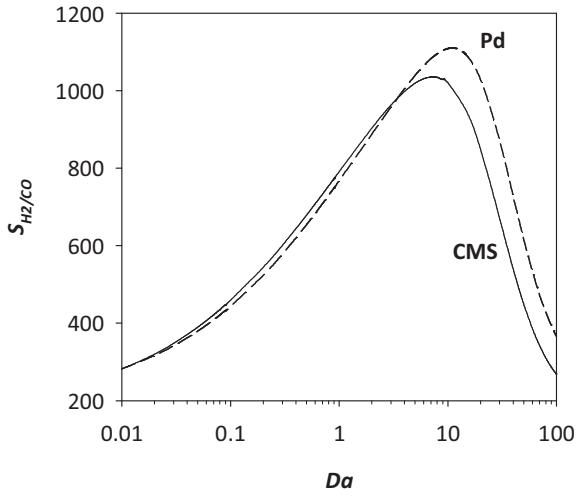

Figure 2.9 – H_2/CO selectivity as a function of Damköhler number for a palladium membrane reactor and a CMS membrane reactor; *S/C* = 1.5, *T* = 473 K, $\Gamma = 2$, $P^{R,out^*} = 1$ and $P^{P^*} = 0.1$.

2.3.3. Hydrogen recovery

The amount of hydrogen that is recovered at the permeate side is an important factor to evaluate the performance of the reactor. Figure 2.10 shows the influence of the permeation contact time and the Damköhler number in the hydrogen recovery, which is defined by (2.29):

$$Rec_{H_2} = \frac{F_{H_2}^{P^*}}{F_{H_2}^{P^*} + F_{H_2}^{R^*}} \tag{2.29}$$

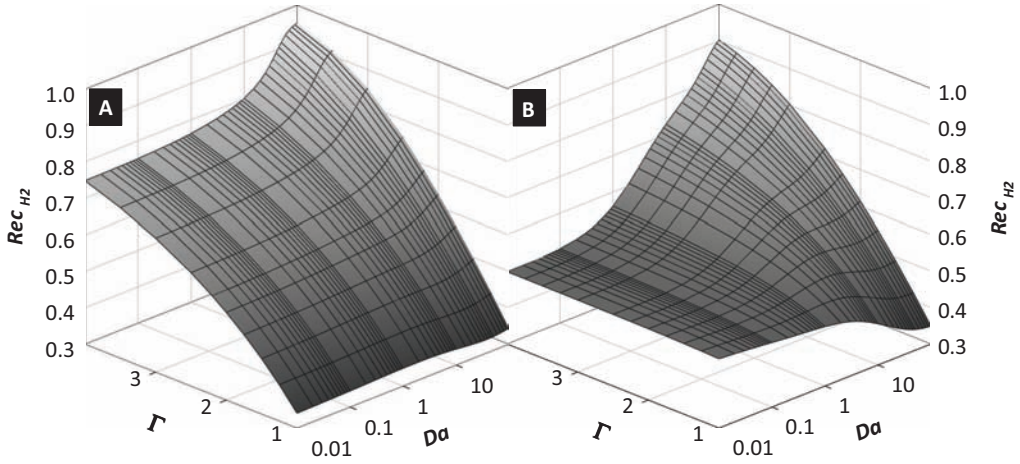

Figure 2.10 – Hydrogen recovery as a function of the dimensionless permeation contact time and the Damköhler number for: **(A) -** CMS membrane reactor; **(B) -** Pd membrane reactor; *S/C* = 1.5, *T* = 473 K, $P^{R,out^*} = 1$ and $P^{P^*} = 0.1$.

As it can be seen, the pattern for both membrane reactors is somehow complex. An increase of the Damköhler number has two different effects, depending on the permeation contact time value. Specifically, at low Γ the membrane reactor operates at low stage cut and the relative hydrogen permeation flux is, therefore, low. With an increase of the *Da* number, the amount of hydrogen produced is higher, but due to low relative permeation flux, the hydrogen recovery at the permeate side decreases. This effect is more pronounced in the Pd-MR than in the CMS-MR because the permeation of water in the CMS-MR causes a decrease of its partial pressure and, subsequently, an increase of the hydrogen partial pressure. On the other hand, higher Γ indicates a higher stage cut, meaning a higher permeation flux relative to the retentate flow rate. When the hydrogen generation increases due to the *Da* number, its partial pressure at the retentate side also increases. Consequently, the hydrogen driving force is higher and its recovery enhanced.

In what concerns the effect of the permeation contact time, the major difference in the performance of these membrane reactors occurs at low Damköhler numbers. While increasing Γ in the Pd-MR seems to have almost no effect, in the CMS-MR it

strongly enhances the hydrogen recovery. According to what was discussed before, when the amount of hydrogen produced is low (low *Da* numbers) the Pd-MR presents a higher driving force than the CMS-MR. Confirming what has been said, Figure 2.10 shows higher hydrogen recovery for the Pd-MR than the CMS-MR at low *Da* and low Γ. However, for low *Da* and high Γ the membrane reactors perform very differently. Beginning with the analysis on the Pd-MR, low *Da* numbers result in low hydrogen production rate, thus low driving force. In this case, where hydrogen is the only permeating species, a change in the permeation contact time has very little effect on the recovery. In fact, the increase of the hydrogen recovery would only be noticeable at very high permeation contact time values. On the other hand, all species permeate in the CMS-MR; although the amount of hydrogen in the reaction side is low, its partial pressure increases with the permeation of the other species, mainly water, towards the permeate side. In fact, the decrease of water partial pressure leads to an increase of the hydrogen partial pressure, resulting in a higher driving force.

2.3.4. Carbon monoxide permeation

As mentioned before, carbon membranes, unlike Pd membranes, are permeable to carbon monoxide, a poison to the anode catalyst of the fuel cells. In order to feed the permeate stream directly to a PEMFC, the amount of CO must be lower than 10 ppm [14]. As so, the effect of the various parameters on the amount of CO that permeates through the membrane is of great importance.

Several authors have shown the advantages of increasing the reaction pressure in order to improve methanol conversion, as well as the hydrogen recovery, in a Pd-MR [18, 33]. Indeed, an increase of the reaction pressure enhances the hydrogen driving force, shifting the reaction equilibrium towards the products. On the other hand, according to the Le Chatelier principle, in reactions where $\sum_i \nu_i > 0$ as steam reforming and methanol decomposition, the increase of pressure shifts the equilibrium towards the reactants and methanol conversion decreases. Figure 2.11 shows the influence of the permeation contact time and the total pressure in the

conversion of methanol. It can be seen that the conversion in the Pd-MR is positively affected by the increase of the pressure due to the higher hydrogen driving force and by the increase of Γ due to the higher stage cut. However, the CMS-MR does not reveal the same behaviour. As there are two ways to consume water, namely, permeation and chemical reaction, there is a value of Γ at which the methanol conversion starts to decrease due to the depletion of water.

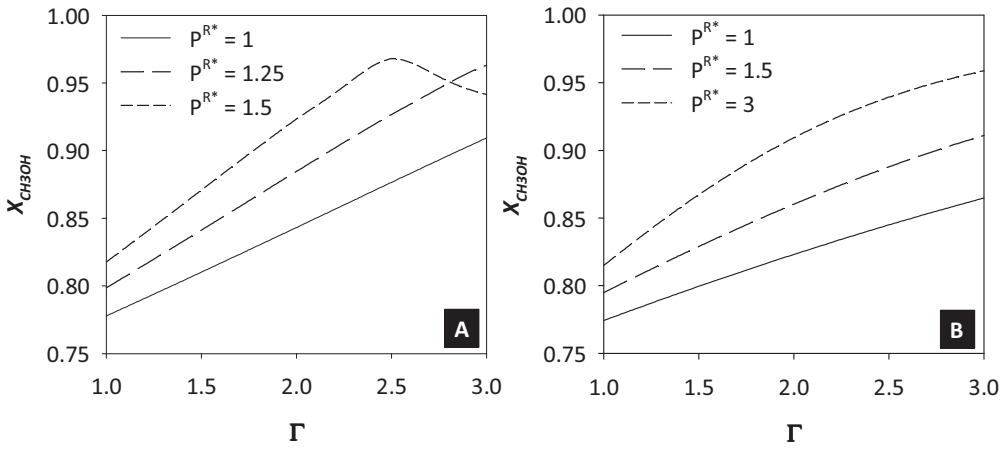

Figure 2.11 – Methanol conversion as a function of the dimensionless permeation contact time, at various retentate pressures, for: **(A) -** CMS membrane reactor. **(B) -** Pd membrane reactor. *S/C* = 1.5, *T* = 473 K, *Da* = 40 and P^{P*} = 0.1 .

Despite the decrease in methanol conversion shown in Figure 2.11, the hydrogen recovery was not penalized by water depletion. In fact, Figure 2.12 (A) shows a small increase of the hydrogen recovery when the conversion starts to decrease. As the amount of hydrogen produced lowers, its recovery rises, so the increase of pressure seems to have a positive effect in the CMS-MR. However, this is not entirely true. The CO permeation also increases with the pressure, inhibiting the stream to be fed directly to the PEMFC - Figure 2.12 (B). As so, unlike Pd, these membranes are better suited for working at low pressures.

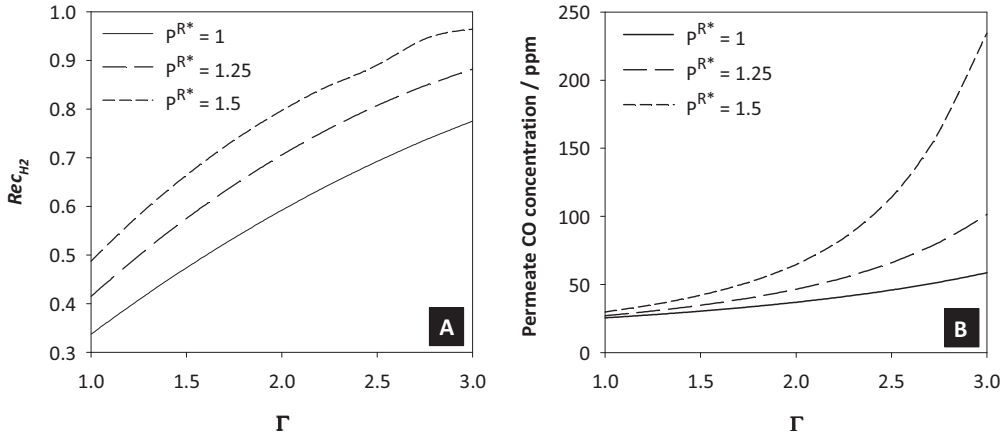

Figure 2.12 – (A) - Hydrogen recovery as a function of the dimensionless permeation contact time, at various retentate pressures for a CMS membrane reactor. **(B) -** Permeate CO concentration as a function of the dimensionless permeation contact time, at various retentate pressures for a CMS membrane reactor. *S/C* = 1.5, *T* = 473 K, *Da* = 40 and P^{P*} = 0.1 .

Carbon monoxide is formed by the endothermic reactions MD and rWGS. Thus, the extent of these reactions can be reduced by lowering the reaction temperature. The increase of the steam to carbon feed ratio is another way of reducing the carbon monoxide formation. The excess of steam will promote the MSR reaction toward the products and less amount of methanol is decomposed to carbon monoxide. In the same way, the WGS reaction is shifted toward the products, producing carbon dioxide and hydrogen and consuming carbon monoxide.

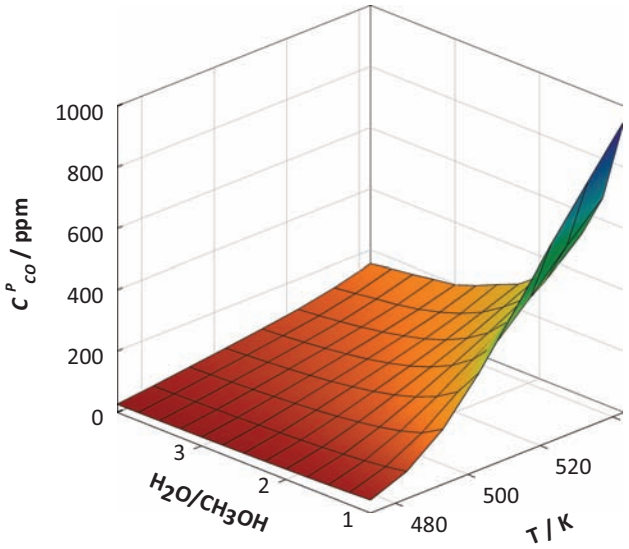

Figure 2.13 – Carbon monoxide concentration at the permeate side as a function of the temperature and the H_2O/CH_3OH feed ratio for a CMS membrane reactor. *Da* = 40, Γ = 2, $P^{R,out*} = 1$ and $P^{P*} = 0.1$.

Figure 2.13 shows the influence of both temperature and steam to carbon ratio on the carbon monoxide concentration at the permeate side. Although the amount of CO decreases with higher steam to carbon ratios and lower reaction temperatures, it is still remaining above 10 ppm and, thus, too high to be fed into a PEMFC. Lower permeation contact time values could be used to decrease the CO content, but this would also decrease the hydrogen recovery. In order to overcome this difficulty, a new membrane reactor configuration was studied as described in the next section.

2.3.5. Combination of Pd and CMS membranes

As discussed above, each membrane has some advantage over the other. As so, an improved system would result from combining in the same reactor a high permeation flux while keeping the CO at the permeation side at low concentrations. In order to find such a system, a new reactor configuration is proposed and simulated, combining a Pd membrane and a CMS membrane, as shown in Figure 2.14.

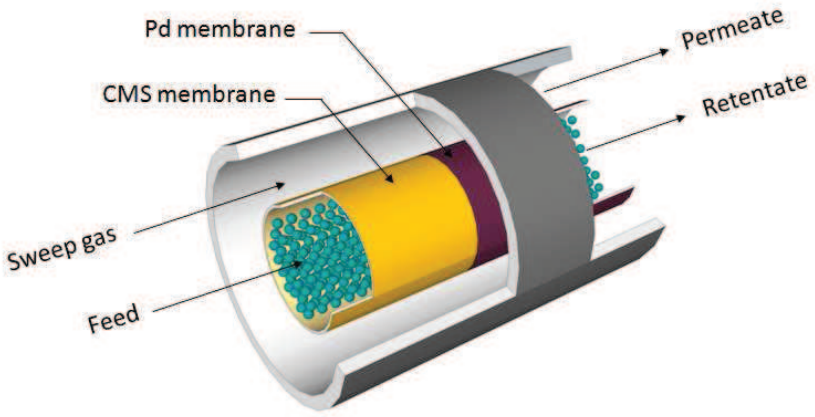

Figure 2.14 – Scheme of the simulated CMS/Pd membrane reactor.

The present simulated reactor comprises two membranes. First the CMS membrane, less selective and less expensive with a higher permeation flux; afterwards, the highly selective Pd membrane with lower permeation flux. A preliminary study was made in order to determine the most adequate ratio of the CMS/Pd membrane length. It was concluded that the value of 1.2 was the most suitable for a large range of the studied operating parameters, keeping the CO concentration at the permeate side below 10 ppm and a high hydrogen recovery.

The major disadvantage of the CMS membrane is the CO permeation. As shown in Figure 2.15, the combination of the membranes overcomes this problem, allowing to produce a permeate stream with an amount of carbon monoxide under 10 ppm. Placing the Pd membrane after the CMS membrane, avoids the permeation of CO where its partial pressure is higher – the end of the reformer.

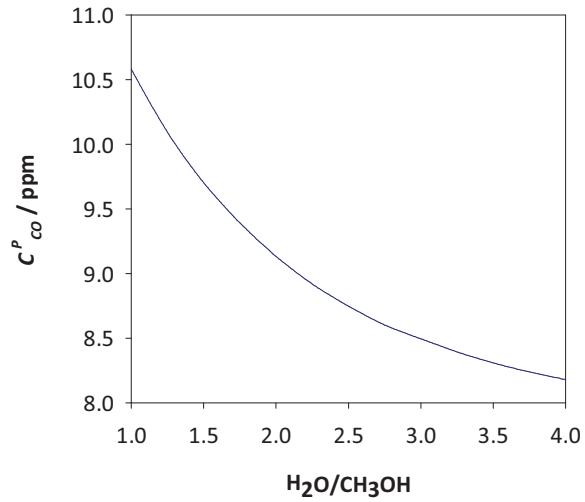

Figure 2.15 – Carbon monoxide concentration in the permeate side as a function of the Damköhler number for a CMS/Pd membrane reactor. T = 473 K, $\Gamma = 2$, $P^{R,out^*} = 1$ and $P^{P^*} = 0.1$.

Concerning the hydrogen permeation flux, Figure 2.16 shows that this new reactor configuration allows a higher recovery of the hydrogen formed. As discussed before, the permeation of water lowers its partial pressure at the reaction side and increases the hydrogen partial pressure. The hydrogen driving force is higher and its permeation flux is increased.

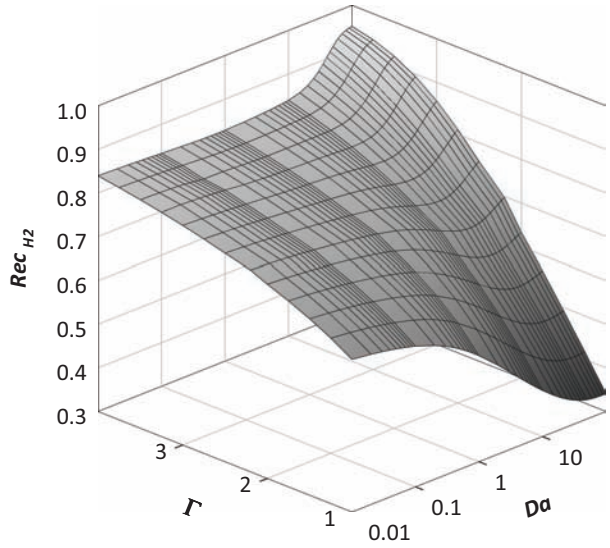

Figure 2.16 – Hydrogen recovery as a function of the dimensionless permeation contact time for a CMS/Pd membrane reactor. *S/C* = 1.5, T = 473 K, *Da* = 40, $P^{R,out^*} = 1$ and $P^{P^*} = 0.1$ **.**

In comparison to the CMS-MR, the hydrogen recovery at low Damköhler numbers is higher due to the presence of the Pd membrane at the end of the reactor. As discussed before, when the production of hydrogen is low, the Pd-MR shows a higher driving force compared to the CMS-MR. In this way, the hydrogen permeation flux increases and the hydrogen recovery is enhanced.

2.4. Conclusions

Two types of membranes were studied to work in a methanol steam reforming membrane reactor. CMS membranes present higher permeabilities, higher hydrogen recovery, and lower selectivities. Pd membranes are more expensive but exhibit much higher selectivity towards hydrogen.

This study was focused on the analysis of the methanol conversion, H_2/CO reaction selectivity, CO concentration at the permeate side and hydrogen recovery. The effect of several parameters was analysed. More specifically, it was concluded that methanol conversion is enhanced by the *Da* number and the reaction

temperature. The H_2/CO reaction selectivity increases with Γ for the Pd-MR but has the opposite effect for the CMS-MR. Hydrogen recovery increases with Γ and *Da* numbers for both MR, although the effect is almost unnoticeable for the Pd-MR and for low *Da* numbers. The CMS-MR presents higher hydrogen recovery than the Pd-MR at high hydrogen concentrations, and the Pd-MR proved to be more advantageous for lower hydrogen concentrations. Finally, the Pd-MR performance is enhanced by high retentate pressures and low permeate pressures, while the CMS-MR performance is enhanced for intermediate values.

A combined CMS+Pd membrane reactor was studied in order to explore the advantages of both membrane systems. The combination of these membranes revealed some advantages towards the CMS-MR; specifically, higher hydrogen recovery is achieved, keeping the CO concentration at the permeate side below 10 ppm. In comparison to the Pd-MR, this membrane combination allows the use of smaller membranes and higher feed flow rates, without prejudice of the membrane reactor performance.

Acknowledgments

The work of Sandra Sá was supported by FCT, grant SFRH/BD/30385/2006. The research was also supported by funds from FCT projects PTDC/EQU-EQU/71617/2006 and POCI/ENR/59323/2004.

List of Abbreviations and symbols

Abbreviations		Definition	Units
A	–	Area	m^2
C_{S1}^T	–	total catalyst surface concentration of site 1	$mol \cdot m^{-2}$
C_{S2}^T	–	total catalyst surface concentration of site 2	$mol \cdot m^{-2}$
C_{S1a}^T	–	total catalyst surface concentration of site 1a	$mol \cdot m^{-2}$
C_{S2a}^T	–	total catalyst surface concentration of site 2a	$mol \cdot m^{-2}$
Da	–	Damköhler number	
D_{ax}	–	axial dispersion coefficient	$m^2 \cdot s^{-1}$
d_p	–	catalyst diameter	m
F_i	–	dimensionless molar flow rate of species *i*	
k_i	–	rate constant for reaction *i,*	$m^2 \cdot s^{-1} \cdot mol^{-1}$
K_j^e	–	equilibrium constant for reaction *j*	
K_i	–	adsorption coefficient for surface species *i*	
$k_{MSR,ref}$	–	rate constant for the steam reforming reaction	$m^2 \cdot s^{-1} \cdot mol^{-1}$
L_i	–	permeance coefficient of species *i*	$kmol \cdot m^{-2} \cdot s^{-1} \cdot kPa^{-n}$
$l_{reactor}$	–	length of the reactor	m
m_{cat}	–	mass of catalyst	kg
M_{ref}	–	reference molar mass	$kg \cdot mol^{-1}$
N_i	–	flux of the component *i* through the membrane	$mol \cdot s^{-1} \cdot m^{-2}$
Pe	–	*Peclet* number for mass transfer	
p_i	–	partial pressure of component *i*	kPa
P_{ref}	–	reference pressure	kPa
P	–	total pressure	kPa
$\Re$	–	gas constant	$kPa\ m^3 \cdot mol^{-1} \cdot K^{-1}$
r_j	–	rate of reaction *j*	$mol \cdot s^{-1} \cdot kgcat^{-1}$

r^R	–	radius of the reactor	m
R_i	–	rate of consumption or formation of species *i*	$mol \cdot s^{-1} \cdot kgcat^{-1}$
S_A	–	surface area of the catalyst	$m^2 \cdot kg^{-1}$
T	–	absolute temperature	K
u	–	interstitial velocity	$m \cdot s^{-1}$
u_{ref}	–	reference velocity	$m \cdot s^{-1}$
x	–	relative length of the reactor	

Greek symbols		**Definition**	**Units**
	–	void fraction of the catalyst bed	
Γ	–	dimensionless permeation contact time	
	–	gas viscosity	$kg \cdot m^{-1} \cdot s^{-1}$
	–	dimensionless time variable	
	–	gas density	$kg \cdot m^{-3}$
$_{cat}$	–	catalyst density	$kg_{cat} \cdot m^{-3}$
$_{ij}$	–	stoichiometric coefficient for species *i* in the reaction *j*	

Superscripts		**Definition**
M	–	membrane
R	–	retentate
P	–	permeate

Subscripts		**Definition**
MD	–	methanol decomposition
MSR	–	methanol steam reforming
rWGS	–	reverse water gas shift
WGS	–	water gas shift

References

[1] G. Cacciola, V. Antonucci, S. Freni, Technology up date and new strategies on fuel cells, J. Power Sources, 100 (2001) 67-79.

[2] J.M. King, M.J. O'Day, Applying fuel cell experience to sustainable power products, J. Power Sources, 86 (2000) 16-22.

[3] D. Ramirez, L.F. Beites, F. Blazquez, J.C. Ballesteros, Distributed generation system with PEM fuel cell for electrical power quality improvement, Int. J. Hydrogen Energy, 33 (2008) 4433-4443.

[4] C. Stone, A.E. Morrison, From curiosity to ''power to change the world'', Solid State Ionics, 152-153 (2002) 1-13.

[5] A.S. Damle, Hydrogen production by reforming of liquid hydrocarbons in a membrane reactor for portable power generation—Model simulations, J. Power Sources, 180 (2008) 516-529.

[6] D.G. Löffler, K. Taylor, D. Mason, A light hydrocarbon fuel processor producing high-purity hydrogen, J. Power Sources, 117 (2003) 84-91.

[7] S. Ahmed, M. Krumpelt, Hydrogen from hydrocarbon fuels for fuel cells, Int. J. Hydrogen Energy, 26 (2001) 291-301.

[8] J.C. Telotte, J. Kern, S. Palanki, Miniaturized Methanol Reformer for Fuel Cell Powered Mobile Applications, Int. J. Chem. Reactor Eng., 6 (2008).

[9] A. Basile, A. Parmaliana, S. Tosti, A. Iulianelli, F. Gallucci, C. Espro, J. Spooren, Hydrogen production by methanol steam reforming carried out in membrane reactor on Cu/Zn/Mg-based catalyst, Catal. Today, 137 (2008) 17–22.

[10] X. Zhang, H. Hu, Y. Zhu, S. Zhu, Methanol Steam Reforming to Hydrogen in a Carbon Membrane Reactor System, Ind. Eng. Chem. Res., 45 (2006) 7997-8001.

[11] D.R. Palo, R.A. Dagle, J.D. Holladay, Methanol Steam Reforming for Hydrogen Production, Chem. Rev., 107 (2007) 3992-4021.

[12] B.A. Peppley, J.C. Amphlett, L.M. Kearns, R.F. Mann, Methanol steam reforming on Cu/ZnO/Al2O3. Part 1: the reaction network, Appl. Catal. A, 179 (1999) 21-29.

[13] B.A. Peppley, J.C. Amphlett, L.M. Kearns, R.F. Mann, Methanol steam reforming on Cu/ZnO/Al2O3 catalysts. Part 2. A comprehensive kinetic model, Appl. Catal. A, 179 (1999) 31-49.

[14] H.P. Dhar, L.G. Christner, A.K. Kush, Nature of CO Adsorption during H2 Oxidation in Relation to Modeling for CO Poisoning of a Fuel Cell Anode, J. Electrochem. Soc., 134 (1987) 3021-3026.

[15] F. Gallucci, L. Paturzo, A. Basile, Hydrogen Recovery from Methanol Steam Reforming in a Dense Membrane Reactor: Simulation Study, Ind. Eng. Chem. Res., 43 (2004) 2420-2432.

[16] A.N. Matzakos, S.L. Wellington, T. Mikus, J.M. Ward, Integrated flameless distributed combustion/steam reforming membrane reactor for hydrogen production and use thereof in zero emissions hybrid power system, USA, 2004.

[17] C.-H. Fu, J.C.S. Wu, Mathematical simulation of hydrogen production via methanol steam reforming using double-jacketed membrane reactor, Int. J. Hydrogen Energy, 32 (2007) 4830-4839.

[18] A. Iulianelli, T. Longo, A. Basile, Methanol steam reforming in a dense Pd–Ag membrane reactor: The pressure and WHSV effects on CO-free H2 production, J. Membr. Sci., 323 (2008) 235–240.

[19] F. Gallucci, A. Basile, S. Tosti, A. Iulianelli, E. Drioli, Methanol and ethanol steam reforming in membrane reactors: An experimental study, Int. J. Hydrogen Energy, 32 (2007) 1201-1210.

[20] B.K.R. Nair, M.P. Harold, Hydrogen generation in a Pd membrane fuel processor: Productivity effects during methanol steam reforming, Chem. Eng. Sci., 61 (2006) 6616–6636.

[21] L. Shao, B.T. Low, T.-S. Chung, A.R. Greenberg, Polymeric membranes for the hydrogen economy: Contemporary approaches and prospects for the future, J. Membr. Sci., 327 (2009) 18-31.

[22] A.F. Ismail, L.I.B. David, A review on the latest development of carbon membranes for gas separation, J. Membr. Sci., 193 (2001) 1-18.

[23] G.A. Sznejer, I. Efremenko, M. Sheintuch, Carbon Membranes for High Temperature Gas Separations: Experiment and Theory, AIChE J., 50 (2004).

[24] A. Harale, H.T. Hwang, P.K.T. Liu, M. Sahimi, T.T. Tsotsis, Experimental studies of a hybrid adsorbent-membrane reactor (HAMR) system for hydrogen production, Chem. Eng. Sci., 62 (2007) 4126 – 4137.

[25] S. Ergun, Fluid flow through packed columns, Chem. Eng. Prog., 48 (1952) 89-94.

[26] P.V. Danckwerts, Continuous flows systems - distribution of residence times, Chem. Eng. Sci., 2 (1953) 1.

[27] J.M. Sousa, A. Mendes, Simulation study of a dense polymeric catalytic membrane reactor with plug–flow pattern, Chem. Eng. J., 95 (2003) 67-81.

[28] P. Cruz, J.C. Santos, F.D. Magalhães, A. Mendes, Simulation of separation processes using finite volume method, Comput. Chem. Eng., 30 (2005) 83-98.

[29] L. Petzold, Automatic Selection of Methods for Solving Stiff and Nonstiff Systems of Ordinary Differential Equations, Siam J. Sci. Stat. Computing, 4 (1983) 136-148.

[30] A. Basile, G.F. Tereschenko, N.V. Orekhova, M.M. Ermilova, F. Gallucci, A. Iulianelli, An experimental investigation on methanol steam reforming with oxygen addition in a flat Pd–Ag membrane reactor, Int. J. Hydrogen Energy, 31 (2006) 1615 – 1622.

[31] F. Gallucci, A. Basile, Pd–Ag membrane reactor for steam reforming reactions: A comparison between different fuels, Int. J. Hydrogen Energy, 33 (2008) 1671 - 1687.

[32] Y.-R. Dong, N. Nishiyama, Y. Egashira, K. Ueyama, H2-Selective Carbon Membranes Prepared from Furfuryl Alcohol by Vapor-Phase Synthesis, Ind. Eng. Chem. Res., (2007).

[33] F. Gallucci, A. Basile, Co-current and counter-current modes for methanol steam reforming membrane reactor, Int. J. Hydrogen Energy, 31 (2006) 2243 - 2249.

[34] A. Basile, F. Gallucci, L. Paturzo, A dense Pd/Ag membrane reactor for methanol steam reforming: Experimental study, Catal. Today, 104 (2005) 244-250.

[35] H.S. Fogler, Elements of Chemical Reaction Engineering, fourth ed., Upper Saddle River, NJ, 2005.

Chapter 3. Methanol steam reforming in a dual-bed membrane reactor for producing PEMFC grade hydrogen[1]

Abstract

This work focus on the advantages of adding a preferential carbon monoxide oxidation (PROX) reactor to a common methanol steam reforming (MSR) membrane reactor (MR). The study was performed using a one-dimensional mathematical model, assuming axially dispersed plug-flow with pressure drop in both retentate and permeate sides. The simulation results showed clear advantages of the MSR+PROX towards the MSR membrane reactor in what concerns the amount of CO in the permeate stream. More specifically, the permeate CO concentration in the MSR+PROX-MR was reduced to levels below 2 ppm, enabling the stream to feed a fuel cell. Additionally, high values of methanol conversion and hydrogen recovery were achieved, and the amount of CO_2 at the permeate side was able to remain below 20 % for all simulations.

[1] S. Sá, J.M. Sousa, A. Mendes, Methanol steam reforming in a dual-bed membrane reactor for producing PEMFC grade hydrogen, Catal. Today, 156 (2010) 254-260.

3.1. Introduction

Polymer electrolyte membrane fuel cells (PEMFC) are a promising source of clean electrical power for small scale and transport applications [1-3]. However, these devices require hydrogen as fuel, which presents storage and transportation problems. The need to overcome these problems makes *in situ* hydrogen production from alcohols and hydrocarbons steam reforming very attractive [4-6]. In comparison to other fuels, methanol presents several advantages which justify its application as a hydrogen carrier for fuel cell applications. More specifically, methanol is liquid at atmospheric conditions, has high hydrogen to carbon ratio, and its reforming temperature is relatively low (200-300 °C) [7-10].

According to the literature [11, 12], there are three chemical reactions to be considered in a methanol steam reformer: the methanol steam reforming (MSR, eq.(3.1)), which is the main reaction, and the methanol decomposition (MD, eq.(3.2)) and water gas shift (WGS, eq.(3.3)) side reactions:

$$CH_3OH + H_2O \rightleftharpoons CO_2 + 3H_2 \qquad \Delta H = 49.7\,kJ\cdot mol^{-1} \qquad (3.1)$$

$$CH_3OH \rightleftharpoons CO + 2H_2 \qquad \Delta H = 92.0\,kJ\cdot mol^{-1} \qquad (3.2)$$

$$CO + H_2O \rightleftharpoons CO_2 + H_2 \qquad \Delta H = -41.2\,kJ\cdot mol^{-1} \qquad (3.3)$$

The major disadvantage of this process is the formation of carbon monoxide as a secondary product. It is known that carbon monoxide poisons the anodic catalyst of the fuel cell, so it must be reduced to levels under than 10 ppm [13]. In the same way, carbon dioxide can also have negative effect on the performance of the fuel cell, and its concentration should be maintained below 20 % [14]. The latter effect is probably due to the formation of carbon monoxide by the reverse water gas shift reaction.

The separation of hydrogen from the resulting gas mixture can be accomplished by using a permselective membrane. The use of palladium (Pd) membranes for hydrogen separation in membrane reactors is very common and is vastly reported in the literature [8, 15-20], due to their high selectivity to hydrogen. However, these

membranes are expensive and have limited applications due to their low permeability compared to porous inorganic membranes [21, 22]. Another type of membranes that can be used to perform this separation is the carbon molecular sieve (CMS). These membranes are less expensive and present higher permeabilities than Pd membranes, enabling the use of higher feed flow rates. However, they are brittle and permeable to other species besides hydrogen. Regarding the application of these membranes, Zhang *et al.* [23] compared a traditional reactor with a CMS membrane reactor for the methanol steam reforming reaction, concluding that higher conversion and lower carbon monoxide yield could be achieved. Harale *et al.* [24] studied a CMS membrane reactor for the water gas shift reaction and presented membranes with very high hydrogen permeation fluxes. These studies showed that higher flow rates and lower membrane areas can be used with CMS membrane reactors. The major drawback of these membranes is the low selectivity towards hydrogen. Due to the CMS permeability to other species, the carbon monoxide concentration at the permeate side can exceed the imposed limit of 10 ppm. To reduce the amount of carbon monoxide, several approaches can be made, namely the preferential oxidation and the water gas shift reactions. Comparing both reactions, the WGS has the advantage of producing hydrogen while consuming carbon monoxide. However, due to thermodynamic limitations, the reaction conversion does not achieve 100 % and the final carbon monoxide concentration exceeds 10 ppm [25]. On the other hand, the PROX reaction can easily convert the majority of the carbon monoxide that permeates through the membrane, but some hydrogen is consumed in the process. Due to the importance of the carbon monoxide removal of the permeate stream, the PROX reaction will be used in this work. According to the literature [26], the CO oxidation (eq. (3.4)) and the H_2 oxidation (eq. (3.5)) reactions must be considered:

$$CO + 1/2O_2 \rightarrow CO_2 \qquad \Delta H = -283\,kJ\cdot mol^{-1} \qquad (3.4)$$

$$H_2 + 1/2O_2 \rightarrow H_2O \qquad \Delta H = -242\,kJ\cdot mol^{-1} \qquad (3.5)$$

This work simulates the production of hydrogen by methanol steam reforming in a carbon molecular sieve membrane reactor. Low CO concentration is assured by a catalyst bed for the PROX reaction at the permeate side. The present work aims to compare the membrane reactor performance with and without the PROX reaction. Ultimately, the objective is to achieve a hydrogen rich permeate stream with low CO and CO_2 concentrations. To this end, a one-dimensional comprehensive mathematical model of a dual packed-bed membrane reactor was developed. The simulation results can help to find the best conditions for the membrane reactor operation. The main goals of this study are the achievement of the highest methanol conversion and hydrogen recovery, keeping the CO concentration at the permeate side below 10 ppm and the one of CO_2 below 20 %.

3.2. Development of the Membrane Reactor Model

Figure 3.1 shows the scheme of the simulated membrane reactor. It consists in a tubular membrane with surface area A^M, housing a packed-bed of a MSR catalyst in the retentate chamber and a packed-bed of a PROX catalyst in the permeate chamber. A gas phase stream of methanol and water is fed to the retentate side, producing hydrogen, carbon dioxide and carbon monoxide. Water vapour is used as sweep gas in the permeate side, flowing in co-current. Oxygen is also fed to the permeate chamber to perform the PROX reaction.

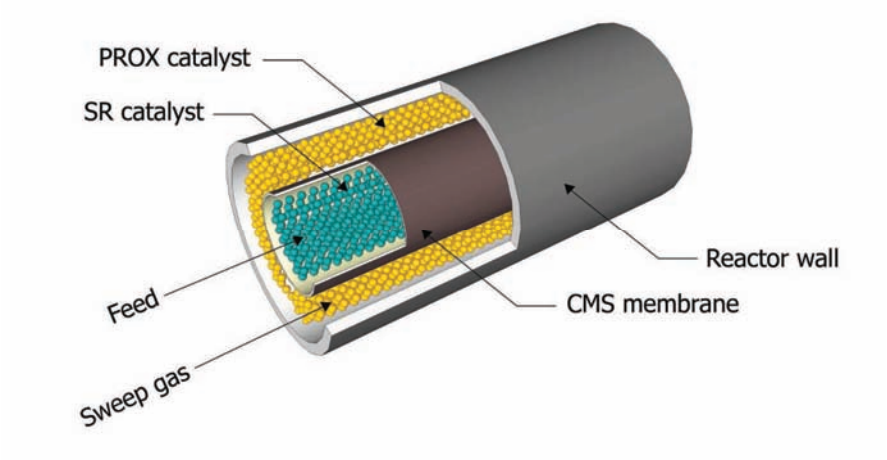

Figure 3.1 – Scheme of the simulated membrane reactor.

The mathematical model proposed comprises the steady-state mass balance equations for the reaction and permeation sides, as well as the respective boundary conditions. This model is based on the following general assumptions: isothermal conditions, ideal gas behaviour, axially dispersed plug flow with pressure drop described by the *Ergun* equation [27], negligible radial gradients and uniform cross-sectional void fraction.

3.2.1. Retentate Side

Partial Mass Balance

$$-\frac{d}{dz}\left(u^R p_i^R\right)+D_{ax}\frac{d}{dz}\left(P^R\frac{d}{dz}\left(\frac{p_i^R}{P^R}\right)\right)-\frac{2}{A^R}\frac{r^M}{\Re TN_i}+\frac{m_{cat}^R}{V^R}\Re TR_i^R=0 \tag{3.6}$$

Total Mass Balance

$$-\frac{d}{dz}\left(u^R P^R\right)-\frac{2\pi r^M}{A^R}\Re T\sum_i N_i+\frac{m_{cat}^R}{V^R}\Re T\sum_i R_i^R=0 \tag{3.7}$$

Pressure drop

$$-\frac{dP^R}{dz} = 150\frac{u^R}{d_p^2}(1- \quad)^2 + \frac{7}{4}\frac{_{gas}\left(u^R\right)^2}{d_p}\frac{1-}{\quad} \tag{3.8}$$

Boundary Conditions

The partial mass balance is a second order differential equation, thus two boundary conditions are needed [28]. When the pressure drop cannot be considered negligible, it must be imposed one boundary condition in z = 0 and other in z = 1, as follows:

$$z=0: \quad D_{ax}\frac{d}{dz}\left(\frac{p_i^R}{P^R}\right) = u^R\frac{p_i^R - p_i^{R,in}}{P^R} \text{ and } u^R = u^{R,in} \tag{3.9}$$

$$z=1: \quad \frac{d}{dz}\left(\frac{p_i^R}{P^R}\right) = 0 \text{ and } P^R = P^{R,out} \tag{3.10}$$

where the superscript R stands for retentate side, i refers to the i^{th} component, z is axial coordinate, u is the interstitial velocity, p is the partial pressure, P is the total pressure, D_{ax} is the effective axial dispersion coefficient, r^M is the internal radius of the membrane, A^R is the cross sectional area of the retentate chamber, V^R is the volume of the retentate chamber, is the void fraction of the catalyst beds (same value for both catalysts), $\Re$ is the gas constant, T is the absolute temperature, N is the flux through the membrane, and m_{cat} is the mass of catalyst, d_P is the catalyst particle diameter, μ is the gas viscosity and ρ_{gas} is the gas density. R is the rate of consumption or formation of the individual species, which is given by:

$$R_i = \sum_j \upsilon_{ij} r_j \tag{3.11}$$

where r_j is the reaction rate of reaction j (described below) and υ_{ij} is the stoichiometric coefficient for species i in the reaction j, taken negative for reactants, positive for reaction products, and null for the components that do not take part in the reaction.

Kinetic Model – MSR reaction

The reaction rate expressions used in this model are the ones developed by Peppley *et al.* [12]. It is assumed that the reaction occurs only at the catalyst surface, and that there is no mass transfer resistance between the bulk gas and the catalyst surface.

$$r_{MSR} = \frac{k_{MSR} K_{CH_3OH^{(1)}} \left(\frac{p_{CH_3OH}}{p_{H_2}^{1/2}} \right) \left(1 - \frac{p_{H_2}^3 p_{CO_2}}{K_{MSR}^e p_{CH_3OH} p_{H_2O}} \right) C_{S1}^T C_{S1a}^T S_A}{\left(1 + K_{CH_3OH^{(1)}} \frac{p_{CH_3OH}}{p_{H_2}^{1/2}} + K_{HCOO^{(1)}} p_{CO_2} p_{H_2}^{1/2} + K_{OH^{(1)}} \frac{p_{H_2O}}{p_{H_2}^{1/2}} \right) \left(1 + K_{H^{(1a)}}^{1/2} p_{H_2}^{1/2} \right)} \tag{3.12}$$

$$r_{WGS} = \frac{k_{WGS} K_{OH^{(1)}} \left(\frac{p_{CO} p_{H_2O}}{p_{H_2}^{1/2}} \right) \left(1 - \frac{p_{H_2} p_{CO_2}}{K_{WGS}^e p_{CO} p_{H_2O}} \right) C_{S1}^{T\ 2} S_A}{\left(\left(1 + K_{CH_3OH^{(1)}} \frac{p_{CH_3OH}}{p_{H_2}^{1/2}} + K_{HCOO^{(1)}} p_{CO_2} p_{H_2}^{1/2} + K_{OH^{(1)}} \frac{p_{H_2O}}{p_{H_2}^{1/2}} \right) \left(1 + K_{H^{(1a)}}^{1/2} p_{H_2}^{1/2} \right) \right)^2} \tag{3.13}$$

$$r_{MD} = \frac{k_{MD} K_{CH_3OH^{(2)}} \left(\frac{p_{CH_3OH}}{p_{H_2}^{1/2}} \right) \left(1 - \frac{p_{H_2}^2 p_{CO}}{K_{MD}^e p_{CH_3OH}} \right) C_{S2}^T C_{S2a}^T S_A}{\left(1 + K_{CH_3OH^{(2)}} \frac{p_{CH_3OH}}{p_{H_2}^{1/2}} + K_{OH^{(2)}} \frac{p_{H_2O}}{p_{H_2}^{1/2}} \right) \left(1 + K_{H^{(2a)}}^{1/2} p_{H_2}^{1/2} \right)} \tag{3.14}$$

where k_j and K_j^e are the reaction rate and equilibrium constants for reaction j, respectively; K_i is the adsorption coefficient for surface species i, C_{S1}^T and C_{S2}^T are the total catalyst surface concentration of sites 1 and 2, respectively, C_{S1a}^T and C_{S2a}^T are the total catalyst surface concentration of sites 1*a* and 2*a*, respectively, and S_A is the surface area of the catalyst.

3.2.2. Permeate Side

Partial Mass Balance

$$-\frac{d}{dz}\left(u^P p_i^P\right) + D_{ax} \frac{d}{dz}\left(P^P \frac{d}{dz}\left(\frac{p_i^P}{P^P} \right) \right) + \frac{2}{A^P} r^M \Re TN_i + \frac{m_{cat}^P}{V^P} \Re TR_i^P = 0 \tag{3.15}$$

Total Mass Balance

$$-\frac{d}{dz}\left(u^P P^P\right)+\frac{2\pi r^M}{A^P}\Re T\sum_i N_i+\frac{m_{cat}^P}{V^P}\Re T\sum_i R_i^P=0 \tag{3.16}$$

Pressure drop

$$-\frac{dP^P}{dz}=150\frac{\mu u^P}{d_p^2}\left(1-\ \right)^2+\frac{7}{4}\frac{\rho_{gas}\left(u^P\right)^2}{d_p}\frac{1-}{} \tag{3.17}$$

Boundary Conditions

$$z=0:\ \ D_{ax}\frac{d}{dz}\left(\frac{p_i^P}{P^P}\right)=u^P\frac{p_i^P-p_i^{P,in}}{P^P}\ \text{and}\ u^P=u^{P,in} \tag{3.18}$$

$$z=1:\ \ \frac{d}{dz}\left(\frac{p_i^P}{P^P}\right)=0\ \text{and}\ P^P=P^{P,out} \tag{3.19}$$

where superscript P stands for permeate side and A^P is the cross sectional area of the permeate chamber.

Kinetic Model – PROX reaction

The reaction rate expressions used in this model are the ones developed by Lee *et al.*[29]:

$$r_{CO}=k_{CO}p_{CO}^{0.91}p_{CO_2}^{-0.37}p_{H_2O}^{-0.62} \tag{3.20}$$

$$r_{H_2}=k_{H_2}p_{H_2}p_{CO_2}^{-0.48}p_{H_2O}^{-0.69} \tag{3.21}$$

3.2.3. Membrane Permeation Equation

The mass transfer of each component through the membrane is assumed to be described by its local driving force and a global mass transfer coefficient, according to the following equation:

$$N_i(z)=L_i\left\{\left(p_i^R(z)\right)^n-\left(p_i^P(z)\right)^n\right\} \tag{3.22}$$

where L is a permeance coefficient and n is equal to 1 (CMS membrane). The film transport resistance supposed at the interface gas/membrane is considered negligible and the permeability coefficients are assumed constant.

3.2.4. Dimensionless Equations

The model variables were made dimensionless with respect to the retentate feed velocity ($u^{R,in}$), to hydrogen (L_{H2} and M_{H2}) and to the reactor length, $l_{reactor}$. Changing for dimensionless variables and introducing suitable dimensionless parameters, equations (2.4)-(3.10), (2.13)-(3.19) and (2.16) become as follows:

$$-\frac{d}{dx}\left(u^{R^*}p_i^{R^*}\right)+\frac{1}{Pe}\frac{d}{dx}\left(P^{R^*}\frac{d}{dx}\left(\frac{p_i^{R^*}}{P^{R^*}}\right)\right)-\Gamma T^* N_i^* + DaT^* R_i^{R^*}=0 \tag{3.23}$$

$$-\frac{d}{dx}\left(u^{R^*}P^{R^*}\right)-\Gamma T^*\sum_i N_i^* + DaT^*\sum_i R_i^{R^*}=0 \tag{3.24}$$

$$-\frac{dP^{R^*}}{dx}=\alpha\mu u^{R^*}+\beta\frac{\rho_{gas}^*}{T^*}\left|u^{R^*}\right|u^{R^*} \tag{3.25}$$

$$x=0:\ \frac{1}{Pe}\frac{d}{dx}\left(\frac{p_i^{R^*}}{P^{R^*}}\right)=u_{x=0}^{R^*}\frac{p_i^{R^*}-p_{i,x=0^-}^{R^*}}{P^{R^*}}\ \text{and}\ u^{R^*}=u^{R,in^*} \tag{3.26}$$

$$x=1:\ \frac{d}{dx}\left(\frac{p_i^{R^*}}{P^{R^*}}\right)=0\ \text{and}\ P^{R^*}=P^{R,out^*} \tag{3.27}$$

$$-\frac{d}{dx}\left(u^{P^*}p_i^{P^*}\right)+\frac{1}{Pe}\frac{d}{dx}\left(P^{P^*}\frac{d}{dx}\left(\frac{p_i^{P^*}}{P^{P^*}}\right)\right)+\Gamma R_A T^* N_i^* + DaR_A R_{m_{cat}} R\ T^* R_i^{P^*}=0 \tag{3.28}$$

$$-\frac{d}{dx}\left(u^{P^*}P^{P^*}\right)-\Gamma R_A T^*\sum_i N_i^* + DaR_A R_{m_{cat}} R\ T^*\sum_i R_i^{P^*}=0 \tag{3.29}$$

$$-\frac{dP^{P^*}}{dx}=\alpha\mu u^{P^*}+\beta\frac{\rho_{gas}^*}{T^*}\left|u^{P^*}\right|u^{P^*} \tag{3.30}$$

$$x=0:\ \frac{1}{Pe}\frac{d}{dx}\left(\frac{p_i^{P^*}}{P^{P^*}}\right)=u_{x=0}^{P^*}\frac{p_i^{P^*}-p_{i,x=0^-}^{P^*}}{P^{P^*}}\ \text{and}\ u^{P^*}=u^{P,in^*} \tag{3.31}$$

$$x=1:\ \frac{d}{dx}\left(\frac{p_i^{P^*}}{P^{P^*}}\right)=0\ \text{and}\ P^{P^*}=P^{P,out^*} \tag{3.32}$$

$$N_i^*(x) = L_i^* \left[\left(p_i^{R*}(x) \right)^n - \left(p_i^{P*}(x) \right)^n \right] \tag{3.33}$$

where $\alpha = \frac{150(1-\varepsilon)^2 u_{ref} l_{reactor}}{\varepsilon^2 d_p^2 P_{ref}}$, $\beta = \frac{1.75(1-\varepsilon) M_{ref} u_{ref}^2 l_{reactor}}{d_p \Re T_{ref}}$, $R_i^{P*} = \frac{R_i^P}{k_{PROX,ref} P_{ref}^{-0.08}}$,

$p_i^* = \frac{p_i}{P_{ref}}$, $P^* = \frac{P}{P_{ref}}$, $u^* = \frac{u}{u_{ref}}$, $R_i^{R*} = \frac{R_i^R}{k_{SR,ref} C_{S1}^T C_{S1a}^T S_A}$, $L_i^* = \frac{L_i}{L_{ref}}$, $x = \frac{z}{l_{reactor}}$,

$Da = \frac{m_{cat}^R \Re T_{ref} k_{SR,ref} C_{S1}^T C_{S1a}^T S_A}{\varepsilon u_{ref} A^R P_{ref}}$, $R_A = \frac{A^R}{A^P}$, $R_{m_{cat}} = \frac{m_{cat}^P}{m_{cat}^R}$, $R = \frac{k_{PROX,ref}}{k_{SR,ref} C_{S1}^T C_{S1a}^T S_A P_{ref}^{0.08}}$,

$\Gamma = \frac{A^M \Re T_{ref} P_{ref}^{n-1} L_{ref}}{\varepsilon u_{ref} A^R}$, $Pe = \frac{l_{reactor} u_{ref}}{D_{ax}}$, M_{ref} is the reference molar mass, L_{ref} is the reference permeance coefficient of the membrane, x is the dimensionless axial coordinate of the reactor, Pe is the Peclet number for mass transfer, Da is the Damköhler number, Γ is the dimensionless permeation contact time (ratio between the permeate flow of reference component when fed pure for null permeate pressure and the total feed flow), $k_{MSR,ref}$ is the rate constant for the steam reforming reaction at the reference temperature, $k_{PROX,ref}$ is the rate constant for the PROX reaction at the reference temperature, P_{ref} is the reference pressure (set to 100 kPa), T_{ref} is the reference temperature (set to 298 K), u_{ref} is the reference velocity and A^M is the permeation area of the membrane.

3.2.5. Numerical solution strategy

To simulate the steam reforming membrane reactor, it is necessary to solve equations (2.17)-(2.19) and (3.28)-(2.22) with the respective boundary conditions. In order to overcome numerical instability problems, it was used the same strategy adopted already [30] for solving the equations: a time derivative term was added to their right-hand side, transforming this problem into a pseudo-transient one. The resultant partial differential equations were spatially discretized using the finite volumes method [31]. The time advancement was accomplished by LSODA [32], a numerical package developed at the Lawrence Livermore National Laboratory. The

solution was considered to be in steady state when the time derivative of each dependent variable and for each of the spatial coordinate was smaller than a pre-defined value.

3.3. Discussion

This study is focused on the advantages of adding a PROX catalyst into the permeate stream of a methanol steam reforming membrane reactor. The effect of several parameters in the enhancement of methanol conversion and hydrogen recovery is also studied. The developed mathematical model was previously validated by Sá *et al.* [33]. The operating parameters for the simulation are presented in Table 3.1. The steam to carbon ratio was varied from 1 to 3 according to what is commonly used in the literature [34]. The temperature was in the range of 473-493 K [35], the permeate pressure was set to 1 bar and the retentate pressure to 4 bar in order to achieve a high driving force. The sweep gas used was water vapour and the sweep ratio (ratio between the inlet permeate velocity and the inlet retentate velocity) was set to 1 [35]. After preliminary simulations, the concentration of oxygen in the permeate stream was set to 5 % in order to achieve high carbon monoxide conversions. The hydrogen permeance was taken from Harale *et al.* [24]. The permeance data were used to estimate the permeation contact time values, using feed flow rates and membrane areas commonly used in the literature [23, 34]. The *Da* number range was estimated using the kinetic data from Peppley *et al.* [12] and the commonly used catalyst mass and feed flow rates [23, 34].

Table 3.1 – Parameters for the simulation

$Da \in [0.01, 100]$	$\Gamma \in [0.5, 4]$
$P^{R,out} = 400$ kPa	$P^{P,out} = 100$ kPa
$T \in [473, 493]$ K	$S/C\ (H_2O/CH_3OH) \in [1, 3]$
L_{ref} = 3.53x10^{-7} kmol·m^{-2}·s^{-1}·kPa^{-1}	$L^*_{H_2}$ = 1
$L^*_{H_2O}$ = 0.313	$L^*_{CH_3OH}$ = 0.001
$L^*_{CO_2} = 0.08$	L^*_{CO} = 0.015
$L^*_{O_2} = 0.07$	

3.3.1. Carbon monoxide permeation

As mentioned before, the CMS membranes present the drawback of being permeable to other species besides hydrogen. Among all compounds present in the reaction mixture, the removal of carbon monoxide is the most imperative once it poisons the anodic catalyst of the fuel cell. The permeation of carbon monoxide through the CMS membranes creates a permeate stream with concentrations above 10 ppm of this species, which must be reduced. As carbon monoxide is formed by the endothermic reactions methanol decomposition and reverse water gas shift (rWGS), their extent can be reduced by lowering the reaction temperature. In addition, the increase of the steam to carbon feed ratio can reduce the formation of carbon monoxide. The excess of steam will promote the MSR reaction toward the products and less amount of methanol is decomposed to carbon monoxide. In the same way, the WGS reaction is shifted toward the products, producing carbon dioxide and hydrogen and consuming carbon monoxide. Figure 3.2 illustrates these effects on the carbon monoxide concentration at the permeate side.

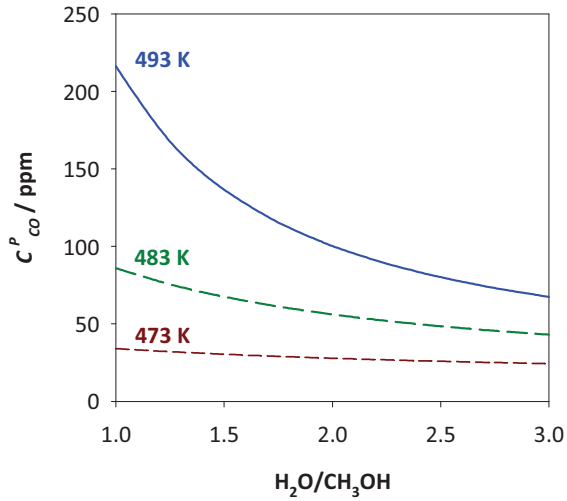

Figure 3.2 – Carbon monoxide concentration at the permeate side as a function of the temperature and the H_2O/CH_3OH feed ratio for a CMS membrane reactor. *Da* = 50 and Γ = 2.

Although the amount of CO decreases with higher steam to carbon ratios and lower reaction temperatures, it still remains above 10 ppm and, thus, too high to be fed into a PEMFC. A strategy to reduce its concentration in the permeate stream is to promote its oxidation to CO_2, by adding a PROX reactor to the system. Some authors [36, 37] placed a PROX reactor at the end of the MSR reactor and reported good results in the decrease the content of CO. However, this implies a larger system with two reactors instead of one. Additionally, if all the CO produced in the MSR reaction is converted to CO_2, a large amount of this species will be fed to the fuel cell, which has a negative effect on its performance [14]. In this line of thought, a different configuration is proposed, as shown in Figure 3.1. By placing a PROX catalyst in the permeate side, the majority of CO that permeates through the membrane can be eliminated by reaction with O_2, producing CO_2. As the CO permeability through CMS membrane is low, only a small part of the CO produced in the retentate side permeates through the membrane, converting to CO_2 by the PROX reaction. This means that the performance of the fuel cell will not be compromised by the increase of the CO_2 concentration. In order to compare the purity of the permeate stream of a

MSR-MR and a MSR+PROX-MR, Figure 3.3 shows the permeate CO concentration for both systems.

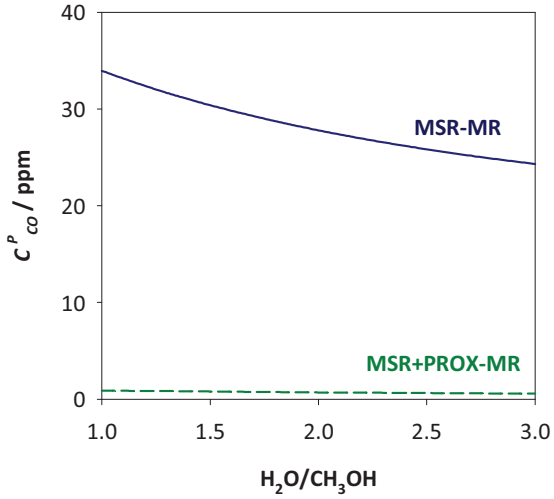

Figure 3.3 - Permeate CO concentration as a function of the steam to carbon (S/C) ratio for a MSR-MR and a MSR+PROX-MR. *Da* = 50, Γ = 2 and *T* = 473 K.

As expected, the system MSR+PROX-MR shows clear advantages in what concerns the permeate CO concentration. The conversion of CO to CO_2 is very high, reducing the CO content to levels below 2 ppm. With this low concentration, is now possible to use the permeate stream to feed a PEMFC.

3.3.2. Carbon dioxide permeation

As mentioned before, in addition to the CO_2 that permeates through the CMS membrane, there is also a small amount that is formed in the PROX reaction at the permeate side. In order to minimize the negative effects of CO_2 on the performance of the fuel cell, its concentration should be maintained below 20 % [14]. Accordingly, the permeation contact time value, Γ, should be lowered as shown in Figure 3.4. This parameter represents the ratio between a reference permeation flow and the feed flow. Accordingly, the higher the value of Γ, the higher is the fraction of the feed flow that permeates - the stage cut.

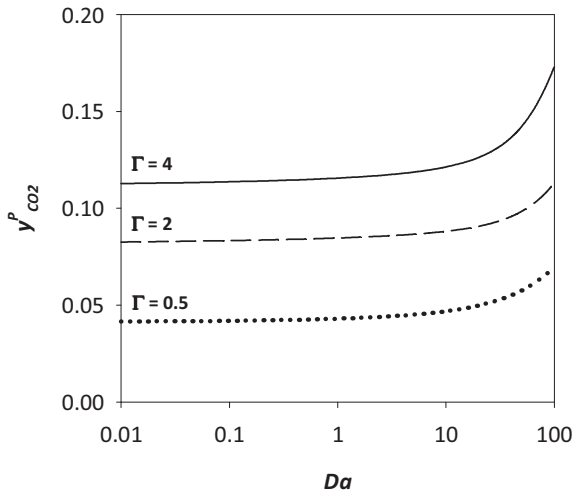

Figure 3.4 - Carbon dioxide molar fraction at the permeate side (dry basis) as a function of the Damköhler number for various dimensionless permeation contact time values. S/C = 3 and *T* = 473 K.

As can be seen in Figure 3.4, lower values of Γ and *Da* result in lower CO_2 concentrations at the permeate side. As desired, the content of CO_2 is kept under 20 % for all simulations. Nevertheless, lowering the permeation contact time value can also present disadvantages by diminishing the amount of hydrogen that permeates. In the same way, small values of *Da* result in low methanol conversions. As so, it is essential to study which conditions enhance the performance of the membrane reactor.

3.3.3. Methanol conversion and hydrogen recovery

At high Damköhler numbers the reaction rates are high, which enhances the production of hydrogen as a consequence of increasing the methanol conversion:

$$X_{CH_3OH} = \frac{F^{R,in*}_{CH_3OH} - F^{R,out*}_{CH_3OH} - F^{P,out*}_{CH_3OH}}{F^{R,in*}_{CH_3OH}} \tag{3.34}$$

where F_i : $F_i^* = \frac{p_i^* u^*}{T^*}$. Without doubt, the conversion should be as high as possible without the prejudice of a high purity permeate stream.

In order to find a compromise between high hydrogen production and high permeate purity, the influence of the *Da* number and the permeation contact time in the methanol conversion is illustrated in Figure 3.5.

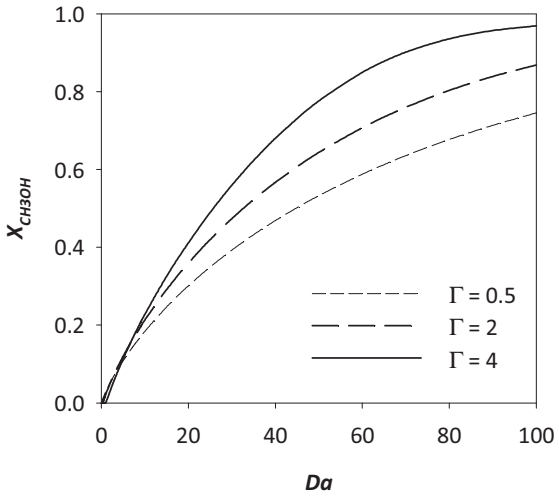

Figure 3.5 - Methanol conversion as a function of the Damköhler number for various dimensionless permeation contact time values. S/C = 3 and *T* = 473 K.

As expected, methanol conversion is enhanced by high *Da* numbers due to the high reaction rates. In addition, high permeation contact time values represent high stage cut, thus high relative permeation flow. The increase of hydrogen permeation decreases its partial pressure at the retentate side and shifts the MSR and the MD reactions toward the products, resulting in higher methanol conversion.

The hydrogen recovery is also an important factor to evaluate the performance of the membrane reactor. It represents the amount of hydrogen produced that is recovered at the permeate side - eq. (3.35). The permeation contact time and the *Da* number have a significant effect in this parameter as shown in Figure 3.6.

$$Rec_{H_2} = \frac{F_{H_2}^{P*}}{F_{H_2}^{P*} + F_{H_2}^{R*}} \tag{3.35}$$

Concerning the hydrogen recovery, the effect of the Damköhler number is different for high and low permeation contact time values, as presented in Figure 3.6. For this reason, the analysis must be made in two steps. First, at low Γ values, the membrane reactor operates at low stage cut. This means that the permeation flow is low compared to the retentate feed flow. At this stage, with the increase of the *Da* number, the amount of hydrogen produced increases and its partial pressure at the retentate side also increases. Consequently, the hydrogen driving force is higher, which should promote the increase of its recovery. However, Figure 3.6 shows the opposite effect. In fact, at low Γ values, the feed flow rate is high and the membrane area is small. As a result, only a minor part of the hydrogen produced is able to permeate through the membrane, being recovered at the permeate side. This means that the permeation does not compensate the increase of the hydrogen production, resulting in lower hydrogen recovery.

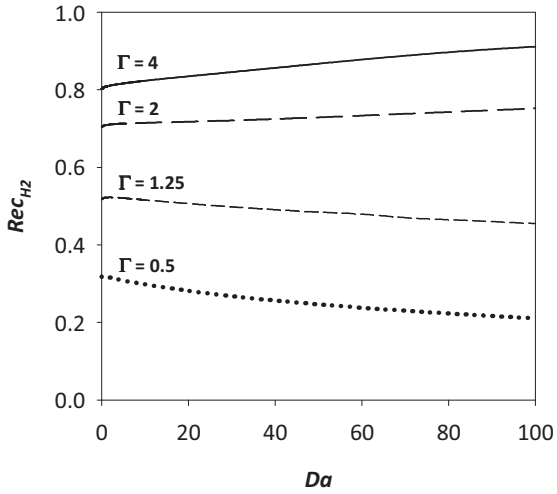

Figure 3.6 - Hydrogen recovery as a function of the Damköhler number for various dimensionless permeation contact time values. S/C = 3 and *T* = 473 K.

On the other hand, at high Γ values, the membrane reactor operates at high stage cut, and the relative permeation flow is also high. As explained before, the increase of the *Da* number results in higher hydrogen partial pressure at the retentate

side, thus in higher driving force. As a result, most of the hydrogen produced permeates through the membrane, increasing the hydrogen recovery.

Compiling all the information gathered from Figure 3.2 to Figure 3.6, this system allows to achieve a hydrogen stream with CO concentrations below 2 ppm, CO_2 below 20 %, high methanol conversion and high hydrogen recovery. If desired, the amount of CO_2 can be lowered to 10 % by using a permeation contact time value of 2 (Figure 3.4), with a conversion of 85 % (Figure 3.5) and a hydrogen recovery of 75 % (Figure 3.6).

3.4. Conclusions

Two membrane reactors configurations were compared concerning the purity of the permeate stream, a common MSR-MR and a MSR+PROX-MR. It was shown that the presence of a PROX reactor at the permeate side positively affects the permeate stream composition. Unlike the MSR-MR, the MSR+PROX-MR converts almost all CO present in the permeate stream to CO_2. More specifically, the CO concentration at the permeate side was kept under 2 ppm and the CO_2 content remained below 20 %. The main advantage of this MR configuration is the possibility of using the permeate stream to feed a PEMFC, without poisoning the anodic catalyst of the fuel cell.

It was also studied in which conditions the performance of the membrane reactor was enhanced in terms of methanol conversion and hydrogen recovery. In particular, it was concluded that methanol conversion is enhanced by the *Da* number and the permeation contact time value. On the other hand, the hydrogen recovery increases with the *Da* number at high Γ, but decreases with the *Da* number at low Γ.

Finally, it was concluded that this system is appropriate to produce a hydrogen stream with CO concentrations below 2 ppm, CO_2 below 20 %, high methanol conversion and high hydrogen recovery. If desired, the amount of CO_2 can be lowered to 10 % by using a permeation contact time value of 2, with a conversion of 85 % and a hydrogen recovery of 75 %.

Acknowledgments

The work of Sandra Sá was supported by FCT, grant SFRH/BD/30385/2006. The research was also supported by funds from FCT projects PTDC/EQU-EQU/71617/2006 and POCI/ENR/59323/2004.

List of Abbreviations and symbols

Abbreviations		Definition	Units
A	–	area	m^2
C_{S1}^T	–	total catalyst surface concentration of site 1	$mol \cdot m^{-2}$
C_{S2}^T	–	total catalyst surface concentration of site 2	$mol \cdot m^{-2}$
C_{S1a}^T	–	total catalyst surface concentration of site 1a	$mol \cdot m^{-2}$
C_{S2a}^T	–	total catalyst surface concentration of site 2a	$mol \cdot m^{-2}$
Da	–	Damköhler number	
D_{ax}	–	axial dispersion coefficient	$m^2 \cdot s^{-1}$
d_p	–	catalyst diameter	m
F_i^*	–	dimensionless rate of species *i*	
k_i	–	rate constant for reaction *i*	$m^2 \cdot s^{-1} \cdot mol^{-1}$
K_j^e	–	equilibrium constant for reaction *j*	
K_i	–	adsorption coefficient for surface species *i*	
$k_{PROX,ref}$	–	rate constant for the prox reaction at the reference temperature	$m^2 \cdot s^{-1} \cdot mol^{-1}$
$k_{SR,ref}$	–	rate constant for the MSR reaction at the reference temperature	$m^2 \cdot s^{-1} \cdot mol^{-1}$
L_i	–	permeance coefficient of species *i*	$kmol\ m^{-2} \cdot s^{-1} \cdot kPa^{-n}$
$l_{reactor}$	–	reactor's length, m	
m_{cat}	–	mass of catalyst	kg
$\boldsymbol{M_{ref}}$	–	reference molar mass	$kg \cdot mol^{-1}$
N_i	–	flux of the component *i* through the membrane	$mol \cdot s^{-1} \cdot m^{-2}$
Pe	–	*Peclet* number for mass transfer	
p_i	–	partial pressure of component *i*	kPa
P_{ref}	–	reference pressure	Pa
P	–	total pressure	kPa
$\Re$	–	gas constant	$kPa\ m^3 \cdot mol^{-1} \cdot K^{-1}$

r_j	–	rate of reaction *j*	$mol \cdot s^{-1} \cdot kg_{cat}^{-1}$
r^R	–	radius of the reactor	m
R_i	–	rate of consumption or formation of species *i*	$mol \cdot s^{-1} \cdot kg_{cat}^{-1}$
R_A	–	ratio between the retentate and permeate areas	
$R_{m_{cat}}$	–	ratio between the permeate and retentate catalyst mass	
S_A	–	surface area of the catalyst	$m^2 \cdot kg^{-1}$
T	–	absolute temperature	K
u	–	interstitial velocity	$m \cdot s^{-1}$
u_{ref}	–	reference velocity	$m \cdot s^{-1}$
x	–	relative length of the reactor	

Greek symbols		**Definition**	**Units**
	–	void fraction of the catalyst beds	
Γ	–	dimensionless permeation contact time	
	–	gas viscosity	$kg \cdot m^{-1} \cdot s^{-1}$
	–	dimensionless time variable	
	–	gas density	$kg \cdot m^{-3}$
$_{cat}$	–	catalyst density	$kg_{cat} \cdot m^{-3}$
$_{ij}$	–	stoichiometric coefficient for species *i* in the reaction *j*	

Superscripts		**Definition**
M	–	membrane
R	–	retentate
P	–	permeate

Subscripts		Definition
MD	–	methanol decomposition
MSR	–	steam reforming
PROX	–	preferential oxidation
rWGS	–	reverse water gas shift
WGS	–	water gas shift

References

[1] D. Ramirez, L.F. Beites, F. Blazquez, J.C. Ballesteros, Distributed generation system with PEM fuel cell for electrical power quality improvement, Int. J. Hydrogen Energy, 33 (2008) 4433-4443.

[2] S.J. Peighambardoust, S. Rowshanzamir, M. Amjadi, Review of the proton exchange membranes for fuel cell applications, Int. J. Hydrogen Energy, 35 (2010) 9349-9384.

[3] Y. Wang, K.S. Chen, J. Mishler, S.C. Cho, X.C. Adroher, A review of polymer electrolyte membrane fuel cells: Technology, applications, and needs on fundamental research, Appl. Energy, 88 (2011) 981-1007.

[4] A.S. Damle, Hydrogen production by reforming of liquid hydrocarbons in a membrane reactor for portable power generation—Model simulations, J. Power Sources, 180 (2008) 516-529.

[5] D.G. Löffler, K. Taylor, D. Mason, A light hydrocarbon fuel processor producing high-purity hydrogen, J. Power Sources, 117 (2003) 84-91.

[6] S. Ahmed, M. Krumpelt, Hydrogen from hydrocarbon fuels for fuel cells, Int. J. Hydrogen Energy, 26 (2001) 291-301.

[7] J.C. Telotte, J. Kern, S. Palanki, Miniaturized Methanol Reformer for Fuel Cell Powered Mobile Applications, Int. J. Chem. Reactor Eng., 6 (2008).

[8] A. Basile, A. Parmaliana, S. Tosti, A. Iulianelli, F. Gallucci, C. Espro, J. Spooren, Hydrogen production by methanol steam reforming carried out in membrane reactor on Cu/Zn/Mg-based catalyst, Catal. Today, 137 (2008) 17–22.

[9] D.R. Palo, R.A. Dagle, J.D. Holladay, Methanol Steam Reforming for Hydrogen Production, Chem. Rev., 107 (2007) 3992-4021.

[10] G.A. Olah, A. Goeppert, G.K.S. Prakash, Beyond Oil and Gas: The Methanol Economy, 2nd ed., WILEY-VCH Verlag GmbH & Co. KGaA, Weinheim, 2006.

[11] B.A. Peppley, J.C. Amphlett, L.M. Kearns, R.F. Mann, Methanol steam reforming on Cu/ZnO/Al2O3. Part 1: the reaction network, Appl. Catal. A, 179 (1999) 21-29.

[12] B.A. Peppley, J.C. Amphlett, L.M. Kearns, R.F. Mann, Methanol steam reforming on Cu/ZnO/Al2O3 catalysts. Part 2. A comprehensive kinetic model, Appl. Catal. A, 179 (1999) 31-49.

[13] H.P. Dhar, L.G. Christner, A.K. Kush, Nature of CO Adsorption during H2 Oxidation in Relation to Modeling for CO Poisoning of a Fuel Cell Anode, J. Electrochem. Soc., 134 (1987) 3021-3026.

[14] A. Bayrakçeken, L. Türker, I. Eroglu, Improvement of carbon dioxide tolerance of PEMFC electrocatalyst by using microwave irradiation technique, Int. J. Hydrogen Energy, 33 (2008) 7527-7537.

[15] B.K.R. Nair, M.P. Harold, Hydrogen generation in a Pd membrane fuel processor: Productivity effects during methanol steam reforming, Chem. Eng. Sci., 61 (2006) 6616–6636.

[16] C.-H. Fu, J.C.S. Wu, Mathematical simulation of hydrogen production via methanol steam reforming using double-jacketed membrane reactor, Int. J. Hydrogen Energy, 32 (2007) 4830-4839.

[17] A. Iulianelli, T. Longo, A. Basile, Methanol steam reforming in a dense Pd–Ag membrane reactor: The pressure and WHSV effects on CO-free H2 production, J. Membr. Sci., 323 (2008) 235–240.

[18] A. Basile, F. Gallucci, L. Paturzo, A dense Pd/Ag membrane reactor for methanol steam reforming: Experimental study, Catal. Today, 104 (2005) 244-250.

[19] M.P. Harold, B. Nair, G. Kolios, Hydrogen generation in a Pd membrane fuel processor: assessment of methanol-based reaction systems, Chem. Eng. Sci., 58 (2003) 2551 - 2571.

[20] M.D. Falco, Pd-based membrane steam reformers: A simulation study of reactor performance, Int. J. Hydrogen Energy, 33 (2008) 3036 – 3040.

[21] G.A. Sznejer, I. Efremenko, M. Sheintuch, Carbon Membranes for High Temperature Gas Separations: Experiment and Theory, AIChE J., 50 (2004).

[22] A.F. Ismail, L.I.B. David, A review on the latest development of carbon membranes for gas separation, J. Membr. Sci., 193 (2001) 1-18.

[23] X. Zhang, H. Hu, Y. Zhu, S. Zhu, Methanol Steam Reforming to Hydrogen in a Carbon Membrane Reactor System, Ind. Eng. Chem. Res., 45 (2006) 7997-8001.

[24] A. Harale, H.T. Hwang, P.K.T. Liu, M. Sahimi, T.T. Tsotsis, Experimental studies of a hybrid adsorbent-membrane reactor (HAMR) system for hydrogen production, Chem. Eng. Sci., 62 (2007) 4126 – 4137.

[25] D.L. Trimm, Minimisation of carbon monoxide in a hydrogen stream for fuel cell application, Appl. Catal., A, 296 (2005) 1-11.

[26] Y. Choi, H.G. Stenger, Kinetics, simulation and insights for CO selective oxidation in fuel cell applications, J. Power Sources, 129 (2004) 246-254.

[27] S. Ergun, Fluid flow through packed columns, Chemical Engineering Progress 48 (1952) 89-94.

[28] P.V. Danckwerts, Continuous flows systems - distribution of residence times, Chem. Eng. Sci., 2 (1953) 1.

[29] H.C. Lee, D.H. Kim, Kinetics of CO and H2 oxidation over CuO-CeO2 catalyst in H2 mixtures with CO2 and H2O, Catal. Today, 132 (2008) 109–116.

[30] J.M. Sousa, A. Mendes, Simulation study of a dense polymeric catalytic membrane reactor with plug–flow pattern, Chem. Eng. J., 95 (2003) 67-81.

[31] P. Cruz, J.C. Santos, F.D. Magalhães, A. Mendes, Simulation of separation processes using finite volume method, Comput. Chem. Eng., 30 (2005) 83-98.

[32] L. Petzold, Automatic Selection of Methods for Solving Stiff and Nonstiff Systems of Ordinary Differential Equations, Siam J. Sci. Stat. Computing, 4 (1983) 136-148.

[33] S. Sá, H. Silva, J.M. Sousa, A. Mendes, Hydrogen production by methanol steam reforming in a membrane reactor: Palladium vs carbon molecular sieve membranes, J. Membr. Sci., 339 (2009) 160-170.

[34] F. Gallucci, A. Basile, Co-current and counter-current modes for methanol steam reforming membrane reactor, Int. J. Hydrogen Energy, 31 (2006) 2243 - 2249.

[35] F. Gallucci, A. Basile, Pd–Ag membrane reactor for steam reforming reactions: A comparison between different fuels, Int. J. Hydrogen Energy, 33 (2008) 1671 - 1687.

[36] Y. Men, G. Kolb, R. Zapf, D. Tiemann, M. Wichert, V. Hessel, H. Löwe, A complete miniaturized microstructured methanol fuel processor/fuel cell system for low power applications, Int. J. Hydrogen Energy, 33 (2008) 1374-1382.

[37] T. Kim, S. Kwon, MEMS fuel cell system integrated with a methanol reformer for a portable power source, Sens. Actuators A: Phys., 154 (2009) 204–211.

Part III

Experimental

Chapter 4. Steam reforming of methanol over a $CuO/ZnO/Al_2O_3$ catalyst. Part I: Kinetic modelling[1]

Abstract

A kinetic study of the methanol steam reforming reaction was performed over a commercial $CuO/ZnO/Al_2O_3$ catalyst (Süd-Chemie, G66 MR), in the temperature range of 200-300 °C. The reactions considered in this work were methanol steam reforming (MSR) and reverse water gas shift (rWGS). Several MSR kinetic rate models developed by different authors were compared and determined the one that best fitted the experimental data. A kinetic Langmuir-Hinshelwood model was proposed based on the work by Peppley *et al.* [1]. The kinetic expressions that presented the best fit were used to simulate the packed bed reactor with a one-dimensional model. A good agreement between the mathematical model and the experimental data was observed.

[1] S. Sá, J.M. Sousa, A. Mendes, Steam reforming of methanol over a $CuO/ZnO/Al_2O_3$ catalyst. Part I: Kinetic modelling, (Submited to Chemical Engineering Science).

4.1. Introduction

The current interest in developing alternative sources of energy for mobile and small scale applications has increased the research in polymer electrolyte membrane fuel cells (PEMFC) [2-4]. With the purpose of producing hydrogen for PEMFC, the reforming of alcohols and hydrocarbons allows a hydrogen production *in situ,* avoiding the problems of hydrogen storage and transportation [5-9]. The advantages of methanol molecule are related to the absence of a strong C-C bond that allows a low temperature reforming (200-300 °C). This low temperature is not possible for other fuels as methane (reformed above 500 °C [10]) or ethanol (reformed around 400 °C [11]).

Methanol steam reforming (MSR), eq. (3.1), has been vastly studied in the literature [1, 12-17].

$$CH_3OH + H_2O \rightleftharpoons CO_2 + 3H_2 \qquad \Delta H = 49.7\,kJ\cdot mol^{-1} \qquad (4.1)$$

Despite the number of studies over $CuO/ZnO/Al_2O_3$ catalysts [1, 13, 18-20], there is still a great discussion over the reaction mechanism. Santacesaria *et al.* [21] proposed that the steam reforming reaction sequence is methanol decomposition (MD) followed by the water gas shift (WGS) :

$$CH_3OH \rightleftharpoons CO + 2H_2 \qquad \Delta H = 92.0\,kJ\cdot mol^{-1} \qquad (4.2)$$

$$CO + H_2O \rightleftharpoons CO_2 + H_2 \qquad \Delta H = -41.2\,kJ\cdot mol^{-1} \qquad (4.3)$$

However, as carbon monoxide is produced first in the reaction system, some authors claim that its concentration should be equal or greater than the one at WGS equilibrium, which is not observed [14, 19, 20]. Takahashi *et al.* [22], on the other hand, suggested a mechanism involving a methyl formate intermediate, which was later supported by Jiang *et al.* [23, 24]. Methanol dehydrogenates to produce methyl formate and hydrogen. Afterwards, methyl formate is hydrolyzed to form formic acid and methanol, followed by decomposition of formic acid to form carbon dioxide [25]:

$$2CH_3OH \rightarrow CH_3OCHO + 2H_2 \qquad (4.4)$$

$$CH_3OCHO + H_2O \rightarrow CH_3OH + HCOOH \quad (4.5)$$

$$HCOOH \rightarrow CO_2 + 2H_2 \quad (4.6)$$

As CO is not formed by methanol decomposition, it has been suggested that its formation is due to the reverse water gas shift (rWGS) reaction [14, 19, 20]:

$$CO_2 + H_2 \rightleftharpoons CO + H_2O \quad (4.7)$$

The reaction scheme remains controversial, which has led to the development of many different kinetic rate expressions. Jiang *et al.* [23, 24] proposed a Langmuir–Hinshelwood (LH) rate expression based in a single kind of active sites. Later, Peppley *et al.* [1] developed a more comprehensive kinetic model involving all three reactions, MSR, WGS and MD. The mechanism is based on two types of active sites, where hydrogen adsorption does not compete for the active sites that the oxygen-containing species adsorb on. More recently, other authors have used Peppley's kinetic expressions to model their own experimental data [13, 26]. On the other hand, some authors have considered methanol decomposition to be negligible due the low concentration of carbon monoxide [14, 19, 20]. More specifically, Patel *et al.* [20] developed a mechanistic kinetic model for the MSR reaction based on the formation of formic acid from formaldehyde as the rate-determining step. The authors also proposed a kinetic expression for the rWGS reaction with the formation of adsorbed CO and surface hydroxyls from formate species as the rate-determining step.

In this work, the commercial $CuO/ZnO/Al_2O_3$ catalyst G66 MR from Süd-Chemie, was used for methanol steam reforming catalytic activity measurements. Due to the low concentration of carbon monoxide in the reaction products, the same approach of Lee *et al.* [19] and Patel *et al.* [20] was made, neglecting the contribution of methanol decomposition. Several kinetic expressions were used to fit the experimental data. The kinetic parameters for each model were estimated by nonlinear regression, minimizing the sum of the residual squares. The best agreement between the experimental data and the model results was obtained for the Langmuir–Hinshelwood models based on the work of Peppley *et al.* [1], for both MSR and rWGS reactions. These kinetic expressions were used to simulate the packed bed

reactor using a one-dimensional model. A good agreement between the mathematical model and the experimental data was observed.

4.2. Experimental

The catalyst used in this study was the commercial $CuO/ZnO/Al_2O_3$ G66 MR, from Süd-Chemie. Its physical properties and chemical composition are listed in Table 4.1. Steam reforming of methanol was performed at atmospheric pressure in a tubular reactor (7.75 mm i.d. and 40 mm lenght) placed inside a temperature controlled oven. A thermocouple placed in the packed bed reactor was used to measure the reaction temperature. Around 200 mg of catalyst previously crushed and sieved to a range of particle sizes of 250-355 μm, was diluted with glass spheres of the same particle size to avoid temperature gradients in the packed bed reactor. The particle size was chosen after preliminary studies regarding intraparticle diffusion limitations. Catalyst particles sizes from 180 μm to 500 μm were tested and it was observed that the conversion of methanol decreased for particles larger than 300 μm. Plug flow conditions were ensured keeping a catalyst bed length to catalyst size ratio above 50 ($l_{reactor}/d_{particle} \geq 50$) and the reactor diameter to size ratio above 30 ($d_{reactor}/d_{particle} \geq 30$) [27].

Table 4.1 - Physical properties of the MSR catalyst, G66 MR, as reported by Süd-Chemie

Chemical composition	
CuO (wt.%)	66
ZnO (wt.%)	23
Al_2O_3 (wt.%)	11
Bulk density ($kg \cdot dm^{-3}$)	1.1
Specific surface area ($m^2 \cdot g^{-1}$)	70

Kinetic experiments were performed in the temperature range of 200-300 °C and space time ratios $W_{cat}/F^0_{CH_3OH}$ of 3-15 $kg_{cat} \cdot s \cdot mol^{-1}$. Prior to the catalytic measurements,

the catalyst was reduced *in situ* with a stream of 10 % H_2 in Ar at 100 $cm^3 \cdot min^{-1}$, from 30 °C to 300 °C, maintaining the final temperature for 1 h. The gas feed flow rate was controlled by mass flow controllers from Bronkhorst (model F-201C ± 0.1 % FS) – Figure 4.1. During the catalytic activity measurements, a CEM-System (Controlled Evaporation and Mixing) from Bronkhorst promoted controlled evaporation of the required methanol aqueous solution before entering the reactor. At the end of the reactor, the stream is composed by the reaction products H_2, CO_2, CO, Ar and the un-reacted water and methanol. The condensable reactants were separated from the gas mixture in a condenser at ca. -10 °C placed outside the oven. The liquid was later collected and analysed in a Karl Fisher titrator from Metrohm for water concentration quantification. On the other hand, the product gas stream was analysed in a quadruple mass spectrometer, Pfeiffer Vacuum OmniStar GSD 320 (detection limit < 1 ppm). Figure 4.1 shows a detailed scheme of the experimental unit.

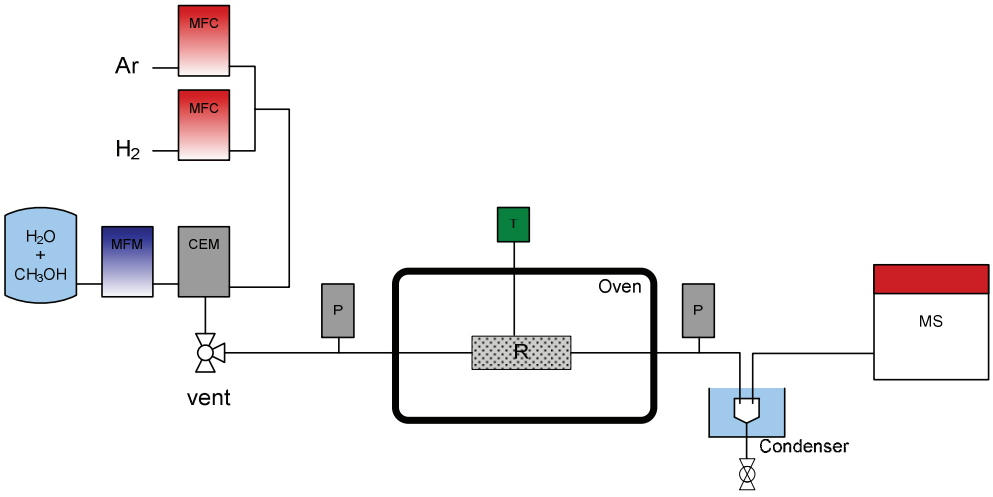

Figure 4.1 – Scheme of the experimental unit. CEM - controlled evaporation and mixing system; MFC - mass flow controller; MFM - mass flow meter; MS - mass spectrometer; P - pressure transducer; T - thermocouple.

4.3. Results and discussion

4.3.1. Catalytic activity

Typical catalytic activity measurements were performed with the packed bed reactor showing the effect of contact time in methanol conversion. The different contact time values were attained keeping the catalyst mass at a constant value and changing the methanol feed flow rate. It is clear from Figure 4.2 that the conversion of methanol is enhanced by the increase of both contact time and temperature, reaching almost complete conversion at 300 °C. Conversely, the hydrogen production rate decreases with the increase of contact time as shown in Figure 4.3. Although the conversion of methanol is high for high contact time values, this corresponds to low feed flow rates, thus the amount of hydrogen produced is low. The obtained results agree well with others reported in the literature with similar catalysts, namely Agrell *et al.* [18] and Purnama *et al.* [14].

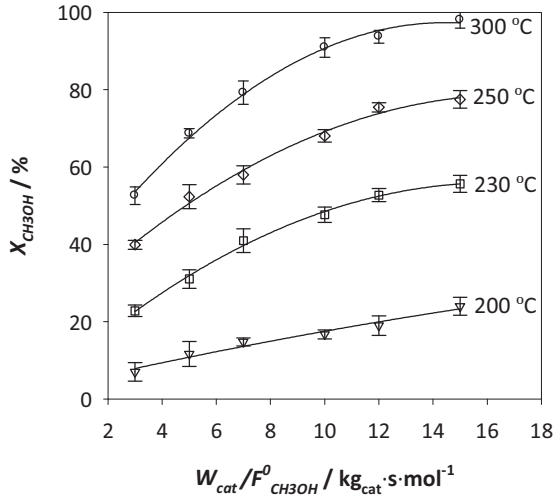

Figure 4.2 – Methanol conversion as a function of $W_{cat}/F^0_{CH_3OH}$ ratio at different temperatures, *S/M* = 1.5, *P* = 1 bar.

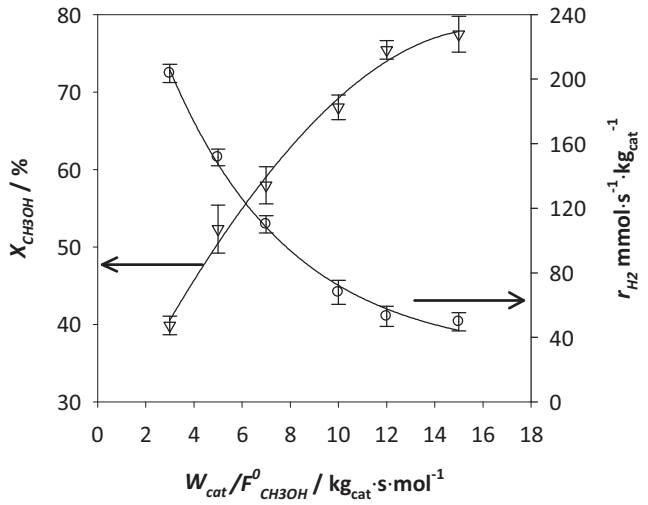

Figure 4.3 – Methanol conversion and hydrogen production rate as a function of $W_{cat}/F^0_{CH_3OH}$ ratio at 250 °C, *S/M* = 1.5, *P* = 1 bar.

4.4. Methanol steam reforming kinetic models

Several studies are reported in the literature regarding the kinetics of the methanol steam reforming reaction over $CuO/ZnO/Al_2O_3$ catalysts [1, 13, 14, 18-20, 28]. While some authors consider all three reactions (3.1)-(3.3) [1, 13, 29], others claim that the amount of carbon monoxide is so low that it can only be produced by the reverse water gas shift reaction, excluding methanol decomposition [19, 20]. In the present work, the concentration of carbon monoxide at the exit of the packed bed reactor was below the rWGS equilibrium one for all experimental runs, as exemplified in Figure 4.4. Accordingly, the contribution of methanol decomposition was neglected and only the methanol steam reforming and the reverse water gas shift reactions were considered. Several kinetic expressions were used to fit the experimental data as presented in the following subsections.

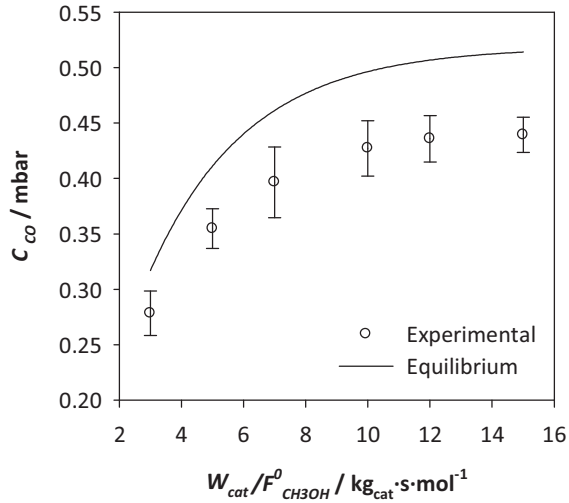

Figure 4.4 – Carbon monoxide partial pressure as a function of $W_{cat}/F^{0}_{CH_3OH}$ ratio, T = 230 °C, S/M = 1.5, P = 1 bar.

4.4.1. Empirical reaction rate models

Although power law models are not based in any reaction mechanism, they have been successfully used to fit experimental data in the literature [14, 19, 26]. In the present study, two different power laws are considered, taken from the work of Lee *et al.* [19] (model 1) and Samms *et al.* [26] (model 2).

Model 1

$$r_{MSR} = k_{MSR} p^{a}_{CH_3OH} \left(\quad + p_{H_2} \right)^{b} \tag{4.8}$$

Model 2

$$r_{MSR} = k_{MSR} p^{a}_{CH_3OH} p^{b}_{H_2O} p^{c}_{CO_2} p^{d}_{H_2} \tag{4.9}$$

4.4.2. Mechanistic derived reaction rate models

The Langmuir-Hinshelwood (LH) mechanisms presented below were proposed by different authors and are based in different reaction mechanisms. Tesser *et al.* [30]

proposed a LH model considering the existence of a detrimental effect of water and hydrogen partial pressure in the reaction rate (model 3).

Model 3

$$r_{MSR} = \frac{k_{MSR} K_{CH_3OH} p_{CH_3OH}}{1 + K_{CH_3OH} p_{CH_3OH} + K_{H_2O} p_{H_2O} + K_{H_2} p_{H_2}} \tag{4.10}$$

The LH model developed by Lee *et al.* [19] assumes the existence of two distinct types of active sites, so that hydrogen does not compete for the same active sites in which methoxy adsorbs on. The adsorption of all oxygen-containing species, with the exception of methoxy, is considered negligible. The dehydrogenation of the adsorbed methoxy to the adsorbed oxymethylene (eq. (4.12)) is considered the rate determining step (RDS). Equation (4.14) was developed by Lee *et al.* [19] based on the following elementary reaction steps:

$$CH_3OH + S_1 + S_{1a} \rightleftharpoons CH_3O^{(1)} + H^{(1a)} \tag{4.11}$$

$$CH_3O^{(1)} + S_{1a} \rightarrow CH_2O^{(1)} + H^{(1a)} \tag{4.12}$$

$$H_2 + 2S_{1a} \rightleftharpoons 2H^{(1a)} \tag{4.13}$$

Model 4

$$r_{MSR} = \frac{k_{MSR} K_{CH_3OH} \left(\frac{p_{CH_3OH}}{p_{H_2}^{1/2}} \right)}{\left(1 + K_{CH_3OH} \frac{p_{CH_3OH}}{p_{H_2}^{1/2}} \right) \left(1 + K_{H_2}^{1/2} p_{H_2}^{1/2} \right)} \tag{4.14}$$

A unique mode of hydrogen adsorption was also proposed by Patel *et al.* [20], where two types of active sites were described. All species containing oxygen or carbon adsorb competitively on a common active site, while hydrogen adsorbs in a different one. The formation of formic acid from formaldehyde, equation (4.17), was

considered the rate determining step. The reaction mechanism proposed by Patel *et al.* [20] was developed based on the following elementary reaction steps:

$$CH_3OH + S_1 + S_{1a} \rightleftharpoons CH_3O^{(1)} + H^{(1a)} \quad (4.11)$$

$$H_2O + S_1 + S_{1a} \rightleftharpoons OH^{(1)} + H^{(1a)} \quad (4.15)$$

$$CH_3O^{(1)} + S_{1a} \rightleftharpoons CH_2O^{(1)} + H^{(1a)} \quad (4.12)$$

$$OH^{(1)} + S_{1a} \rightleftharpoons O^{(1)} + H^{(1a)} \quad (4.16)$$

$$CH_2O^{(1)} + O^{(1)} \rightarrow HCOOH^{(1)} + S_1 \quad (4.17)$$

$$HCOOH^{(1)} + S_{1a} \rightleftharpoons HCOO^{(1)} + H^{(1a)} \quad (4.18)$$

$$HCOO^{(1)} + S_{1a} \rightleftharpoons H^{(1a)} + CO_2{}^{(1)} \quad (4.19)$$

$$HCOO^{(1)} + S_1 \rightleftharpoons OH^{(1)} + CO^{(1)} \quad (4.20)$$

$$2H^{(1a)} \rightleftharpoons 2S_{1a} + H_2 \quad (4.21)$$

$$CO^{(1)} \rightleftharpoons S_1 + CO \quad (4.22)$$

$$CO_2{}^{(1)} \rightleftharpoons S_1 + CO_2 \quad (4.23)$$

Model 5

$$r_{MSR} = \frac{k_{MSR} K_{O^{(1)}} K_{CH_2O^{(1)}} \left(\frac{p_{CH_3OH} p_{H_2O}}{p_{H_2}^2} \right) \left(1 - \frac{p_{H_2}^3 p_{CO_2}}{K_{MSR} p_{CH_3OH} p_{H_2O}} \right)}{\left(1 + \frac{K_{CH_3O^{(1)}} p_{CH_3OH}}{p_{H_2}^{1/2}} + \frac{K_{OH^{(1)}} p_{H_2O}}{p_{H_2}^{1/2}} + \frac{K_{O^{(1)}} p_{H_2O}}{p_{H_2}} + \frac{K_{CH_2O^{(1)}} p_{CH_3OH}}{p_{H_2}} + K^*_{HCOO^{(1)}} p_{CO_2} p_{H_2}^{1/2} \right)^2} \quad (4.24)$$

Finally, the LH rate expression proposed by Peppley *et al.* [1] was based on the dehydrogenation of adsorbed methoxy as rate determining step – equation (4.12). Similarly to Patel *et al.* [20], oxygen-containing species adsorb competitively on one kind of active sites, while hydrogen adsorbs in a different one. The kinetic expression developed by Peppley *et al.* [1], equation (4.29), was based on the following elementary reaction steps:

$$CH_3OH + S_1 + S_{1a} \rightleftharpoons CH_3O^{(1)} + H^{(1a)} \quad (4.11)$$

$$H_2O + S_1 + S_{1a} \rightleftharpoons OH^{(1)} + H^{(1a)} \quad (4.15)$$

$$CO^{(1)} \rightleftharpoons S_1 + CO \quad (4.22)$$

$$CO_2{}^{(1)} \rightleftharpoons S_1 + CO_2 \quad (4.23)$$

$$2S_{1a} + H_2 \rightleftharpoons 2H^{(1a)} \quad (4.13)$$

$$CH_3O^{(1)} + S_{1a} \rightleftharpoons CH_2O^{(1)} + H^{(1a)} \quad (4.12)$$

$$CH_3O^{(1)} + CH_2O^{(1)} \rightleftharpoons CH_3OCH_2O^{(1)} + S_1 \quad (4.25)$$

$$CH_3OCH_2O^{(1)} + S_{1a} \rightleftharpoons CH_3OCHO^{(1)} + H^{(1a)} \quad (4.26)$$

$$CH_3OCHO^{(1)} + OH^{(1)} \rightleftharpoons HCOOH^{(1)} + CH_3O^{(1)} \quad (4.27)$$

$$HCOOH^{(1)} + S_{1a} \rightleftharpoons H^{(1a)} + HCOO^{(1)} \quad (4.18)$$

$$OH^{(1)} + CO^{(1)} \rightleftharpoons HCOO^{(1)} + S_1 \quad (4.28)$$

$$HCOO^{(1)} + S_{1a} \rightleftharpoons H^{(1a)} + CO_2{}^{(1)} \quad (4.19)$$

Model 6

$$r_{MSR} = \frac{k_{MSR}\dfrac{K_{CH_3O^{(1)}}P_{CH_3OH}}{P_{H_2}^{1/2}}\left(1-\dfrac{P_{H_2}^3 P_{CO_2}}{K_{MSR}P_{H_2O}P_{CH_3OH}}\right)}{\left(1+\dfrac{K_{CH_3O^{(1)}}P_{CH_3OH}}{P_{H_2}^{1/2}}+\dfrac{K_{OH^{(1)}}P_{H_2O}}{P_{H_2}^{1/2}}+K_{HCOO^{(1)}}P_{H_2}^{1/2}P_{CO_2}\right)\left(1+\sqrt{K_{H^{(1a)}}P_{H_2}}\right)} \quad (4.29)$$

4.5. Reverse water gas shift kinetic model

Peppley *et al.* [1] developed a reaction rate expression for the water gas shift reaction where the formation of adsorbed formate from adsorbed hydroxyls and adsorbed CO was the rate determining step. In this work, the elementary reactions proposed by Peppley *et al.* [1] were used to write the reverse water gas shift reaction rate expression – eq. (4.30). Accordingly, the rate determining step was considered to be the formation of adsorbed CO and surface hydroxyls from formate species – eq. (4.20). The elementary reaction that differ from the ones of Peppley *et al.* [1] are as follows:

$$HCOO^{(1)} + S_1 \rightarrow OH^{(1)} + CO^{(1)} \quad (4.20)$$

$$CO_2{}^{(1)} \rightleftharpoons S_1 + CO_2 \quad (4.23)$$

$$CO^{(1)} \rightleftharpoons S_1 + CO \quad (4.22)$$

$$2H^{(1a)} \rightleftharpoons 2S_{1a} + H_2 \quad (4.21)$$

Model 6a

$$r_{rWGS} = \frac{k_{rWGS} K_{HCOO^{(1)}} P_{CO_2} P_{H_2}^{1/2} \left(1 - \frac{P_{H_2O} P_{CO}}{K_{rWGS} P_{CO_2} P_{H_2}}\right)}{\left(1 + \frac{K_{CH_3O^{(1)}} P_{CH_3OH}}{P_{H_2}^{1/2}} + \frac{K_{OH^{(1)}} P_{H_2O}}{P_{H_2}^{1/2}} + K_{HCOO^{(1)}} P_{H_2}^{1/2} P_{CO_2}\right)^2} \quad (4.30)$$

4.6. Parameter estimation

The kinetic parameters were determined by non linear regression, minimizing the sum of the residual squares. The MSR models (eqs. (4.8)-(4.10), (4.14), (4.24), (4.29) and (4.30)) were compared using the mean residual sum of squares parameter, *MRSS*. This parameter was used due to the difference between the number of parameters of each model, and was calculated according to eq. (4.31):

$$MRSS = \frac{\sum_{i=1}^{N} \left(r_{\exp,i} - r_{calc,i}\right)^2}{N - N_P} \quad (4.31)$$

where, $r_{exp,i}$ and $r_{calc,i}$ are the measured and predicted rates in experiment *i,* respectively, *N* is the number of experimental runs (N = 24) and N_P is the number of estimated parameters. The experimental reaction rates were obtained with the differential method:

$$-\left(r_{CH_3OH}\right) = \frac{dX_{CH_3OH}}{d\left(W_{cat} / F^{in}_{CH_3OH}\right)} \quad (4.32)$$

In each experimental run, the partial pressures of all the reaction species were measured at the exit if the reactor. The outlet gas composition was used to determine the conversion of methanol according to eq. (4.33):

$$X_{CH_3OH} = \frac{F_{CO}^{out} + F_{CO_2}^{out}}{F_{CH_3OH}^{in}} \tag{4.33}$$

The equilibrium constants of the adsorbed species were estimated using van't Hoff expression:

$$K_i = \exp\left[\frac{\Delta S_i}{\Re} - \frac{\Delta H_i}{\Re T}\right] \tag{4.34}$$

In kinetic models with a large number of parameters, such as models 5 and 6, a common strategy to decrease the correlation degree is to reduce the number of estimated parameters. For instance, Peppley *et al.* [1] and Patel *et al*. [20] set some heats of adsorption at values consistent with the ones reported in the literature, excluding them from the nonlinear regression. In the present study, the same approach was followed as shown in Table 4.2 - the parameters that were not included in the nonlinear regression are indicated and were taken from the work by Peppley *et al.* [1]. Temperature centering was used to reduce the correlation coefficient between the activation energies and pre-exponential factors of the Arrhenius equation. It has been reported to provide more robust parameters and reduce the nonlinearity of the correlation [20, 31]:

$$k = k\left(T_m\right)\exp\left[-\frac{E_a}{\Re}\left(\frac{1}{T} - \frac{1}{T_m}\right)\right] \tag{4.35}$$

where $k(T_m)$ is the rate constant evaluated at the mean temperature. The same applies for the equilibrium constants of the absorbed species:

$$K_i = K_i\left(T_m\right)\exp\left[-\frac{\Delta H_i}{\Re}\left(\frac{1}{T} - \frac{1}{T_m}\right)\right] \tag{4.36}$$

where $K_i(T_m)$ is the adsorption equilibrium constant evaluated at the mean temperature. The estimated kinetic parameters for the proposed models concerning the MSR reaction are presented in Table 4.2, as well as the respective *MRSS* value.

Table 4.2 – Estimated kinetic parameters for all studied models of the steam reforming reaction

Parameter	Model 1	Model 2	Model 3	Model 4	Model 5	Model 6
k_0	3.9×10^{9}	1.3×10^{7}	1.3×10^{9}	2.0×10^{9}	9.1×10^{9}	9.0×10^{9}
E_a	104.0	80.0	100.0	108.0	97.9	106.7
a	0.47	0.35	–	–	–	–
b	-0.55	0.16	–	–	–	–
c	–	-0.09	–	–	–	–
d	–	-0.07	–	–	–	–
	0.30	–	–	–	–	–
ΔS_{CH_3OH}	–	–	-22.9	-12.9	–	–
ΔS_{H_2O}	–	–	-29.8	–	–	–
ΔS_{H_2}	–	–	-78.7	-88.1	–	–
ΔH_{CH_3OH}	–	–	-33.1	-12.0	–	–
ΔH_{H_2O}	–	–	-18.1	–	–	–
ΔH_{H_2}	–	–	-56.6	-49.7	–	–
$\Delta S_{CH_3O^{(1)}}$	–	–	–	–	-64.6	-29.3
$\Delta S_{CH_2O^{(1)}}$	–	–	–	–	-51.1	–
$\Delta S_{OH^{(1)}}$	–	–	–	–	-84.2	-84.6
$\Delta S_{O^{(1)}}$	–	–	–	–	-47.8	–
$\Delta S_{HCOO^{(1)}}$	–	–	–	–	160.6	198.9
$\Delta S_{H^{(1a)}}$	–	–	–	–	–	-191.5
$\Delta H_{CH_3O^{(1)}}$	–	–	–	–	-20*	-20*
$\Delta H_{CH_2O^{(1)}}$	–	–	–	–	-22.6	–
$\Delta H_{OH^{(1)}}$	–	–	–	–	-20*	-20*
$\Delta H_{O^{(1)}}$	–	–	–	–	-28.9	–
$\Delta H_{HCOO^{(1)}}$	–	–	–	–	100*	100*
$\Delta H_{H^{(1a)}}$	–	–	–	–	–	-50*
MRSS	1.7×10^{-5}	1.1×10^{-5}	2.2×10^{-5}	7.2×10^{-6}	1.0×10^{-5}	5.7×10^{-6}

*Values based on data by Peppley *et al.* [1] and not included in the nonlinear regression.

Figure 4.5 shows that all models describe quite well the experimental data. However, analysing the *MRSS* values in Table 4.2, it is clear that model 3 presents the worst fit, followed by the power-laws models 1 and 2. Although the power-law models can fit well the experimental results, they are not mechanistic derived and, thus were discarded. Among the remaining models 4, 5 and 6, the ones with the lowest *MRSS* values consider very similar reaction mechanisms, models 4 and 6, which suggests that model 5 can be discarded as well. These results indicate that the rate determining step for the MSR reaction is the dehydrogenation of adsorbed methoxy, since both models (4 and 6) are based in that same assumption. The difference between these two models is in the species that are assumed to adsorb in site 1. While in model 6 all oxygen-containing species are assumed to adsorb in site 1, in model 4 the adsorption of all components, with the exception of methoxy, is assumed to be negligible. In other words, model 4 is a simplified version of model 6, which can explain why its *MRSS* value is higher than the one of model 6.

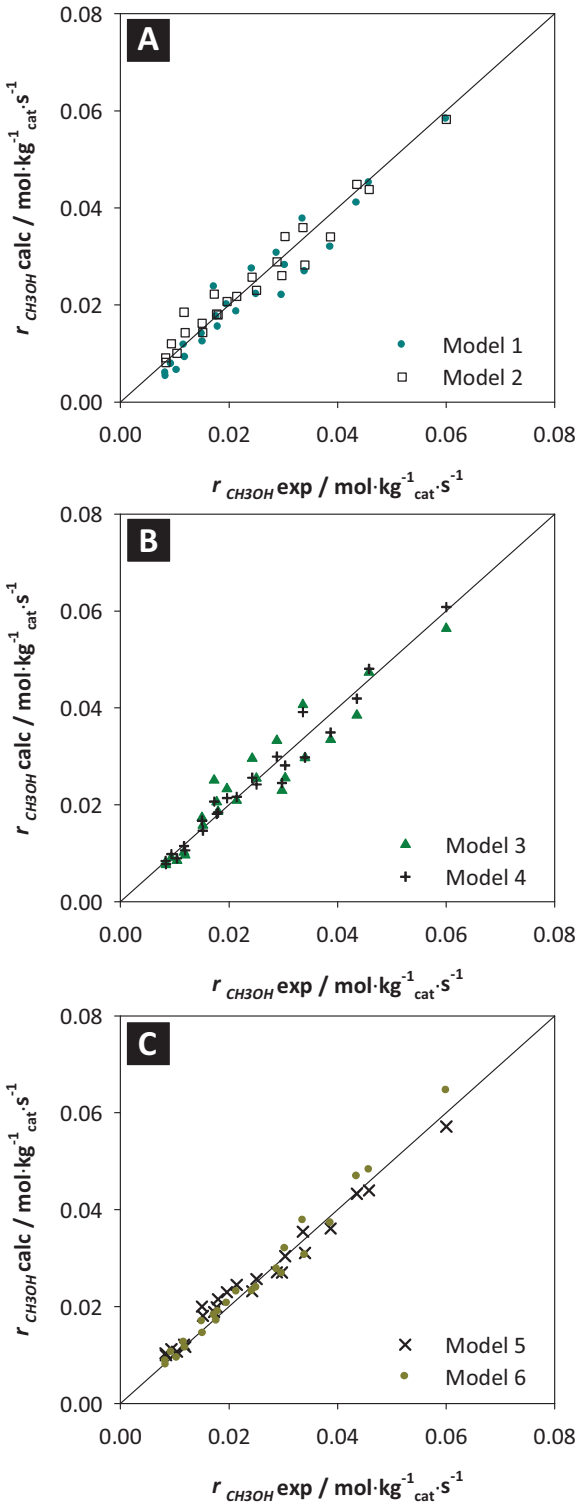

Figure 4.5 – Parity plots of experimental and predicted CH_3OH consumption rates; **(A) -** models 1 and 2; **(B) -** models 3 and 4; **(C) -** models 5 and 6.

Although the predicted rate of methanol consumption is quite precise for all models, this is not enough to describe the overall reaction. In fact, the production of carbon monoxide can only be estimated with a kinetic expression for the rWGS reaction. Among all the works from which the kinetic models were taken, only two have proposed a kinetic expression involving the formation of carbon monoxide. Peppley *et al.* [1] developed a kinetic expression for the WGS reaction while Patel *et al.* [20] developed a kinetic model for the rWGS reaction. Since Patel's model for MSR (model 5) was not among the ones with lower *MRSS* values, the corresponding rWGS model was excluded. As mentioned before, the best fit was obtained for model 4 [19] and model 6 [1]. Accordingly, only Peppley's models will be considered from this point on. As explained in section 3.3, a rWGS kinetic rate expression was written using the same assumptions of Peppley *et al.* [1] – model 6a.

Table 4.3 – Estimated kinetic parameters for rWGS reaction model

Parameter	Model 6a
k_0	9.2×10^{6}
E_a	70.0
$\Delta S_{CH_3O^{(1)}}$	-29.3
$\Delta S_{OH^{(1)}}$	-84.6
$\Delta S_{HCOO^{(1)}}$	198.9
$\Delta S_{H^{(1a)}}$	-191.5
$\Delta H_{CH_3O^{(1)}}$	-20.0
$\Delta H_{OH^{(1)}}$	-20.0
$\Delta H_{HCOO^{(1)}}$	100.0
$\Delta H_{H^{(1a)}}$	-50.0
MRSS	3.0×10^{-9}

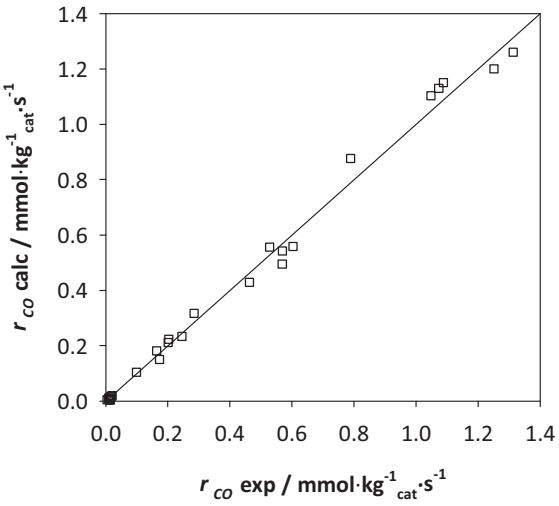

Figure 4.6 – Parity plot of experimental and predicted CO production rates.

As show in Figure 4.6, a good fitting was obtained; the predicted carbon monoxide production rates are very close to the measured ones. These results confirm that the selection of Models 6 and 6a are appropriate to fit the experimental data. Accordingly, these models were used to simulate the packed bed reactor with a one-dimensional model as described in section 4.7.

4.7. Model validation

The Langmuir–Hinshelwood models 6 and 6a developed based on the work of Peppley *et al.* [1] were used to simulate the packed bed reactor with a one-dimensional model. The mathematical model of the reactor comprises steady-state mass balance equations as well as the respective boundary conditions. The reactor operates isothermally with axially dispersed plug flow pattern and pressure drop described by the *Ergun* equation [32]. The model equations as well as the numerical solution strategy are described elsewhere [33]. The accuracy of the model for describing the experimental reactor's performance was assessed for all the operating conditions range. As shown in Figure 4.7, the reactor's model fits well the

experimental results for the entire temperature range (200 °C) and contact time values (3-15 $kg_{cat}·s·mol^{-1}$) considered. A typical S-shape curve describes the conversion of methanol as a function of the reactor temperature; as expected, the conversion is favoured by the temperature increase.

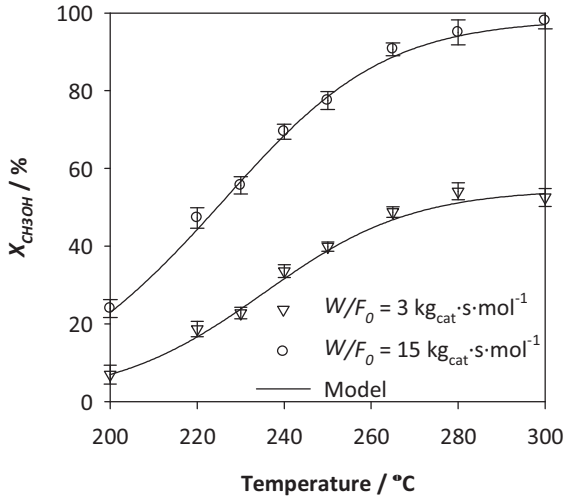

Figure 4.7 – Methanol conversion as a function of temperature, $W_{cat}/F^0_{CH_3OH}$ = 15 $kg_{cat}·mol·s^{-1}$, *S/M* = 1.5, *P* = 1 bar.

The model validation is not complete before assuring that the predicted carbon monoxide production is accurate. Accordingly, the experimental CO concentration was compared to the modelled one as shown in Figure 4.8. Once again, the model reproduces very closely the experimental data for the entire temperature range (200-300 °C). It is important to notice how the CO production increases with temperature due to the endothermic reaction of rWGS.

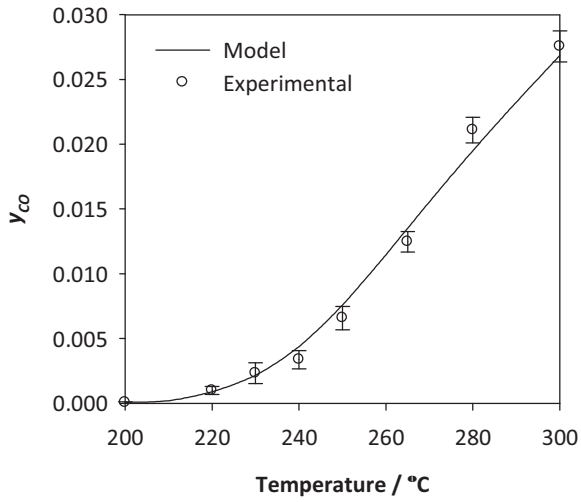

Figure 4.8 – Carbon monoxide molar fraction as a function of temperature, $W_{cat}/F^{0}_{CH_3OH}$ = 15 $kg_{cat}\cdot mol\cdot s^{-1}$, *S/M* = 1.5, *P* = 1 bar.

These results clearly validate both kinetic and reactor's models, which is essential for future modelling works. Although several kinetic studies with commercial $CuO/ZnO/Al_2O_3$ catalysts have already been published, it is important to develop kinetic rate expressions for each catalyst. Similar catalysts can present different performances and thus different models are required. In our following work [34] the kinetic model proposed and validated in this study will be used for the simulation of methanol steam reforming in a carbon membrane reactor.

4.8. Conclusion

A kinetic study of the methanol steam reforming reaction over a commercial $CuO/ZnO/Al_2O_3$ (Süd-Chemie, G66 MR) catalyst has been performed. The reaction was carried out at atmospheric pressure, in a temperature range from 200 °C to 300 °C, and a contact time interval of 3-15 $kg_{cat}\cdot s\cdot mol^{-1}$. The carbon monoxide concentration was below the equilibrium concentration of the reverse water gas shift reaction in all experimental runs, which suggests that methanol decomposition can be neglected. Even though there are several kinetic studies in the literature concerning commercial

$CuO/ZnO/Al_2O_3$ catalysts, a complete kinetic model that is able to predict the formation of carbon monoxide is missing for this particular catalyst. In order to develop such a model, several kinetic rate models expressions developed by different authors were compared. A good agreement between the measured methanol consumption rates and predicted ones was attained by LH models 4 and 6. To predict the production of carbon monoxide, a kinetic expression for the rWGS reaction was developed based on the work of Peppley *et al.* [1]. A good agreement between measured and predicted carbon monoxide production rates was attained. Models 6 and 6a were, thus, chosen as the most appropriate ones to fit the experimental data and were used to simulate the packed bed reactor with a one-dimensional model. The mathematical model was validated comparing predicted conversion and CO concentration to the experimental data.

Acknowledgments

The work of Sandra Sá was supported by FCT, grant SFRH/BD/30385/2006. The research was also supported by funds from FCT projects PTDC/EQU-EQU/71617/2006 and PTDC/EQU-EQU/104217/2008.

List of Abbreviations and symbols

Abbreviations		Definition	Units
a, b, c, d	–	apparent reaction orders for CH_3OH, H_2O, CO_2 and H_2, respectively	
$d_{particle}$	–	diameter of the catalyst particles	m
E_a	–	activation energy	$kJ \cdot mol^{-1}$
$F^0_{CH_3OH}$	–	methanol feed flow rate	$mol \cdot s^{-1}$
H_i	–	heat of adsorption of component *i*	$kJ \cdot mol^{-1}$
k_j	–	rate constant of reaction *j*	*
$k_j(T_m)$	–	rate constant of reaction j evaluated at T_m	*
K_i	–	adsorption equilibrium constant of species *i*	**
$K_i(T_m)$	–	adsorption equilibrium constant of species *i* evaluated at T_m	**
K^e_j	–	equilibrium constant of reaction *j*	***
LH	–	Langmuir-Hinshelwood	
$l_{reactor}$	–	length of the reactor	m
MD	–	methanol decomposition	
MSR	–	methanol steam reforming	
N	–	number of experimental runs	
N_P	–	number of estimated parameters	
P	–	total pressure	bar
PEMFC	–	polymer electrolyte membrane fuel cell	
p_i	–	partial pressure of component *i*	bar
r_j	–	rate of reaction *j*	$mol \cdot s^{-1} \cdot kg_{cat}^{-1}$
$\Re$	–	ideal gas constant	$kJ \cdot mol^{-1} \cdot K^{-1}$

rWGS	–	reverse water gas shift	
Se	–	criteria for comparing goodness-of-fit of the different models	
S_i	–	entropy of adsorption of component *i*	$J \cdot mol \cdot K^{-1}$
S / M	–	steam to methanol feed ratio	
T	–	absolute temperature	K
T_m	–	temperature used in the centering of the Arrhenius and van't Hoff equations	K
W_{cat}	–	mass of catalyst	kg
WGS	–	water gas shift	
X_{CH_3OH}	–	conversion of methanol	%

*units are specific to the form of the rate expression: $mol \cdot kg_{cat}^{-1} \cdot s^{-1}$; $mol \cdot kg_{cat}^{-1} \cdot s^{-1} \cdot bar^{0.08}$; $mol \cdot kg_{cat}^{-1} \cdot s^{-1} \cdot bar^{-0.35}$.

**units are specific to the form of the rate expression: dimensionless; bar; bar^{-1}; $bar^{-1.5}$; $bar^{-0.5}$.

***dimensionless for MSR; bar^{-2} for rWGS.

Greek symbols		**Definition**	**Units**
	–	kinetic parameter	bar

References

[1] B.A. Peppley, J.C. Amphlett, L.M. Kearns, R.F. Mann, Methanol steam reforming on Cu/ZnO/Al2O3 catalysts. Part 2. A comprehensive kinetic model, Appl. Catal. A, 179 (1999) 31-49.

[2] L.C. Pérez, L. Brandão, J.M. Sousa, A. Mendes, Segmented polymer electrolyte membrane fuel cells--A review, Renewable Sustainable Energy Rev., 15 (2011) 169-185.

[3] L. Peng, J. Mai, P. Hu, X. Lai, Z. Lin, Optimum design of the slotted-interdigitated channels flow field for proton exchange membrane fuel cells with consideration of the gas diffusion layer intrusion, Renewable Energy, 36 (2011) 1413-1420.

[4] A.S. Danerol, C. Bas, L. Flandin, E. Claude, N.D. Alberola, Influence of ageing in fuel cell on membrane/electrodes interfaces, J. Power Sources, 196 (2011) 3479-3484.

[5] J.C. Telotte, J. Kern, S. Palanki, Miniaturized Methanol Reformer for Fuel Cell Powered Mobile Applications, Int. J. Chem. Reactor Eng., 6 (2008).

[6] Y. Men, G. Kolb, R. Zapf, D. Tiemann, M. Wichert, V. Hessel, H. Löwe, A complete miniaturized microstructured methanol fuel processor/fuel cell system for low power applications, Int. J. Hydrogen Energy, 33 (2008) 1374-1382.

[7] A.S. Damle, Hydrogen production by reforming of liquid hydrocarbons in a membrane reactor for portable power generation—Model simulations, J. Power Sources, 180 (2008) 516-529.

[8] D.G. Löffler, K. Taylor, D. Mason, A light hydrocarbon fuel processor producing high-purity hydrogen, J. Power Sources, 117 (2003) 84-91.

[9] S. Ahmed, M. Krumpelt, Hydrogen from hydrocarbon fuels for fuel cells, Int. J. Hydrogen Energy, 26 (2001) 291-301.

[10] Y. Chen, Y. Wang, H. Xu, G. Xiong, Hydrogen production capacity of membrane reformer for methane steam reforming near practical working conditions, J. Membr. Sci., 322 (2008) 453-459.

[11] S. Tosti, A. Basile, F. Borgognoni, V. Capaldo, S. Cordiner, S.D. Cave, F. Gallucci, C. Rizzello, A. Santucci, E. Traversa, Low temperature ethanol steam reforming in a Pd-Ag membrane reactor Part 1: Ru-based catalyst, J. Membr. Sci., 308 (2008) 250–257.

[12] B.A. Peppley, J.C. Amphlett, L.M. Kearns, R.F. Mann, Methanol steam reforming on Cu/ZnO/Al2O3. Part 1: the reaction network, Appl. Catal. A, 179 (1999) 21-29.

[13] V. Agarwal, S. Patel, K.K. Pant, H2 production by steam reforming of methanol over Cu/ZnO/Al2O3 catalysts: transient deactivation kinetics modeling, Appl. Catal. A, 279 (2005) 155–164.

[14] H. Purnama, T. Ressler, R.E. Jentoft, H. Soerijanto, R. Schlögl, R. Schomäcker, CO formation/selectivity for steam reforming of methanol with a commercial CuO/ZnO/Al2O3 catalyst, Appl. Catal. A, 259 (2004) 83-94.

[15] D.R. Palo, R.A. Dagle, J.D. Holladay, Methanol Steam Reforming for Hydrogen Production, Chem. Rev., 107 (2007) 3992-4021.

[16] A. Basile, A. Parmaliana, S. Tosti, A. Iulianelli, F. Gallucci, C. Espro, J. Spooren, Hydrogen production by methanol steam reforming carried out in membrane reactor on Cu/Zn/Mg-based catalyst, Catal. Today, 137 (2008) 17–22.

[17] L. Gao, G. Sun, S. Kawi, A study on methanol steam reforming to CO2 and H2 over the La2CuO4 nanofiber catalyst, J. Solid State Chem., 181 (2008) 7–13.

[18] J. Agrell, H. Birgersson, M. Boutonnet, Steam reforming of methanol over a Cu/ZnO/Al2O3 catalyst: a kinetic analysis and strategies for suppression of CO formation, J. Power Sources, 106 (2002) 249-257.

[19] J.K. Lee, J.B. Ko, D.H. Kim, Methanol steam reforming over Cu/ZnO/Al2O3 catalyst: kinetics and effectiveness factor, Appl. Catal. A, 278 (2004) 25-35.

[20] S. Patel, K.K. Pant, Experimental study and mechanistic kinetic modeling for selective production of hydrogen via catalytic steam reforming of methanol, Chem. Eng. Sci., 62 (2007) 5425-5435.

[21] E. Santacesaria, S. Carrá, Kinetics of catalytic steam reforming of methanol in a cstr reactor, Appl. Catal., 5 (1983) 345-358.

[22] K. Takahashi, N. Takezawa, H. Kobayashi, The mechanism of steam reforming of methanol over a copper-silica catalyst, Appl. Catal., 2 (1982) 363-366.

[23] C.J. Jiang, D.L. Trimm, M.S. Wainwright, N.W. Cant, Kinetic mechanism for the reaction between methanol and water over a Cu-ZnO-Al2O3 catalyst, Appl. Catal. A, 97 (1993) 145-158.

[24] C.J. Jiang, D.L. Trimm, M.S. Wainwright, N.W. Cant, Kinetic study of steam reforming of methanol over copper-based catalysts, Appl. Catal. A, 93 (1993) 245-255.

[25] H. Jeong, K.I. Kimb, T.H. Kimb, C.H. Ko, H.C. Park, I.K. Song, Hydrogen production by steam reforming of methanol in a micro-channel reactor coated with Cu/ZnO/ZrO2/Al2O3 catalyst, J. Power Sources, 159 (2006) 1296–1299.

[26] S.R. Samms, R.F. Savinell, Kinetics of methanol-steam reformation in an internal reforming fuel cell, J. Power Sources, 112 (2002) 13-29.

[27] G.F. Froment, K.B. Bischoff, Chemical reactor analysis and design, second ed., Wiley, New York, 1990.

[28] A. Basile, F. Gallucci, L. Paturzo, Hydrogen production from methanol by oxidative steam reforming carried out in a membrane reactor, Catal. Today, 104 (2005) 251–259.

[29] S.P. Asprey, B.W. Wojciechowski, B.A. Peppley, Kinetic studies using temperature-scanning: the steam-reforming of methanol, Appl. Catal. A, 179 (1999) 51-70.

[30] R. Tesser, M. Di Serio, E. Santacesaria, Methanol steam reforming: A comparison of different kinetics in the simulation of a packed bed reactor, Chem. Eng. J., 154 (2009) 69-75.

[31] K.K. Pant, D. Kunzru, Catalytic Pyrolysis of n-Heptane: Kinetics and Modeling, Ind. Eng. Chem. Res., 36 (1997) 2059-2065.

[32] S. Ergun, Fluid flow through packed columns, Chem. Eng. Prog., 48 (1952) 89-94.

[33] S. Sá, H. Silva, J.M. Sousa, A. Mendes, Hydrogen production by methanol steam reforming in a membrane reactor: Palladium vs carbon molecular sieve membranes, J. Membr. Sci., 339 (2009) 160-170.

[34] S. Sá, J.M. Sousa, A. Mendes, Steam reforming of methanol over a CuO/ZnO/Al2O3 catalyst. Part II: A carbon membrane reactor Chem. Eng. Sci., (Submited paper).

Chapter 5. Steam reforming of methanol over a $CuO/ZnO/Al_2O_3$ catalyst Part II: A carbon membrane reactor[1]

Abstract

The reaction of methanol steam reforming was studied in a carbon membrane reactor over a commercial $CuO/ZnO/Al_2O_3$ catalyst (G66 MR, Süd-Chemie). Carbon molecular sieve membranes supplied by Carbon Membranes Ltd. were tested at 150 °C and 200 °C. The carbon membrane reactor was operated at atmospheric pressure and with vacuum at the permeate side, at 200 °C. High methanol conversion and hydrogen recovery were obtained with low carbon monoxide permeate concentrations. A sweep gas configuration was simulated with a one-dimensional model. The experimental mixed-gas permeance values at 200 °C were used in a mathematical model that showed a good agreement with the experimental data. The advantages of using water as sweep gas were investigated in what concerns methanol conversion and hydrogen recovery. The concentration of carbon monoxide at the permeate side was under 20 ppm in all simulation runs. These results indicate that the permeate stream can be used to feed a polymer electrolyte membrane fuel cell.

[1] S. Sá, J.M. Sousa, A. Mendes, Steam reforming of methanol over a $CuO/ZnO/Al_2O_3$ catalyst. Part II: A carbon membrane reactor (Submited to Chemical Engineering Science).

5.1. Introduction

Polymer electrolyte membrane fuel cells (PEMFC) are an attractive power source for small scale applications. Electricity is generated using hydrogen as fuel in an electrochemical reaction where only water is produced. The lack of an easy and efficient way to transport and store hydrogen is leading to the development of *in situ* hydrogen production systems. The reforming of alcohols and hydrocarbons [1-5] are a good example of that. In comparison to other fuels, methanol presents several advantages as a hydrogen carrier. Although it is known for its high toxicity, it has the advantages of being biodegradable, liquid at atmospheric conditions and having a high hydrogen to carbon ratio. Moreover, the temperature range for the methanol steam reforming (MSR) is low (200-300 °C), unlike the one of methane (above 500 °C [6]), or ethanol (around 400 °C [7]). As methanol is a reliable source of hydrogen for fuel cell applications, several studies of MSR reaction, eq. (3.1) have been reported in the literature [8-14].

$$CH_3OH + H_2O \rightleftharpoons CO_2 + 3H_2 \qquad \Delta H = 49.7\,kJ\cdot mol^{-1} \qquad (5.1)$$

The resulting gas mixture is composed by hydrogen and carbon dioxide. However, another reaction between these products place, the so-called reverse water gas shift reaction (rWGS):

$$CO + H_2O \rightleftharpoons CO_2 + H_2 \qquad \Delta H = -41.2\,kJ\cdot mol^{-1} \qquad (5.2)$$

As a consequence, the resulting gas mixture contains a certain amount of carbon monoxide, thus a purification step is needed before feeding the produced stream to the PEMFC. This is particularly important in what concerns the carbon monoxide concentration. CO poisons the anodic catalyst of PEM fuel cells, thus its concentration must be lower than 10 ppm [15].

This separation step can be integrated in the reaction unit using a membrane reactor. Several authors have reported significant improvements in the reactor's performance when using a hydrogen selective membrane [13, 16-18]. Although palladium membranes are the most common ones for this application, promising

results with carbon molecular sieve (CMS) membrane reactors have also been reported [17, 19, 20]. In fact, CMS membranes can be particularly advantageous for low temperature membrane reactors. With the increasing development of catalysts for this reaction, several studies have been published with significant catalytic activities at increasingly lower temperatures (150-200 °C) [21-25]. For this temperature range, CMS membranes present high permeabilities and high selectivities. Palladium membranes, on the other hand, present very low permeabilities under 200 °C and thus are not suitable for this application.

In this work, a membrane module of carbon molecular sieve hollow fibres from Carbon Membranes Ltd. was assembled. Permeance measurements were performed at 150 and 200 °C for single gas and gas mixtures. A carbon membrane reactor (CMR) with a $CuO/ZnO/Al_2O_3$ catalyst from Süd-Chemie was assembled to produce PEMFC grade hydrogen from methanol steam reforming. The effects of the total feed flow rate in methanol conversion, hydrogen yield and hydrogen recovery were studied. Model simulations were carried out to evaluate how the water permeation affects the reactor's performance. In general, this work aims to show that a carbon membrane reactor can produce a hydrogen rich permeate stream to feed a PEMFC.

5.2. Membrane reactor model

The mathematical model used in this work comprises steady-state mass balance equations for the reaction and permeation sides, as well as the respective boundary conditions. Isothermal conditions and ideal gas behaviour were considered. The retentate, filled with a methanol steam reforming catalyst, was assumed to have an uniform cross-sectional void fraction and follow an axially dispersed plug flow pattern with pressure drop described by the *Ergun* equation [26]. The permeate side was assumed to be plug flow with no axial dispersion and with no pressure drop. The model equations as well as the numerical solution strategy are described elsewhere [17]. Due to the lack of a complete kinetic study for this specific catalyst, several

reaction rate expressions were tested and compared in a previous work [27] (see Chapter 4), in order to find the one that best fits to the experimental data. The MSR kinetic model proposed by Peppley *et al.* [9] was the one with better results. A kinetic expression for the rWGS reaction was proposed by the authors based in the same assumptions of Peppley *et al.* [9].

5.3. Experimental

A scheme of the experimental set-up used in both permeation and reaction experiments is presented in Figure 5.1. The membrane module for permeation experiments and the carbon membrane reactor (7.75 mm i.d. and 80 mm lenght) were placed inside a temperature-controlled oven. The temperature of the reactor and the membrane module were measured with type K thermocouples. Mass flow controllers from Bronkhorst (model F-201C, ± 0.1 % FS) were used to control the gas feed flow rate. A CEM-System (Controlled Evaporation and Mixing) from Bronkhorst promoted controlled evaporation of the required methanol aqueous solution before entering the oven. Both feed and permeate pressures were monitored with Druck pressure transducers (PMP 4010, ± 0.08 % FS) and the respective flow rates were measured with Bronkhorst mass flow meters (models F-111B and F-110C, ± 0.1 % FS). The un-reacted water and methanol were separated from the gas mixture in a condenser at ca. -10 °C placed outside the oven. The composition of this mixture was analysed in a Karl Fisher titrator from Metrohm. The retentate and permeate gas streams were analysed in a quadrupole mass spectrometer, Pfeiffer Vacuum OmniStar GSD 320 (detection limit < 1 ppm).

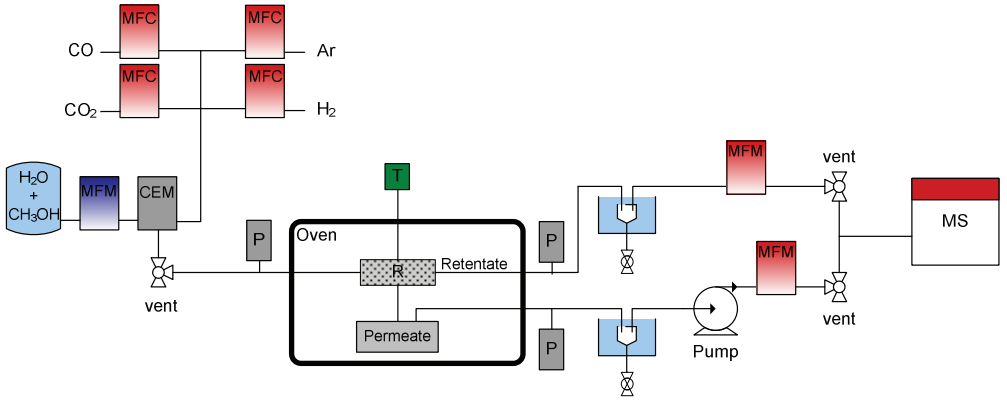

Figure 5.1 – Scheme of the experimental unit. CEM - controlled evaporation and mixing system; MFC - mass flow controller; MFM - mass flow meter; MS - mass spectrometer; P - pressure transducer; T - thermocouple.

5.4. Results and discussion

5.4.1. Carbon membranes permeance

The membranes used in this work are carbon molecular sieve hollow fibres from Carbon Membranes Ltd. - Figure 5.2. These membranes were produced by pyrolysis of dense cellulose cupra-amonia hollow fibres in an inert atmosphere, following a strict temperature history. Afterwards, they were subjected to several carbon chemical vapour deposition/activation steps, this last performed at elevated temperature using air. This post-treatment assigns to the membranes a precise pore size distribution that allows very high permeabilities and selectivities. A more detailed description of the membrane's production and characteristics can be found elsewhere [28].

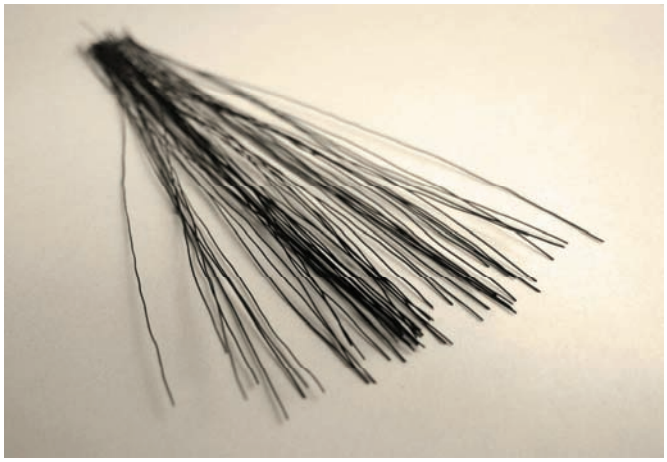

Figure 5.2 – Carbon molecular sieve hollow fibres from Carbon Membranes Ltd.

Gas permeation experiments were performed in a permeation module according to the scheme on Figure 5.3. As summarized in Table 5.1, the prepared module contained 15 fibres of 6.5 cm long, housed in a ¼'' stainless steel tube. Preliminary tests were performed to choose the sealant for the membrane module. Several epoxy glues and silicon adhesives were tested for gas permeability, resistance to water, temperature and pressure. The best performance was obtained with high temperature silicon glue from Shin-Etsu Chemical.

Table 5.1 – Characteristics of the assembled membrane module

Number of fibres	15
Length (m)	0.065
Outer diameter (m)	1.7×10^{-4}
Membrane thickness, ℓ (m)	9×10^{-6}
Effective module membrane area (m^2)	5.0×10^{-4}

The feed was applied to the shell side of the module, while vacuum was applied to the permeate side. The time-lag method [29] was applied to determine the permeation flux across the membranes. After performing vacuum to the permeate side, the gas

permeates driven by the pressure difference between feed and permeate sides. The permeation flux is obtained from the permeate pressure derivative at quasi steady state read in the calibrated volume – Figure 4.1. To confirm the results, a mass flow meter was also used to measure the flow rate of the permeating species.

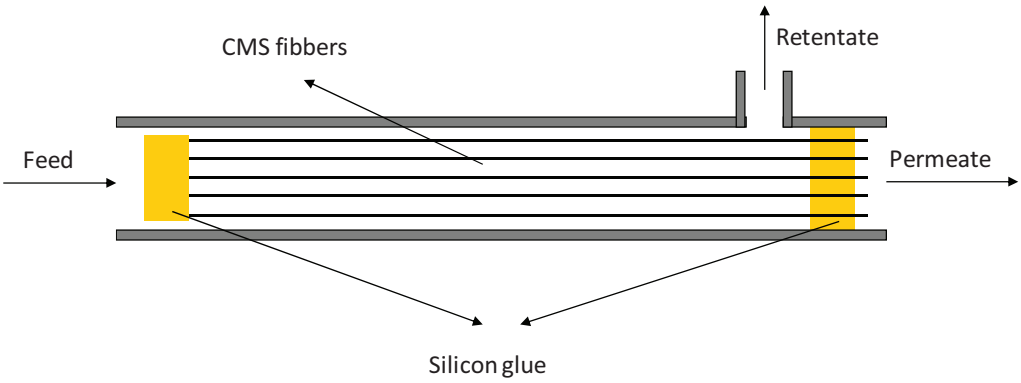

Figure 5.3 – Scheme of the CMS membrane module.

The pure component permeability, L_i, is given by eq. (5.3):

$$L_i = \frac{Q_i}{A^m \Delta p_i / \ell} \tag{5.3}$$

where, Q_i is the flow rate of component *i* through the membrane, Δp_i is the partial pressure difference of component *i* between retentate and permeate, A^m is the effective membrane area and ℓ is the membrane thickness. The gas permeance is defined by the permeability divided by the membrane thickness:

$$L_i^* = \frac{L_i}{\ell} \tag{5.4}$$

In this work, hydrogen was considered the reference component for defining the ideal selectivity, $_{H_2/i}$, given by eq. (5.5):

$$_{H_2/i} = \frac{L_{H_2}}{L_i} \tag{5.5}$$

This ideal selectivity is valid for pure component permeabilities. The separation factor, $'_{H_2/i}$, is defined as the ratio of multicomponent permeabilities, L_i', and is given by:

$$\alpha'_{H_2/i} = \frac{L'_{H_2}}{L'_i} \tag{5.6}$$

The permeance results at 150 °C and 200 °C are summarized in Table 5.2. Monocomponent results show that the permeance of all components increases with temperature, while the higher ideal selectivities are attained at 150 °C. At low temperatures the transport is controlled by activated diffusion and adsorption, whereas at higher temperatures the transport is mostly controlled by the activated diffusion. Comparing the mono and multicomponent permeances at 200 °C, it can be seen that the values are quite similar, which indicates that transport mechanism is mainly diffusion controlled.

In a general analysis, smaller molecules (H_2O and H_2) are considerably more permeable than bulkier ones due to the molecular sieving effect. On the other hand, carbon dioxide is a small species that strongly adsorbs on the pore walls of the carbon membranes, crossing the CMS faster than bulkier and weaker adsorbable species such as carbon monoxide or argon. It was not detected any permeation of methanol either in mono or multicomponent experiments. The results at 150 °C are very interesting in terms of ideal selectivity. Although the commercial catalyst used in this study is not active at this temperature, some studies have been published reporting catalysts with high activities at temperatures lower than 200 °C [21-25]. In a low temperature regime as 150-200 °C, palladium membranes are not a suitable option for a membrane reactor, due to their low permeability. CMS membranes, on the other hand, could be a good option, as they present reasonably high permeabilities and selectivities - Table 5.2.

Table 5.2 – Mono and multicomponent permeance ($m^3_{PTN}·m^{-2}·s^{-1}·kPa^{-1}$) x$10^8$, selectivity and separation factor at 150 °C and 200 °C.

		Monocomponent 150 °C		**Monocomponent 200 °C**		**Multicomponent 200 °C**	
	Kinetic diameter (Å) [30]	**Permeance**	$_{H_2/i}$	**Permeance**	$_{H_2/i}$	**Permeance**	$'_{H_2/i}$
H_2O	2.64	-	-	-	-	254.9	0.4
H_2	2.89	90.0	1	105.2	1	106.4	1
CO_2	3.3	6.2	14.5	7.5	14.0	7.8	13.6
CO	3.69	1.1	81.8	1.9	55.4	1.9	56.0
Ar	3.54	1.0	90.0	1.7	61.9	1.8	59.1

5.5. Membrane reactor

The membrane reactor used in this study contained 100 carbon molecular sieve hollow fibres of 6.5 cm length, and 1.5 g of the commercial CuO/ZnO/Al_2O_3 G66 MR catalyst from Süd-Chemie. The catalyst was previously crushed, sieved to a range of particle sizes of 250-355 µm and diluted with glass spheres of the same particle size, to ensure a homogeneous temperature in the reactor. The catalyst bed was homogeneously distributed in the shell side of the carbon membranes as shown in Figure 5.4.

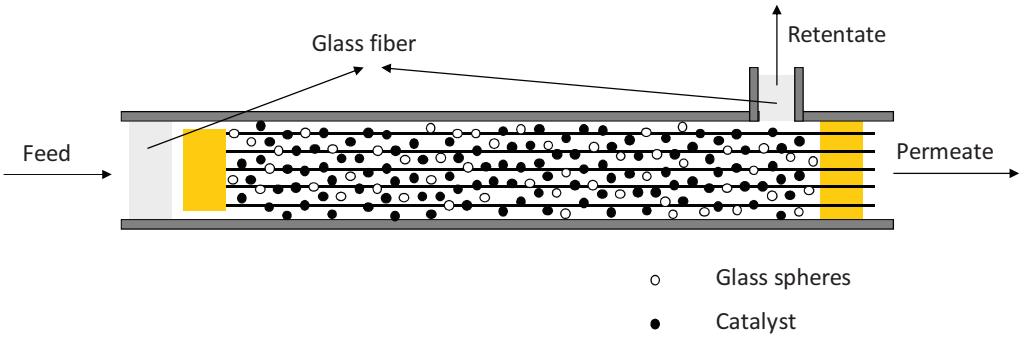

Figure 5.4 – Scheme of the carbon membrane reactor.

The reaction temperature was chosen taking into account several factors. The temperature must be high enough so that the catalyst remains active, but not too high in order to keep the amount of carbon monoxide produced at low levels. Additionally, the membrane selectivities towards hydrogen are favoured at lower temperatures. A good compromise was found at 200 °C. All experiments were performed at atmospheric pressure in the retentate side and vacuum (15 mbar) in the permeate side. The feed flow rate varied between 20 and 180 $cm^3 \cdot min^{-1}$, and the space time ratio range, $W_{cat}/F^0_{CH_3OH}$, was from 93 to 560 $kg_{cat} \cdot s \cdot mol^{-1}$. Due to the high permeability of water through the CMS membranes, the steam to methanol ratio (*S*/*M*) was set to 4. It is important to avoid water depletion in the reaction side due to permeation, otherwise the conversion of methanol will decrease.

It is known that the presence of the membrane in the reactor has a positive influence in its performance [13, 16-18]. The selective removal of hydrogen through the membrane shifts the MSR reaction towards the products, increasing the conversion of methanol. The improvement in the reactor's performance by the presence of the carbon membranes can be measured by the hydrogen yield, defined in the following:

$$Y_{H_2} = \frac{F^P_{H_2} + F^R_{H_2}}{F^0_{CH_3OH}} \tag{5.7}$$

where F_i is the flow rate of component *i*, and superscripts *R* and *P* stand for retentate and permeate respectively. The hydrogen yield is presented in Figure 5.5 as a function of the feed flow rate for the packed bed reactor (PBR) and for the CMR. As expected, the selective removal of hydrogen from the retentate side shifts the MSR equilibrium towards the products, thus increasing the methanol conversion and the hydrogen production. Figure 5.5 also shows a decrease of the hydrogen yield with the total feed flow rate. This happens because higher feed flow rates correspond to lower residence times in the reactor and, consequently, the amount of hydrogen produced per methanol feed flow rate is lower.

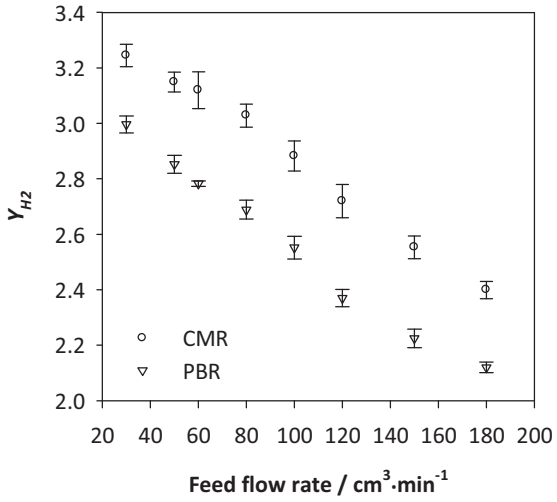

Figure 5.5 – Hydrogen yield as a function of the feed flow rate for the packed bed reactor and the carbon membrane reactor, S/M = 4, P^R = 1 bar, P^P = 15 mbar.

Methanol conversion and hydrogen recovery (eqs. (5.8) and (5.9)) are also affected by the total feed flow rate as illustrated in Figure 5.6. Both conversion and hydrogen recovery are enhanced at lower feed flow rates due higher residence times. The lines in Figure 5.6 correspond to the membrane reactor model, which are very close to the experimental results.

$$X_{CH_3OH} = \frac{F_{CH_3OH}^{R,0} - F_{CH_3OH}^{R,0} - F_{CH_3OH}^{P,0}}{F_{CH_3OH}^{R,0}} \tag{5.8}$$

$$Rec_{H_2} = \frac{F_{H_2}^{P}}{F_{H_2}^{P} + F_{H_2}^{R}} \tag{5.9}$$

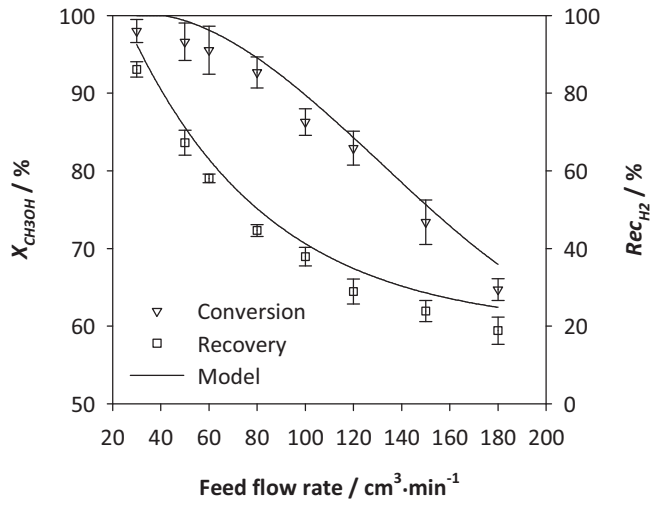

Figure 5.6 – Methanol conversion and hydrogen recovery as a function of the total feed flow rate at 200 °C, S/M = 4, P^R = 1 bar, P^P = 15 mbar.

As mentioned above, carbon monoxide poisons the anodic catalyst of the PEMFC, thus its concentration in permeate side must be lower than 10 ppm [15]. Although a low feed flow rate has a positive effect in methanol conversion and hydrogen recovery, it has the drawback of enhancing the production carbon monoxide. The increase of methanol conversion leads to an increase of the carbon monoxide concentration in the retentate side, thus increasing its driving force through the CMS membranes. The carbon monoxide concentration in the permeate side as a function of the total feed flow rate is shown in Figure 5.7. Once again, the developed model agrees well with the experimental data. Although low CO concentration values can be attained in the CMR, this is attained at the cost of low hydrogen recovery. In order to improve these results, a simulation study was performed as described in section 4.3. The mathematical model was validated with the experimental data as shown in Figure **4.2** 5.6 and Figure 5.7.

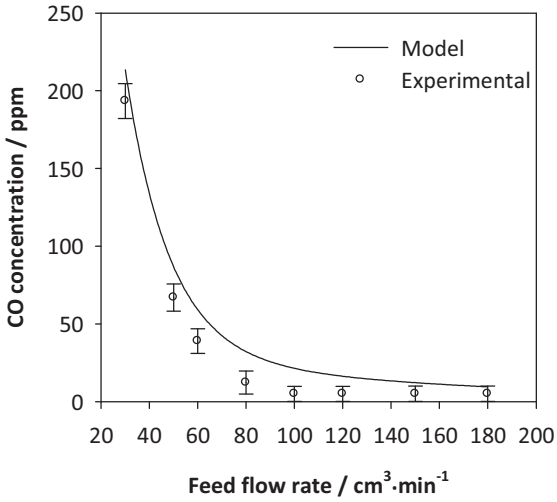

Figure 5.7 – Carbon monoxide concentration at the permeate side as a function of the total feed flow rate at 200 °C, S/M = 4, P^R = 1 bar, P^P = 15 mbar.

5.6. Water as sweep gas

The amount of hydrogen that does not permeate through the membrane cannot be used to feed a PEMFC, thus must be minimized. To improve the hydrogen recovery, the residence time can be increased. Another approach is the increase of hydrogen driving force with a higher retentate pressure. However, the higher the hydrogen permeation is, the higher the water permeation will be as well. This can lead to water depletion in the reaction side (retentate), decreasing the conversion of methanol. In order to illustrate this, a simulation of the CMR was performed considering argon as sweep gas in counter current mode at atmospheric pressure. In comparison to the experimental operating conditions, the residence time was doubled and the reaction pressure was set to 2 bar. As shown in Figure 5.8, the permeation of water is too high, leading to its depletion on the reaction side. The absence of water shifts the rWGS reaction towards the products, producing more carbon monoxide. It is clear in the reactor's profile of Figure 5.8 that the

concentration of carbon monoxide drastically increases when the molar fraction of water is near zero.

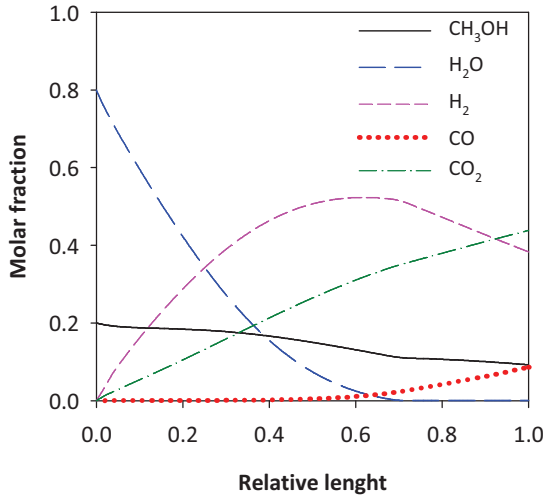

Figure 5.8 – Simulated composition profile at the reaction side (retentate), Q_{total} = 120 $cm^3 \cdot min^{-1}$, S/M = 4, P^R = 2 bar, P^P = 1 bar.

In order to avoid this from happening, water can be used as sweep gas in the permeate side. Another advantage of using water vapour instead of an inert gas, is that water is easily separated from the permeate gas stream in a condenser. The previous simulation was repeated, replacing argon for water as sweep gas - Figure 5.9. Comparing these results with the ones obtained with vacuum at the permeate side (Figure **4.2** 5.6), it is possible to see that the hydrogen recovery was significantly enhanced. Concerning the conversion of methanol, two factors must be analysed. According to the Le Chatelier principle, the increase of the reaction pressure shifts the equilibrium towards the side with fewer moles (reactants), decreasing the conversion of methanol. On the other hand, the increase of the reaction pressure leads to a higher hydrogen driving force, as long as the sweep gas flow rate is high. This leads to higher hydrogen permeation, which shifts the MSR reaction towards the products. In this case, the higher conversion values attained show that the latter effect is more pronounced.

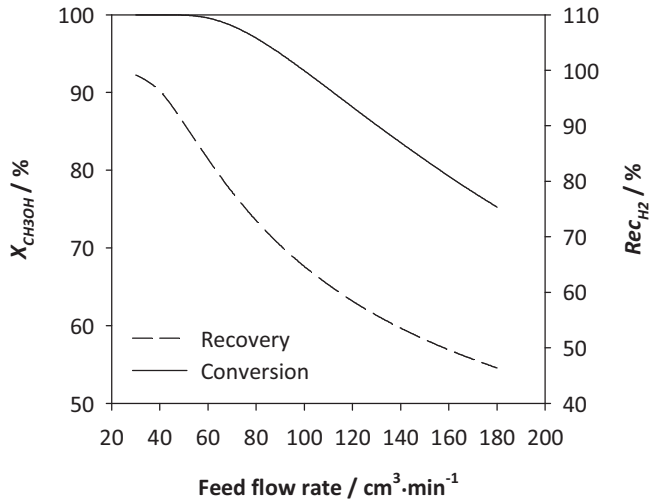

Figure 5.9 – Simulated methanol conversion and hydrogen recovery as a function of the total feed flow rate, with water as sweep gas in counter current mode, S/M = 4, P^R = 2 bar, P^P = 1 bar.

As explained before, the concentration of carbon monoxide in the permeate side must be minimized due to the poisoning of the anodic catalyst of the PEMFC. In order to attain this without reducing the hydrogen permeability, the amount of carbon monoxide produced must be lowered. Using water vapour as sweep gas, its partial pressure at the reaction side remains high enough to keep the rWGS equilibrium shifted towards the reactants side, decreasing the carbon monoxide production rate. This effect is clearly shown in Figure 5.10, where the concentration of carbon monoxide is always below 12 ppm at the permeate side. With such low CO concentration values, the permeate stream can be used to feed a PEMFC without poisoning the platinum electrocatalyst.

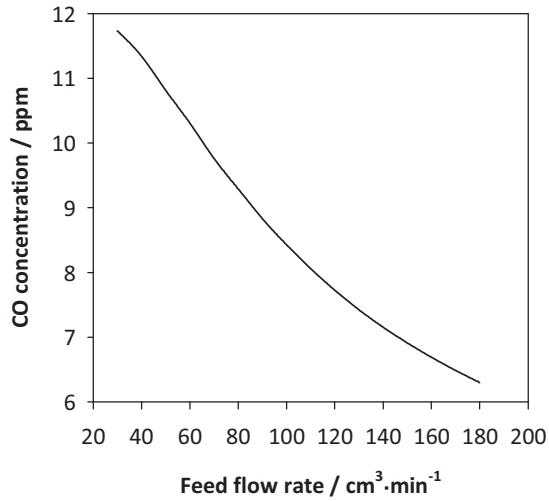

Figure 5.10 – Simulated carbon monoxide concentration at the permeate side as a function of the total feed flow rate, with water as sweep gas in counter current mode, S/M = 4, P^R = 2 bar, P^P = 1 bar.

There is, however, a major drawback in this approach, the energy necessary for vaporizing larger amounts of water. Even though water can be recycled and re-used as reactant, there is still an increase in the process expenses due to the production of steam. In order to reduce the costs, water flow rate must be reduced as well. However, if the sweep gas flow rate is too low, the hydrogen partial pressure at the permeate side will increase, decreasing the driving force across the membrane, thus lowering its recovery. As mentioned before, the advantage of using steam as sweep gas is that water depletion on the reaction side never occurs. In fact, water is always in excess when compared to methanol, due to its permeation from the permeate to the retentate side. In this way, instead of reducing the water flow rate in the permeate side, its amount can be optimised in the retentate side. To facilitate the comparison between both systems (steam or argon as sweep gases), an equivalent steam to methanol ratio, S/M^*, is defined as follows:

$$S/M^* = \frac{F_{H_2O}^{R,in} + F_{H_2O}^{P,in}}{F_{CH_3OH}^{R,in}} \tag{5.10}$$

A simulation study was performed to evaluate the effect of the equivalent steam to methanol ratio in the reactor's performance (Figure 5.11). It was considered constant methanol feed flow rate, while the water feed flow rate was changed to obtain the various S/M^* values. The total feed flow rate was kept constant (100 $cm^3 \cdot min^{-1}$) by adjusting the inert argon flow rate. Figure 5.11 shows that both methanol conversion and hydrogen recovery are enhanced by increasing the equivalent steam to methanol ratio. The effect of steam to methanol feed ratio has been studied by other authors such as Gallucci *et al.* [31], who reported a decrease in the conversion of methanol at high *S*/*M* values. However, this behaviour was controlled by the increase of the total feed flow ratio and thus by the residence time decrease. Zhang *et al.* [19], on the other hand, reported an increase of methanol conversion with steam to methanol feed ratio, in agreement to the results obtained in this work. Despite the similarity in methanol conversion, the CMR simulated in this work is quite different from the one of Zhang *et al.* [19]. In the present work, the excess of steam in the retentate side decreases water permeation from the permeate side, keeping the sweep gas at high flow rates. Therefore, the permeate hydrogen partial pressure remains low and its driving force high. With enhanced hydrogen recovery without depletion of water, the conversion of methanol increases as shown in Figure 5.11.

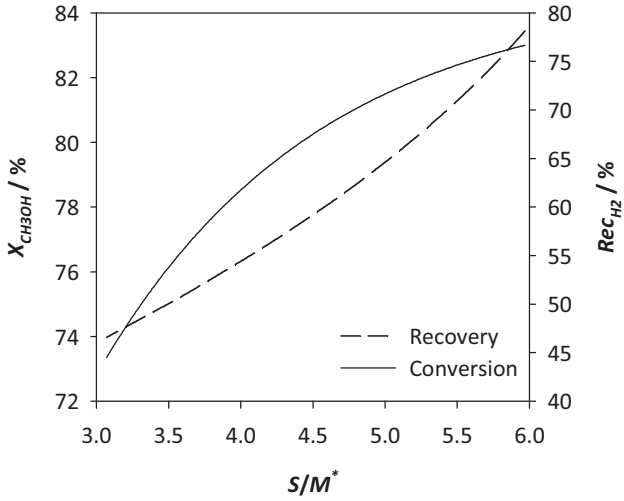

Figure 5.11 – Simulated methanol conversion and hydrogen recovery as a function of the equivalent steam to carbon ratio, with water as sweep gas in counter current mode, $W_{cat} / F^{0}_{CH_3OH}$ = 100 kg_{cat}·s·mol^{-1}, P^R = 2 bar, P^P = 1 bar.

The inhibitory effect of water in the production of carbon monoxide has been reported in the literature [32-34]. The excess of water shifts the WGS reaction towards the products consuming carbon monoxide. In the present work, another factor must be taken into account, the significant increase of methanol conversion. With the increase of water content in the feed, methanol conversion increases as shown above. Consequently, the production of carbon monoxide also increases - Figure 5.12.

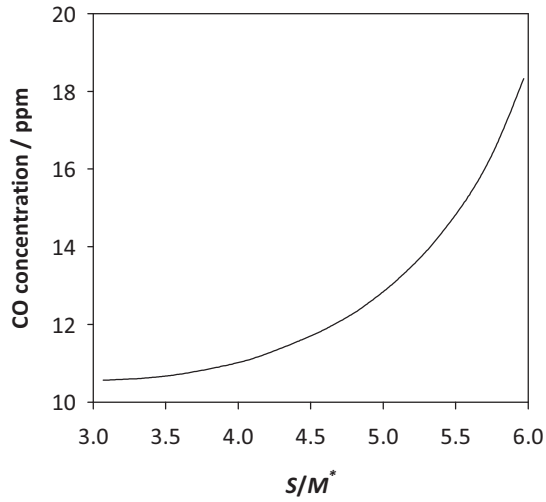

Figure 5.12 – Simulated carbon monoxide concentration at the permeate side as a function of the equivalent steam to carbon ratio, with water as sweep gas in counter current mode, $W_{cat} / F^0_{CH_3OH}$ = 100 kg_{cat}·s·mol^{-1}, P^R = 2 bar, P^P = 1 bar.

Comparing the vacuum results (Figure **4.2** 5.6) with the sweep gas simulations (Figure 5.12), it is possible to conclude that similar methanol conversion and hydrogen recovery values can be obtained using the same amount of water (S/M^* = 4). The steam sweep gas system has the clear advantage of reducing the production of carbon monoxide as shown in Figure 5.12. It is important to notice that permeate CO concentration was kept below 20 ppm when steam was used as sweep gas, while it reaches up to 200 ppm under vacuum (Figure 5.7). In the MR with sweep gas configuration, the same amount of water vapour originated a permeate hydrogen stream containing a significantly smaller concentration of CO. After condensing the excess of water, this humidified hydrogen stream can be directly used for feeding PEMFC.

5.7. Conclusion

The reaction of methanol steam reforming has been studied in a carbon membrane reactor. A commercial $CuO/ZnO/Al_2O_3$ catalyst from Süd-Chemie, G66 MR, was used and the carbon molecular sieve hollow fibres were supplied by Carbon Membranes Ltd. All experiments were performed at 200 °C, atmospheric pressure in the retentate side and vacuum (15 mbar) in the permeate side. The feed flow rate varied between 20 and 180 $cm^3 \cdot min^{-1}$, and space time ratio range, $W_{cat} / F^0_{CH_3OH}$, was from 93 to 560 $kg_{cat} \cdot s \cdot mol^{-1}$. Single and mixed gas permeance measurements were performed at 150 °C and 200 °C. The mixed-gas permeance values were later used in the CMR model. A good agreement between the mathematical model and the experimental data was observed. It was found that methanol conversion, hydrogen recovery and hydrogen yield are enhanced by lower feed flow rates due to higher residence times, with the drawback of higher production of carbon monoxide. The simulation study showed that using water as sweep gas brings several advantages. In addition to an increase in both methanol conversion and hydrogen recovery, the production of carbon monoxide decreases drastically. It was also concluded that water in the retentate feed can be decreased due to its permeation from the permeate side. The results presented in this study confirm the potential of using methanol steam reforming in a CMR to produce humidified hydrogen directly usable for PEMFC applications.

Acknowledgments

The work of Sandra Sá was supported by FCT, grant SFRH/BD/30385/2006. The research was also supported by funds from FCT projects PTDC/EQU-EQU/71617/2006 and PTDC/EQU-EQU/104217/2008.

List of Abbreviations and symbols

Abbreviations		Definition	Units
A_m	–	effective membrane area	m^2
CMR	–	carbon membrane reactor	
CMS	–	carbon molecular sieve	
F_i	–	flow rate of component *i*	$mol \cdot s^{-1}$
ℓ	–	membrane thickness	m
L_i	–	permeability of pure component *i*	$m^3_{PTN} \cdot m \cdot m^{-2} \cdot s^{-1} \cdot kPa^{-1}$
L_i'	–	multicomponent permeability of component *i*	$m^3_{PTN} \cdot m \cdot m^{-2} \cdot s^{-1} \cdot kPa^{-1}$
L_i^*	–	permeance of component *i*	$m^3_{PTN} \cdot m \cdot m^{-2} \cdot s^{-1} \cdot kPa^{-1}$
MSR	–	methanol steam reforming	
P	–	total pressure	bar
PEMFC	–	polymer electrolyte membrane fuel cell	
Q_i	–	flow rate of component	$m^3 \cdot s^{-1}$
Rec_{H2}	–	hydrogen recovery	%
rWGS	–	reverse water gas shift	
S/M	–	steam to methanol feed ratio	
S/M^*	–	equivalent steam to methanol ratio	
W_{cat}	–	mass of catalyst	kg
WGS	–	water gas shift	
X_{CH_3OH}	–	conversion of methanol	%
Y_{H_2}	–	hydrogen yield	

Greek symbols	Definition	Units
	membrane ideal selectivity	
′	separation factor	
Δp	partial pressure difference	bar

Superscripts		Definition
R	–	retentate
P	–	permeate
0	–	feed conditions

References

[1] J.C. Telotte, J. Kern, S. Palanki, Miniaturized Methanol Reformer for Fuel Cell Powered Mobile Applications, Int. J. Chem. Reactor Eng., 6 (2008).

[2] Y. Men, G. Kolb, R. Zapf, D. Tiemann, M. Wichert, V. Hessel, H. Löwe, A complete miniaturized microstructured methanol fuel processor/fuel cell system for low power applications, Int. J. Hydrogen Energy, 33 (2008) 1374-1382.

[3] A.S. Damle, Hydrogen production by reforming of liquid hydrocarbons in a membrane reactor for portable power generation—Model simulations, J. Power Sources, 180 (2008) 516-529.

[4] D.G. Löffler, K. Taylor, D. Mason, A light hydrocarbon fuel processor producing high-purity hydrogen, J. Power Sources, 117 (2003) 84-91.

[5] S. Ahmed, M. Krumpelt, Hydrogen from hydrocarbon fuels for fuel cells, Int. J. Hydrogen Energy, 26 (2001) 291-301.

[6] Y. Chen, Y. Wang, H. Xu, G. Xiong, Hydrogen production capacity of membrane reformer for methane steam reforming near practical working conditions, J. Membr. Sci., 322 (2008) 453-459.

[7] S. Tosti, A. Basile, F. Borgognoni, V. Capaldo, S. Cordiner, S.D. Cave, F. Gallucci, C. Rizzello, A. Santucci, E. Traversa, Low temperature ethanol steam reforming in a Pd-Ag membrane reactor Part 1: Ru-based catalyst, J. Membr. Sci., 308 (2008) 250–257.

[8] B.A. Peppley, J.C. Amphlett, L.M. Kearns, R.F. Mann, Methanol steam reforming on Cu/ZnO/Al2O3. Part 1: the reaction network, Appl. Catal. A, 179 (1999) 21-29.

[9] B.A. Peppley, J.C. Amphlett, L.M. Kearns, R.F. Mann, Methanol steam reforming on Cu/ZnO/Al2O3 catalysts. Part 2. A comprehensive kinetic model, Appl. Catal. A, 179 (1999) 31-49.

[10] V. Agarwal, S. Patel, K.K. Pant, H2 production by steam reforming of methanol over Cu/ZnO/Al2O3 catalysts: transient deactivation kinetics modeling, Appl. Catal. A, 279 (2005) 155–164.

[11] H. Purnama, T. Ressler, R.E. Jentoft, H. Soerijanto, R. Schlögl, R. Schomäcker, CO formation/selectivity for steam reforming of methanol with a commercial CuO/ZnO/Al2O3 catalyst, Appl. Catal. A, 259 (2004) 83-94.

[12] D.R. Palo, R.A. Dagle, J.D. Holladay, Methanol Steam Reforming for Hydrogen Production, Chem. Rev., 107 (2007) 3992-4021.

[13] A. Basile, A. Parmaliana, S. Tosti, A. Iulianelli, F. Gallucci, C. Espro, J. Spooren, Hydrogen production by methanol steam reforming carried out in membrane reactor on Cu/Zn/Mg-based catalyst, Catal. Today, 137 (2008) 17–22.

[14] L. Gao, G. Sun, S. Kawi, A study on methanol steam reforming to CO2 and H2 over the La2CuO4 nanofiber catalyst, J. Solid State Chem., 181 (2008) 7–13.

[15] H.P. Dhar, L.G. Christner, A.K. Kush, Nature of CO Adsorption during H2 Oxidation in Relation to Modeling for CO Poisoning of a Fuel Cell Anode, J. Electrochem. Soc., 134 (1987) 3021-3026.

[16] A. Basile, F. Gallucci, L. Paturzo, A dense Pd/Ag membrane reactor for methanol steam reforming: Experimental study, Catal. Today, 104 (2005) 244-250.

[17] S. Sá, H. Silva, J.M. Sousa, A. Mendes, Hydrogen production by methanol steam reforming in a membrane reactor: Palladium vs carbon molecular sieve membranes, J. Membr. Sci., 339 (2009) 160-170.

[18] S.H. Israni, M.P. Harold, Methanol steam reforming in single-fiber packed bed Pd-Ag membrane reactor: Experiments and modeling, J. Membr. Sci., 369 (2011) 375-387.

[19] X. Zhang, H. Hu, Y. Zhu, S. Zhu, Methanol Steam Reforming to Hydrogen in a Carbon Membrane Reactor System, Ind. Eng. Chem. Res., 45 (2006) 7997-8001.

[20] A. Harale, H.T. Hwang, P.K.T. Liu, M. Sahimi, T.T. Tsotsis, Experimental studies of a hybrid adsorbent-membrane reactor (HAMR) system for hydrogen production, Chem. Eng. Sci., 62 (2007) 4126 – 4137.

[21] L. Gao, G. Sun, S. Kawi, A study on methanol steam reforming to CO2 and H2 over the La2CuO4 nanofiber catalyst, J. Solid State Chem., 181 (2008) 7-13.

[22] J. Agrell, H. Birgersson, M. Boutonnet, I. Melián-Cabrera, R.M. Navarro, J.L.G. Fierro, Production of hydrogen from methanol over Cu/ZnO catalysts promoted by ZrO2 and Al2O3, J. Catal., 219 (2003) 389-403.

[23] G. Águila, J. Jiménez, S. Guerrero, F. Gracia, B. Chornik, S. Quinteros, P. Araya, A novel method for preparing high surface area copper zirconia catalysts: Influence of the preparation variables, Appl. Catal. A, 360 (2009) 98-105.

[24] B. Lindström, L.J. Pettersson, P. Govind Menon, Activity and characterization of Cu/Zn, Cu/Cr and Cu/Zr on -alumina for methanol reforming for fuel cell vehicles, Appl. Catal. A, 234 (2002) 111-125.

[25] C.-Z. Yao, L.-C. Wang, Y.-M. Liu, G.-S. Wu, Y. Cao, W.-L. Dai, H.-Y. He, K.-N. Fan, Effect of preparation method on the hydrogen production from methanol steam reforming over binary Cu/ZrO2 catalysts, Appl. Catal. A, 297 (2006) 151-158.

[26] S. Ergun, Fluid flow through packed columns, Chem. Eng. Prog., 48 (1952) 89-94.

[27] S. Sá, J.M. Sousa, A. Mendes, Steam reforming of methanol over a CuO/ZnO/Al2O3 catalyst. Part I: Kinetic modelling Chem. Eng. Sci., (Submited paper).

[28] S. Lagorsse, F.D. Magalhães, A. Mendes, Carbon molecular sieve membranes. Sorption, kinetic and structural characterization, J. Membr. Sci., 241 (2004) 275–287.

[29] P. Taveira, A. Mendes, C. Costa, On the determination of diffusivity and sorption coefficients using different time-lag models, J. Membr. Sci., 221 (2003) 123-133.

[30] S. Sircar, Basic Research Needs for Design of Adsorptive Gas Separation Processes, Ind. Eng. Chem. Res., 45 (2006) 5435-5448.

[31] F. Gallucci, A. Basile, Co-current and counter-current modes for methanol steam reforming membrane reactor, Int. J. Hydrogen Energy, 31 (2006) 2243 - 2249.

[32] S. Patel, K.K. Pant, Experimental study and mechanistic kinetic modeling for selective production of hydrogen via catalytic steam reforming of methanol, Chem. Eng. Sci., 62 (2007) 5425-5435.

[33] M. Yang, S. Li, G. Chen, High-temperature steam reforming of methanol over ZnO-Al2O3 catalysts, Appl. Catal. B, 101 409-416.

[34] S. Patel, K.K. Pant, Activity and stability enhancement of copper-alumina catalysts using cerium and zinc promoters for the selective production of hydrogen via steam reforming of methanol, J. Power Sources, 159 (2006) 139-143.

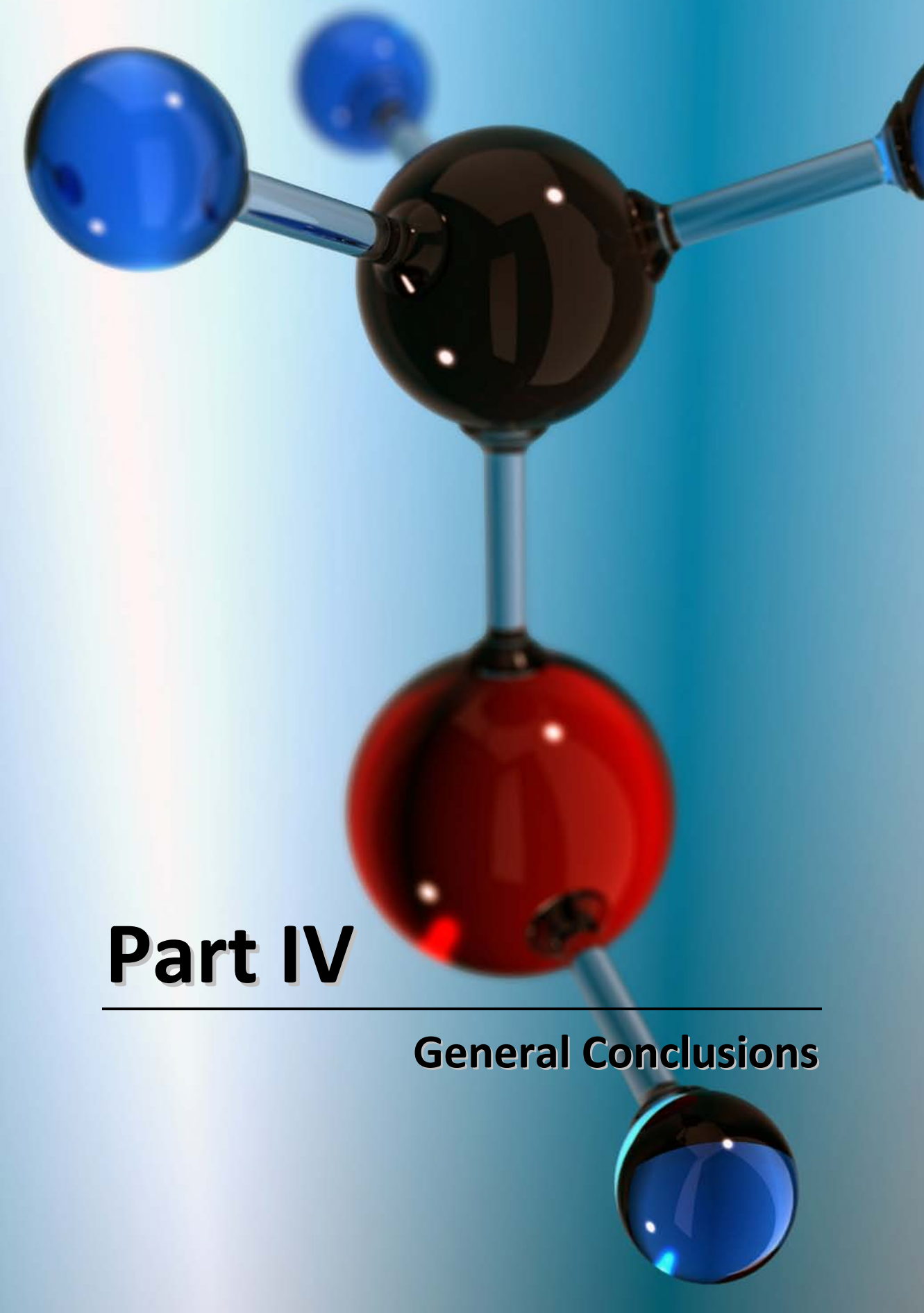

Part IV

General Conclusions

Chapter 6. General Conclusions and Future Work

The present thesis aimed the study of hydrogen production by methanol steam reforming for PEMFC applications. In two simulation studies, **Part II**, the operating and design conditions at which conditions a membrane reactor can produce a PEMFC grade hydrogen stream were investigated. First, a comparative study between carbon molecular sieve and palladium membrane reactors was performed. An innovative configuration was also studied, where the membrane reactor comprised two membrane sections, one made of CMS and the other made of palladium. It was observed that carbon molecular sieve membranes present higher permeabilities, higher hydrogen recovery, and lower selectivities, while palladium membranes are more expensive but exhibit much higher selectivity towards hydrogen. The effect of several parameters on methanol conversion, H_2/CO reaction selectivity, CO concentration at the permeate side and hydrogen recovery was analysed. The CMS-MR presented higher hydrogen recovery than the Pd-MR at high hydrogen concentrations, and the Pd-MR proved to be more advantageous for lower hydrogen production rates. The combination of both membranes revealed some advantages towards each MR. In comparison to the Pd-MR, this configuration allows the use of higher feed flow rates. On the other hand, higher hydrogen recovery and lower CO concentration at the permeate side were achieved compared to the CMS-MR.

In the second simulation study, a new membrane reactor configuration was proposed, with a preferential oxidation catalyst in the permeate side of a MSR-MR. The enhancement of the CMS-MR performance by the presence of a preferential oxidation catalyst in the permeate side was addressed. It was found that the presence of the PROX catalyst in the permeate side was able to convert almost all of the carbon monoxide into carbon dioxide. It was concluded that this system is appropriate to produce a PEMFC grade hydrogen stream with CO concentrations below 2 ppm, CO_2 below 20 %, and more than 80 % of methanol conversion and hydrogen recovery.

Part III of this thesis comprises two experimental studies using a commercial $CuO/ZnO/Al_2O_3$ catalyst from Süd-Chemie, G66 MR. A kinetic study of the MSR reaction was performed, where several kinetic expressions were used to fit the experimental data. The best agreement between the experimental data and the model results was obtained for the Langmuir–Hinshelwood models based on the work of Peppley *et al.*[1]. It was considered that the dehydrogenation of adsorbed methoxy is the rate determining step in MSR reaction, and the formation of adsorbed formate from adsorbed hydroxyls and adsorbed CO is the rate determining step of the rWGS reaction. The kinetic rate expressions were used to simulate the packed bed reactor with a one-dimensional model, which was able to predict very accurately the experimental conversion of methanol and the CO concentration.

A membrane module of CMS hollow fibres from Carbon Membranes Ltd. was assembled. Permeance measurements were performed at 150 and 200 °C for single gas and gas mixtures. In was observed that smaller molecules (H_2O and H_2) are considerably more permeable than the bulkier ones (Ar, CO_2 and CO) due to the molecular sieving effect. On the other hand, carbon dioxide is a small species that strongly adsorbs on the pore walls of the carbon membranes, crossing the CMS faster than bulkier and weaker adsorbable species such as carbon monoxide or argon. The results at 150 °C were particularly interesting in terms of ideal selectivity for CMS application in low temperature MSR membrane reactors.

A carbon membrane reactor was assembled with the CMS hollow fibres and the commercial $CuO/ZnO/Al_2O_3$ catalyst from Süd-Chemie, G66 MR. The catalytic activity experiments were performed at 200 °C, atmospheric pressure in the retentate side and vacuum (15 mbar) in the permeate side. High methanol conversion (40-100 %) and hydrogen recovery (20-98 %) were obtained with low carbon monoxide permeate concentrations (200-5 ppm).

The previously developed mathematical model was validated with the experimental data and was used to simulate a sweep gas configuration in the

[1] B.A. Peppley, J.C. Amphlett, L.M. Kearns, R.F. Mann, Appl. Catal., A 179 (1999) 31-49.

membrane reactor. The simulation study showed that using water as sweep gas brings several advantages to the reactor's performance. Higher methanol conversion and hydrogen recovery were achieved, and the production of carbon monoxide decreased drastically. It was also concluded that the amount of water in the retentate feed can be decreased due to its permeation from the permeate side. The results confirmed the potential of using MSR in a carbon membrane reactor to produce humidified hydrogen directly usable for PEMFC applications.

As future work, it would be important to test and compare the performance of other catalysts besides the commercial G66 MR from Süd-Chemie. Our group is currently developing new catalysts for low temperature MSR operation (150-180 °C). Preliminary tests have revealed high catalytic activities at 180 °C with low carbon monoxide formation, comparable to the one of the commercial catalyst at 240 °C. A comparison between their catalytic activity and the commercial catalyst would be interesting. Our group is now starting to work on dimethyl ether steam reforming and on the development of new low temperature catalysts. The comparison of this process with MSR will soon be possible.

Despite the good results attained with the carbon molecular sieve hollow fibres from Carbon Membranes Ltd., their configuration brought some problems during the module assembly, particularly in the module sealing. A different membrane configuration, such as tubular, that would not require a sealant adhesive should be tested.

Another approach is the use of palladium membranes for hydrogen separation. Our group has a strong experience in composite ultrathin palladium membranes with high hydrogen permeation flow rates. A membrane reactor with this type of membranes should be studied.

Finally, the mathematical model used in this work is very simple and could be improved with the addition of the energy balance. Our group is currently developing a complex mass transport model for gas separation with membranes. This model

assumes multicomponent Darken activated diffusivity. The membrane reactor mathematical model could be significantly improved with the addition of this mass transport model.

Appendix A

Assembled units

Appendix A. Assembled units

A.1. Batch reactor

The experimental unit of Figure A.1 was built to study the methanol steam reforming reaction in a batch reactor.

Figure A.1 – Batch reactor experimental set-up.

A detailed scheme of this unit is presented in Figure A.2. The reactor is placed in an oven, at the required temperature, with the catalyst inside. The feed mixture of methanol and water is introduced in a vessel placed also inside the oven and homogenised using a magnetic stirrer. After reaching the thermal equilibrium, the valve between the reactor and vessel is opened and then closed, allowing the mixture to flow into the reactor, which is under vacuum. The reaction progress is followed by

the pressure variation and by periodic sampling of the reaction mixture, analysed in a gas chromatographer with a thermal conductivity detector (TCD).

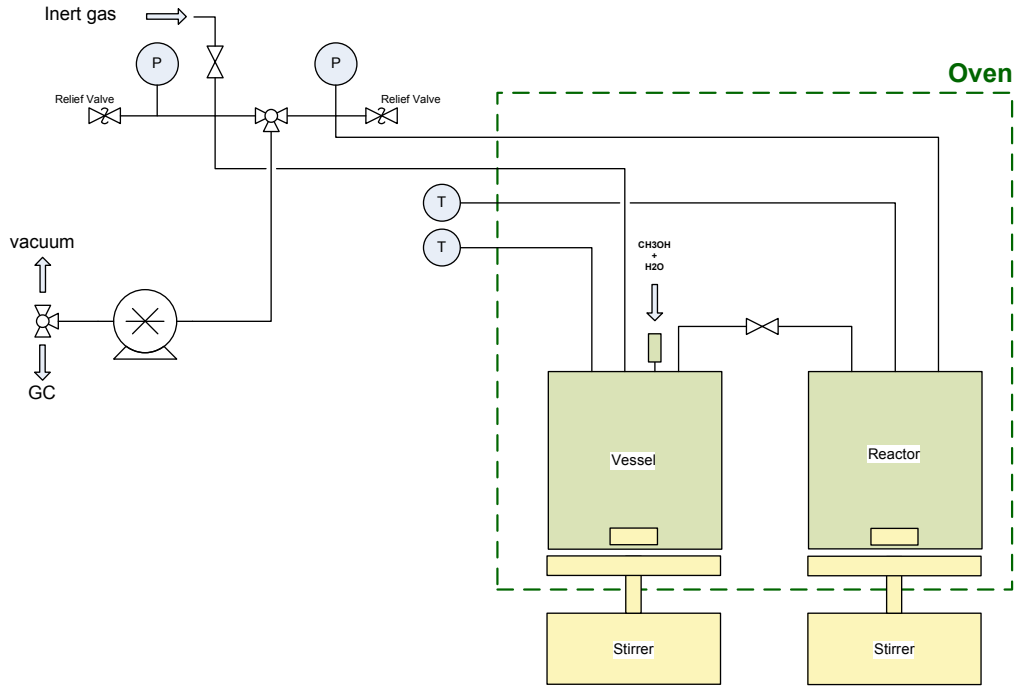

Figure A.2 – Set-up design for batch reactor unit for the methanol steam reforming reaction.

Due to the high operating temperatures (200-300 °C), the magnetic stirrers could not be placed inside the oven, thus had to be adapted. As show in Figure A.3, the control system of the stirrers was kept outside the oven while the plate remained inside the oven.

(A) **(B)**

Figure A.3 – (A) - View of the magnetic stirrers adapted for high temperatures from outside the oven; (**B) –** View of the mixture vessel, reactor and magnetic stirrers' plates at the inside of the oven.

Figure A.4 shows the gasket which holds the methanol steam reforming catalyst. The gasket is placed inside the reactor and is kept under rotation to promote good gas phase mixture (reactants and reaction products). Its rotation is controlled by the magnetic stirrer presented in Figure A.3.

Figure A.4 – Gasket for holding the methanol steam reforming catalyst.

To avoid water and methanol condensation in the tubes placed outside the oven, heating tapes were used to keep the temperature at 150 °C as show in Figure A.5.

Figure A.5 – Heating tapes to avoid the reactants condensation.

This unit employs Swagelok™ stainless steel valves, more specifically: 1/8" 3-ways valves (ref. SS-41GXS2), 1/8" on-off valve (ref. SS-41GS2) and 1/4'' relief valves (ref. SS-RL3S4). The pressure sensors used, model PMP 4010 from Druck, have a range from 0 to 10 bar with a precision of 0.08 % FS.

A data acquisition system was developed based on LabVIEW software (National Instruments) and its front page can be seen in Figure A.6.

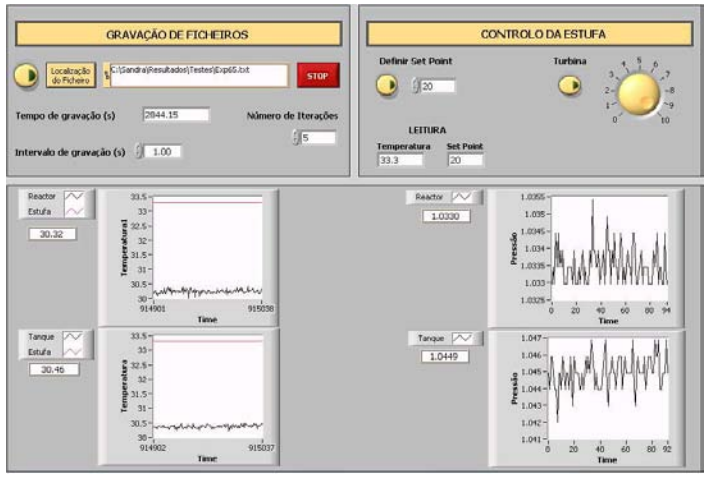

Figure A.6 – Front page of the LabVIEW data acquisition system used for controlling the experimental unit.

A.2. Continuous reactor and permeation unit

The experimental unit of Figure A.7 was built for both reaction and permeation studies, as described below.

Figure A.7 – Experimental unit of the continuous reactor and permeation.

This unit is suitable for studying the steam reforming reaction in a packed bed reactor or a membrane reactor. Mono and multicomponent permeation measurements can also be performed in this unit. Figure A.8 shows the different modules as well as the MSR catalyst.

Figure A.8 – (A) – Membrane module with 15 fibbers; **(B) –** Membrane module with 1 fibber; **(C) –** MSR catalyst; **(D) –** View of the membrane reactor module placed inside the oven.

A detailed scheme of this unit is presented in chapter 5. The packed bed/membrane module/membrane reactor is placed inside a temperature-controlled oven. Mass flow controllers from Bronkhorst (model F-201C, ± 0.1 % FS) are used to control the gas feed flow rate. A CEM-System (Controlled Evaporation and Mixing) from Bronkhorst promotes controlled mixing and evaporation of the feed mixture. A Back Pressure Regulator from Swagelok™ ensures a constant pressure in the reactor. Both feed and permeate pressures are monitored with Druck pressure transducers (PMP 4010, ± 0.08 % FS) and the respective flow rates are measured with Bronkhorst mass flow meters (models F-111B and F-110C, ± 0.1 % FS).

The condensable reactants are separated from the gas mixture in two condensers (permeate and retentate) at ca. -10 °C placed outside the oven (Figure A.9 (A)). The liquid is collected in a small vessel (Figure A.9 (B)) and analysed in a Karl Fisher titrator from Metrohm for water concentration quantification (Figure A.10 (A)). The product gas stream is analysed in a quadruple mass spectrometer, Pfeiffer Vacuum OmniStar GSD 320 (detection limit < 1 ppm) (Figure A.10 (B)).

(A) **(B)**

Figure A.9 – (A) - Condensers placed outside the oven; **(B) –** Vessel for collecting condensed reactants.

(A) **(B)**

Figure A.10 – (A) - Karl Fisher titrator from Metrohm for water concentration quantification; **(B) -** Quadruple mass spectrometer, Pfeiffer Vacuum OmniStar GSD 320.

This unit employs Swagelok™ stainless steel valves, more specifically: 1/8" 3-ways valves (ref. SS-41GXS2), 1/8" on-off valve (ref. SS-41GS2) and 1/4'' relief valves (ref. SS-RL3S4). The pressure transducers used, model PMP 4010 from Druck, have a range from 0 to 10 bar and 0 to 350 mbar, with a precision of 0.08 % FS.

A data acquisition system was developed based on LabVIEW software (National Instruments) and its front page can be seen in Figure A.11.

Figure A.11 – Front page of the LabVIEW data acquisition system used for controlling the experimental unit.